Title

Bioengineered Materials for the Investigation of Adipose Tissue and Adipocytes

Author

Zushin, Peter-James Heliker

Publication Date

2021

Peer reviewed|Thesis/dissertation

Bioengineered Materials for the Investigation of Adipose Tissue and Adipocytes

By

Peter-James H. Zushin

A dissertation submitted in partial satisfaction of the

requirements for the degree of

Doctor of Philosophy

in

Metabolic Biology

in the

Graduate Division

of the

University of California, Berkeley

Committee in Charge:

Professor Andreas Stahl, Chair
Professor Hei Sook Sul
Professor Sona Kang
Professor Sanjay Kumar

Spring 2022

Abstract

Bioengineered Materials for the Investigation of Adipose Tissue and Adipocytes

By

Peter-James H. Zushin

Doctor of Philosophy in Metabolic Biology

University of California, Berkeley

Professor Andreas Stahl, Chair

Obesity and the metabolic diseases that result from it continue to increase across the developing and developed world with little slow down in sight. As such, novel mechanisms for the study and treatment of these metabolic outcomes are needed to combat the ever-increasing epidemic. Our lab has focused on the development of two mechanisms geared toward the understanding of adipose tissue's role in these abnormal metabolic processes through the development of an *in* situ forming implant whose goal is to burn excess circulating glucose and lipids, and through the characterization of a microphysiological device (MPS) to model insulin resistance formation in adipocytes. Our hyaluronic acid (HA)-based hydrogels are ideal scaffolds to build upon to accomplish the three main aims of our *in situ*-forming implant: recruit host stem cells, differentiate those stem cells to a beige adipocyte fate, and then maintain activation of these cells over a long period of time. Using two well characterized chemistries, thiol-acrylate Michael addition and Strain Promoted Azide Alkyne click (SPAAC), we can tailor our hydrogels to the targeted niche using short adhesion peptides, growth factors, degradable crosslinkers, and compounds that bind receptors on a cell's surface. To this end we have shown that molecular weight plays no role in adipocyte function *in vitro*, but altering the hydrogel in increase the loss, or viscous, modulus of a hydrogel can alter morphology and migration. In addition, peptides and growth factors seem to enhance the ingression of host stem and immune cells when injected into an animal and may provide further tailoring opportunities down the road for this therapeutic. I also created a bifunctional HA version of our implant with the goal of pushing forward aim three of the hydrogel project. Modifying the HA backbone with a DBCO group would allow us to conjugate in a tri-azole modified compound like Mirabegron, a β_3-adrenergic agonist responsible for the differentiation of beige adipocytes. I was able to illustrate the efficacy of this bi-chemical modification and determine the final ability of the gels to perform in both capacities, which will be crucial for the beige adipocyte therapeutic in the future. Finally, we created a MPS that reproduces obese metabolic disease states in adipose tissue using induced pluripotent stem cells (iPSC) to differentiate them toward adipocytes and macrophages, modelling the interactions and development of these two cell types to validate this method as a testable platform for insulin resistance.

Table of Contents

Dedication Page

This work is for Laura and Auggie, the two reasons why I'm finishing.

Acknowledgments

First, I would like to acknowledge all the mentors who helped me with these projects over the years. Andreas Stahl for his advice and support within the lab, letting me investigate these novel hydrogels and make the mistakes required to learn. I would also like to thank my Dissertation committee members Hei Sook Sul, Sona Kang, and Sanjay Kumar for their useful advice throughout this process. I'd also like to thank James Olzmann for his astute and always welcome career advice. Kevin Tharp for initially teaching me the hydrogel ropes that allowed me to make the advances outlined here. Sanjay Kumar and Kayla Wolf for helping me transition to the new chemistries as well as being a source of information regarding Hyaluronic acid use as a hydrogel. I'd like to also thank Lin Qi for spearheading the microphysiological device projects and allowing me to take part in the generation of the mature MPS by using my hydrogels. His support and advice during his time here has been greatly appreciated.

My lab mates over the years have been a system of support that has kept me going throughout my Ph.D. Ching-Fang Chang for being my rotation mentor and then someone who I could bounce experimental and data analysis ideas off of for our entire time here. Diyala Shihadih for being my cohort buddy and moral compass. Garrett Dempsey for keeping me company in the morning and upping my coffee game. Xue Wang for being a fun bay/bench/refrigerator friend that does not take any more or less space than absolutely necessary. I would also like to thank Amanda Gunawan, Irene Liparulo, and Kaitlyn Vitangcol for their injection of new blood into the Stahl lab system during Covid.

I'd also like to acknowledge all of the undergraduate volunteers that have worked with me over the years: Jazlyn Chong, Karen Huang, Christina Eldabaugh, Amy Kim, John Xiao, Bowoo Lee, Dan Luca, Adrian Valladarez, Riley Henderson, Jason Feinberg, Shereen Aziz, Jueun Pyun, Jae Hyun Lyu, and Yu Harishima.

I would like to especially thank Steve Ruzin and Denise Schichnes in the College of Natural Resources Bioimaging Facility for their imaging support over the years. Cryosectioned tissue presented here was supported in part by the National Institutes of Health S10 program under award number 1S10RR026866-01. The content is solely the responsibility of the authors and does not necessarily represent the official views of the National Institutes of Health.

Finally, I would like to thank Danielle Jorgens, the director of the Electron Microscopy lab who did quite a bit of the heavy lifting when it came to the sample prep for the SEM imaging of the hydrogels

Chapter 3 Adapted with permission from John Wiley and Sons, DOI: 10.1002/smll.202103157, Lin Qi, Peter-James H. Zushin, Ching-Fang Chang, Yue Tung Lee, Diana L. Alba, Suneil K. Koliwad, and Andreas Stahl, "Probing Insulin Sensitivity with Metabolically Competent Human Stem Cell-Derived White Adipose Tissue Microphysiological Systems."

Chapter 1:
Dual Chemistry Hyaluronic Acid Based implant for Beige Adipogenesis

Summary

Obesity and the comorbidities that go along with it are increasing across the world, and not just in select developed countries. There is much research going into the amelioration of these diseases with the goal of creating a therapeutic. There are many avenues that labs are pursuing this goal from a perspective of increasing the body's metabolic rate by increasing the amount of beige fat in the body with the goal of burning excess energy substrate that is then wasted as heat. Our therapeutic attempt revolves around the creation of a novel hydrogel system that is capable of inducing host stem cell ingression, differentiating them to thermogenic beige adipocytes, and then maintaining activation over the lifetime of the implant. Here, we describe a novel bifunctional hydrogel that presents a conjugated compound for persistent β_3-adrenergic receptor agonism as well as maintaining its ability to present short adhesion peptide and crosslink into a viscoelastic solid, creating a conducive environment for long-term beige adipogenesis and activation.

1.1 - Introduction

1.1.1 Obesity amelioration with beige adipogenesis

Adipose tissue is a complex organ that is made of many different cell types, acting in concert, to guide whole body energy homeostasis[1]. Dysregulation of adipose tissue occurs when chronic nutrient excess leads to obesity. Decades long obesity can in turn effect other tissues like muscle and liver, leading to insulin resistance and eventually diabetes. In addition, this will affect other systems in the body like the circulatory system/cardiac tissue leading to cardiovascular disease, stroke, and heart attack. Because of this, many groups are looking into ways to ameliorate the worst parts of this disease by helping shed excess calories through the activation of inducible beige adipocytes, a thermogenic fat cell that relies on fatty acid catabolism to generate heat at the cost of ATP synthesis, usually through drugs. Here we propose an alternative method of deployment of this idea, using an implantable material to increase the amount of beige adipose tissue in the body by recruiting the host's stem cells, differentiating them toward a beige fate, and then maintaining the activation over the life of the implant. We identified a promising method that utilizes hyaluronic acid as a scaffold, functionalizing it for reaction with two separate click chemistries, in order to create a niche that will hopefully increase the metabolic tone of the differentiating stem cells as they ingress into the hydrogel. While the development of this system is not yet finalized, we have discovered interesting details resulting from our experiments that have pointed us in the right direction.

1.1.2 Beige adipogenesis and activation

Beige adipocytes are thermogenically capable cells arising from white adipose tissue that are plastic in their physiology and behavior, often becoming white-like when not activated[2,3].

Beige adipocytes, like brown adipocytes, are multilocular lipid droplet containing cells with a large mitochondrial load. They generate heat by taking up fatty acids from circulation, shunting them to the mitochondria to undergo β-oxidation creating acetyl CoA, NADH and $FADH_2$. These products then enter the electron transport chain resulting in protons crossing from the matrix of the mitochondria to the intermembrane space where they flow back down their electrochemical gradient through Uncoupling Protein 1 producing heat. Because of their wasteful use of lipids liberated from white adipocytes they represent a tantalizing target for the obesity epidemic.

Thermogenesis capable adipocytes have long been described in rodent model organisms[4,5], mostly focusing on interscapular brown fat which develops prenatally, but an inducible version was discovered that arose from inside the WAT that seemed morphologically similar[6]. Similarly, while it was long known that humans lose their Brown adipose tissue around one year of age[7], an inducible version similar to beige adipocytes was discovered in adult humans[8] leading to the feasibility of the therapeutic targeting of obesity through the activation of human beige adipocytes.

Beige, or Brite as they are sometimes called, adipocytes are plastic cells that can appear as a white adipocyte until receiving an activation signal[9], or may be differentiated from beige adipocyte precursor cells that occur around microvasculature[10]. Often this signal comes as a result of cold challenge activating the β_3-Adrenergic receptor[11], but it can also occur as a result of exercise as well[12]. This begs the question then, which method is more predominantly utilized? In Lee *et al.* mice were housed at room temperature and then give a cold challenge, resulting in roughly 50% of beige adipocytes coming from de novo biogenesis[13]. When revisited in 2015, this group performed a cold challenge but instead housed the animals at thermoneutrality (30°C) first resulting in a much larger population of beige adipocytes (88%) coming from new, differentiated, cells. This data is backed up in a recent study that showed $CD81^+$ cells within $PDGFR\alpha^+/SCA1^+$ cells from the stromovascular fraction that become proliferative upon cold exposure and give rise to beige adipocytes in mouse inguinal WAT[14].

In adult humans, beige adipocyte induction has been targeted to great effect recently by focusing on the β_3-Adrenergic receptor[15,16]. Mirabegron, a β_3 agonist used for the treatment of overactive bladder, has been shown to increase not only the amount of beige/brown adipose tissue in humans, but also improve other biomarkers to a healthier level like HDL, improved insulin sensitivity, and increased circulating adiponectin. We propose to do something similar, using a modified Mirabegron to induce these changes in human adipocytes, but on a more local level by being anchored into a hydrogel scaffold that could conceivably maintain activation of these cells as long as the receptor/agonist remain in contact.

1.1.3 Hyaluronic acid as a basis for an implantable therapeutic

Hyaluronic acid (HA) is an integral part of many connective tissues in the body, made up by a repeating pattern of D-Glucuronic acid and *N*-acetyl-D-glucosamine. This unique glycosaminoglycan is non-sulfated, forms in the plasma membrane and not the Golgi, and can be anywhere from a few hundred repeats[17] to millions[18]. Interestingly, a third of this extracellular matrix component is turned over daily making the synthesis and breakdown of this molecule highly energy intensive. HA has also been implicated in proper adipocyte function. During diet-induced obesity (DIO), total HA content is increased in insulin resistant skeletal muscle and

adipose tissue. When given a recombinant form of hyaluronidase the authors noted reduced HA accumulation and an increase in insulin sensitivity[19]. During adipogenesis, HA synthesis is increased possibly through a positive feedback loop that incorporates PPARγ and C/EBPα[20]. Due to HA's positive role in adipogenesis, as well as its ready degradability, it is an attractive target for an adipose tissue implant that would help increase the number of beige adipocytes in the body, creating a higher metabolic tone in the host and burning excess energy over time.

HA is a highly modifiable substrate, with many published methods that allow alterations to the molecule to functionalize them. To accomplish this lipid and glucose burning implant, we have proposed a novel hydrogel that is modified in two ways. The first is conversion of the glucosamine hydroxyl to a methacrylate group that allows for a click chemistry reaction called Michael Addition that reacts the acrylate group to a thiol group where the nucleophilic addition of a carbanion results in a conjugate addition. The next reaction is conversion of the glucuronic acid carboxyl group to a dibenzocyclooctyne (DBCO) which facilitates strain-promoted azide alkyne click reactions with compounds containing a terminal triazole group. With this difunctionalized HA, we plan to create an injectable therapeutic that crosslinks *in vivo* and presents a viable beige adipocyte niche with the addition of short adhesion peptides through Michael addition. Second, it presents a SPAAC-capable β_3-Adrenergic receptor agonist, triazole-modified Mirabegron, that activates beige adipogenesis.

1.2 - Results

1.2.1 – Generation of a bifunctional hyaluronic acid hydrogel

Hyaluronic acid hydrogels are eminently modifiable due to three functional groups as outlined in Figure 1. The glucuronic acid group contains the carboxyl moiety in magenta that we have identified as an ideal candidate for modification to a DBCO group that would allow for SPAAC chemistry to append a triazole-functionalized Mirabegron onto the HA. Additionally, we wanted to include a Michael addition-based chemistry from the hydroxyl group of the N-acetylglucosamine chemistry (Figure 1, Blue) to provide the crosslinking functionality as well as any other peptides for cell adhesion, differentiation, physiological performance. Both of these chemistries have been well characterized individually[21,22], but never together.

Individual gels for each chemistry were created according to the published methods using 60kDa sodium hyaluronate, reconstituted in deuterated H2O (D2O), and scanned on the College of Chemistry NMR facility NEO-500 automated spectrometer using their general 1H method. The resulting peaks match what has been previously published. The methacrylate functionalized hydrogel (Figure 1-2A) shows the peaks used for quantitative estimation of functionalization. The left-hand arrow denotes the methacrylate methylene peak at 6.1 while the right-hand arrow denotes the HA methyl signal at 1.9. The DBCO functionalized hydrogel (Figure 1-2B) pertinent peaks are also picked out, where the left-hand peak at 6.9 show the aromatic ring hydrogens, the middle arrow picks out the peaks from the NHS ester linker region, and the final right-hand peak picks out the Carbon-Carbon triple bond.

After NMR validation of both chemistries on their own, we then set out to determine an ideal order in which to perform the sequential reactions. Starting with the methacrylate HA reaction and putting it through the DBCO amine reaction after yielded the most robust recovery

of the product, and even seemed to result in a cleaner methacrylate signal in the end. Figure 1-2C illustrates a 1H spectra that shows all the peaks one would expect from an HA molecule that was functionalized with these two chemistries. Methacrylate peaks are picked out in black (arrow points left to right) and DBCO peaks are picked out in Blue (arrows point right to left), illustrating a modified HA molecule with upwards of 90% methacrylate functionalization and 10-12% DBCO functionalization (MDHA).

1.2.2 – Crosslinking characteristics of the bifunctional MDHA

The first test of the MDHA hydrogel was whether the methacrylate and DBCO groups remained functional over the course of synthesis. To determine this, we set up a crosslinking test that would illustrate the results of gels that were solidified through the methacrylate chemistry with dithiothreitol (DTT), DBCO chemistry with a 4-arm triazole-modified PEG, or both. 4 wt% MDHA was reconstituted and crosslinked overnight in a 9mm plastic mold that was trimmed down to 8mm before being placed on our Discovery HR10 rheometer for bulk storage and loss modulus testing. As seen in Figure 1-3A, 200µM PEG was the lowest concentration of this crosslinker that could be used to obtain a solid hydrogel. The highest concentration tested here yielded a storage modulus of 240 Pa and loss of 42 which seemed to be about the max modulus we could obtain with this chemistry. DTT-based crosslinking kinetics performed as reported in the past, where a 0.4 thiol to HA monomer (T:M) ratio was used to obtain a gel that was close to 900 Pa (the storage modulus of white adipose tissue). We next mixed the two chemistries for crosslinking to determine if the effects were additive or multiplicative. And found that with the lowest concentration of the 4-arm AzidoPEG mixed with the 0.4 T:M DTT we obtained an almost 2.5-fold increase in the storage modulus, that did not seem to increase with an increased concentration of the PEG. Lastly, we used a much lower T:M ratio, 0.2, with the lowest concentration of the PEG and was able to achieve a gel of middling storage modulus in comparison to the other 0.4 T:M gels.

We lastly wanted to determine if the MDHA gels behaved in a viscoelastic manner, so a frequency sweep was performed (Figure 1-3B). After crosslinking for 240 minutes on the rheometer in a temperature controlled and humified chamber, we see a gel that isn't fully to the final storage modulus of Figure 1-3A, but it is reasonably close at 638 Pa. The loss modulus of this gel also changes as the top plate angular frequency is changed, suggesting the viscoelasticity properties of the MDHA gels is intact. These rheological outcomes show the individual chemistries as independently functional within the hydrogel and the synthesis process has no noticeable effect on the ability of the hydrogels to behave rheologically as previously published.

1.2.3 - Quantification of DBCO functionality and sequestration capability

To discover the definitive maximum amount of sequestered compound our MDHA hydrogels could conceivably hold, we employed a fluorescence-based approach by utilizing a triazole-modified Cy5 fluorophore. Because of the triazole modification, this fluorophore can participate in SPAAC chemistry reactions. At 10% functionalization, the max reported here[21], we can assume that a 3 wt% MDHA gel could conceivably hold 15µM worth of the triazole compound so we titrated various concentrations of the azido-Cy5 into the MDHA as well as MeHA and then

crosslinked each hydrogel with DTT to a 0.4 T:M ratio in the bottom of a poly-L-lysine coated 24 well tissue culture plate. After crosslinking overnight, we then performed washes every 12 hours with PBS. After 2 days the plates were measured, and the concentrations were compared across the two hydrogels. As seen in Figure 1-4A, the MDHA is able to maintain fluorescence signal better than the MeHA which has no DBCO group. The MDHA fluorescence signal also increases with increasing Cy5 addition which begged the question if we could go higher.

To test this, we added in a roughly 2-fold molar excess of azido-Cy5 relative to the theoretical sequestration concentration of MDHA, 40μM, prior to crosslinking the hydrogels as previously mentioned. The next day the gels were submerged in PBS and their fluorescence was immediately read to determine the baseline levels of the gels. Next the gels were washed twice per day, measuring the hydrogel fluorescence immediately after the second PBS wash. At the end of the first day of washing we see a 90% drop in fluorescence signal in the MeHA gels that tapers off to below 1% of baseline by day 4. The MDHA gels however dropped to just above 50% and then held steady at 47-48% for the next three days. In all the hydrogels show through their azido-Cy5 leak and sequestration actions that they can perform in reliable ways and can be used in their intended dual chemistry approach.

1.2.4 – Azide-functionalized Mirabegron gel and cell functionality

We next obtained a β_3-Adrenergic receptor agonist, Mirabegron, that had been modified in two ways to contain a triazole group (AzMira) by the Goun Lab at the University of Missouri (Figure 1-5A, B Top). To determine their ability to conjugate into the MDHA gel, we reconstituted the MDHA at 1 wt% in D_2O with 2uM of one of the two AzMira compounds. The resulting spectra were then analyzed according to the methods outlined in Figure 1-2C. PK169, but not 143, was capable of quenching the peaks at 6.9 and 1.0ppm, leaving the NHS linker region spectra intact, suggesting that this compound was reacting successfully with the MDHA hydrogels (Figure 1-5A, B Bottom).

To further prove the efficacy of these compounds, we tested their ability to stimulate physiological responses *in vitro*. Using sWAT cells, preadipocytes capable of differentiating reliably toward a beige fate, we treated the cells with another β-Adrenergic receptor agonist isoproterenol as well as unmodified Mirabegron to compare their effectiveness at stimulating UCP1 gene expression as well as releasing glycerol, a byproduct of lipolysis secreted from adipocytes. After 4 hours treatment, PK143 and 169 both induced lipolysis at a rate similar to Isoroterenol, and 4 times higher in comparison to DMSO treatment (Figure 1-5C). This result was also dose dependent as the 5μM concentrations of both were only 2-fold higher. This result was replicated in another adipocyte cell line, a Brown one, called sBAT (Figure 1-5D) UCP1 induction in these cells was also increased in sWAT cells with AzMira administration, though not at an isoproterenol or even unmodified Mirabegron level (Figure 1-5E). These data show the AzMira compounds provided to us are not only able to be conjugated into the MDHA hydrogels, they also still maintain some efficacy for β_3-Adrenergic receptor agonism.

1.2.5 – Post-conjugation physiological stimulation of Azmira compounds

Next, a DBCO chemistry-isolating step was used to determine if the DBCO-AzMira conjugation allowed for the physiological stimulation of sWAT cells as we saw in the previous section. PK169 was conjugated to DBCO-functionalized magnetic beads that would allow for the 2M excess loading of the AzMira as well as being washable after the conjugation step was over. After washing 3x's in PBS, a 20 and 5μM concentration of AzMira-bound beads was loaded into pre-differentiated beige sWAT cells and gene expression was measured (Figure 1-6A). No noticeable change in FABP4 or beige transcription factor EBF2 occurred, but a significant increase in UCP1 levels did in the 20uM version compared to the bead-only control. In addition, no noticeable morphological change occurred that would suggest the intolerance of the treatment groups as indicated by brightfield microscopy (Figure 1-6B). Finally, these treatments also had a much more noticeable effect on the amount of glycerol released with beads conjugated to both versions of AzMira (Figure 1-6C).

1.2.6 – AzMira-conjugated HA has no physiological effect on cells

Finally, we tested the ability of a MDHA hydrogel preconjugated with 20μM Pk169 and Pk143 (MiraHA) to stimulate UCP1 expression in beige adipocytes. MDHA was reconstituted and functionalized overnight with a short adhesion peptide, cyclic RGD 1.2. The next day, the hydrogels were crosslinked and plated in a 24 well tissue culture plate. After crosslinking overnight and undergoing 3x PBS washes, D6 beige differentiated sWAT cells were trypsinized and replated onto 4 wt% MiraHA hydrogels crosslinked at 0.4 T:M ratio. After 24 hours there was no change in any beige-specific genes compared to DMSO or non-modified Mirabegron controls (Figure 1-7A). UCP1 and total HSL protein levels also remained unchanged after 24 hours on the MiraHA as well (Figure 17B). While the AzMira looks functional across all of the other methods we tested them with, it seems like conjugation to the HA backbone inactivates them.

1.3 - Discussion

The obesity epidemic is not going away any time soon, so the development of novel therapeutics are necessary to push back the tide. Here, we have described the beginning of such a device, an implantable therapeutic that is able to maintain activation of beige adipocytes over the lifespan of the implant by using a bound β_3-Adrenergic receptor agonist, mirabegron, that has already been used successfully in humans as an offlabel treatment[23,24]. While the work is not quite complete yet, we have shown here that the material foundation of such a therapeutic is sound and the ability of beige adipogenesis is unhindered while cells are grown on top of it.

Recently, there was another attempt at using HA to deliver an adrenergic agonist to adipose tissue with the goal of protecting again diet-induced obesity. They created an injectable that was a carrier for Clenbuterol, a β_2-adrenergic agonist originally created for the treatment of equine asthma[25]. While effective at inducing the inhibition of lipogenesis in the perigonadal adipose tissue they injected near, no beiging characteristics were measured. This is in contrast to our implant where we would hopefully increase the overall number of beige adipocytes available

for thermogenic disposal of excess energy substrate and not just limit lipogenesis and induce some lipolysis.

The chemistries used to create this bifunctional MDHA gel have never been combined within an HA scaffold. In Figure 1-2 we illustrated the feasibility of the combination of these two disparate chemistries, creating a hydrogel that have a ^{1}H NMR spectra with combination of peaks from each of the two chemistries that are readily identifiable and quantifiable. The resulting bifunctional gel also is capable of reacting through both chemistries as evidenced by still being able to be crosslinked by DTT, as well as being crosslinked by a 4-arm azido-PEG to a much lesser storage modulus. Interestingly, the combination of the two click chemistries as crosslinkers seem to have a multiplicative effect on the final stiffness of the gel without affecting the loss modulus too much, giving a potential mechanism to further increase the stiffness of these gels to accomplish some unknown need.

Next, the functionalization of the mirabegron compounds were an unknown before they were tried in tissue culture, so it was a relief to see them behave on par with Mirabegron and Isoproterenol for lipolytic stimulation on their own (Figure 1-5C,D) as well as conjugated to the DBCO magnetic beads (figure 1-6C). While the increased UCP1 gene expression is lacking in the AzMira compounds compared to the unmodified version, some stimulation did occur (Figure 1-5E and 1-6A). This might be a blessing in disguise as chronic β-Adrenergic receptor agonism has long been known to decrease in effectiveness due to receptors being endocytosed into the cytoplasm and not returning[26].

Finally, when mature beige adipocytes were placed on top of AzMira-conjugated MDHA no evidence of β-Adrenergic receptor agonism was seen after a 24-hour period when looking at gene expression. This is an unfortunate outcome considering the success of the material up to this point, even when bound to DBCO on a magnetic bead. One possibility is that the Mirabegron is too close to the larger DBCO group, leading to steric hindrance and an inability of the agonist to bind to the receptor. At the moment we are waiting on a new synthesis of AzMira that contains a long linker region that may help alleviate the non-reactivity in the gel which we hope to test out in the near future as the dual chemistry hydrogel looks functional otherwise.

1.4 - Figures
Figure 1-1

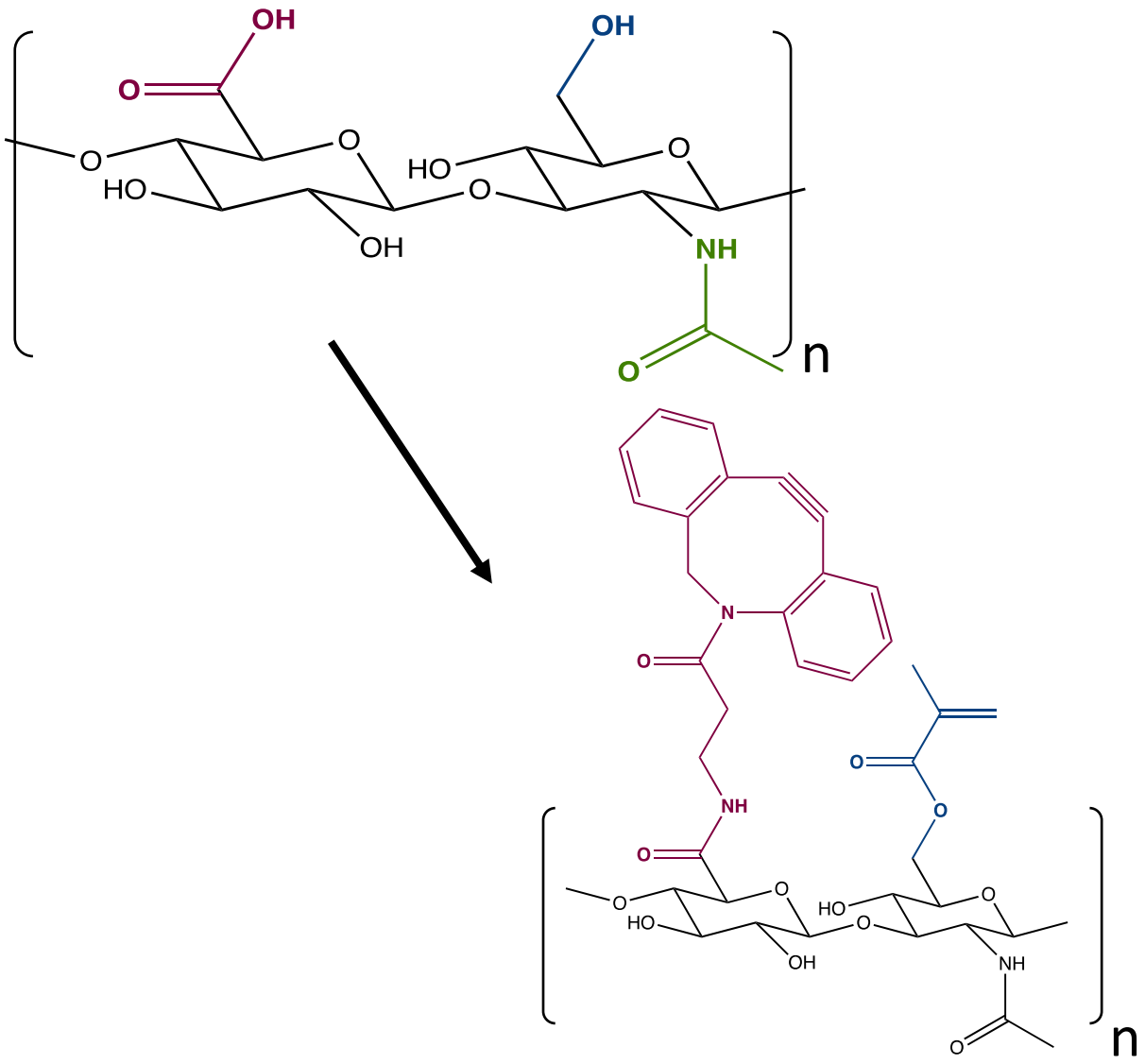

Figure 1-1: Schematic of the hydrogel that outlines the function. (Top) HA monomer with modifiable groups colored, glucuronic acid carboxyl (magenta), *N*-acetylglucosamine C6-hydroxyl (blue), or amine group (green). (Bottom) Proposed difunctional hyaluronic acid structure with the carboxyl group changed to a DBCO moiety (magenta), and the hydroxyl group changed to a methacrylate group (blue).

Figure 1-2:

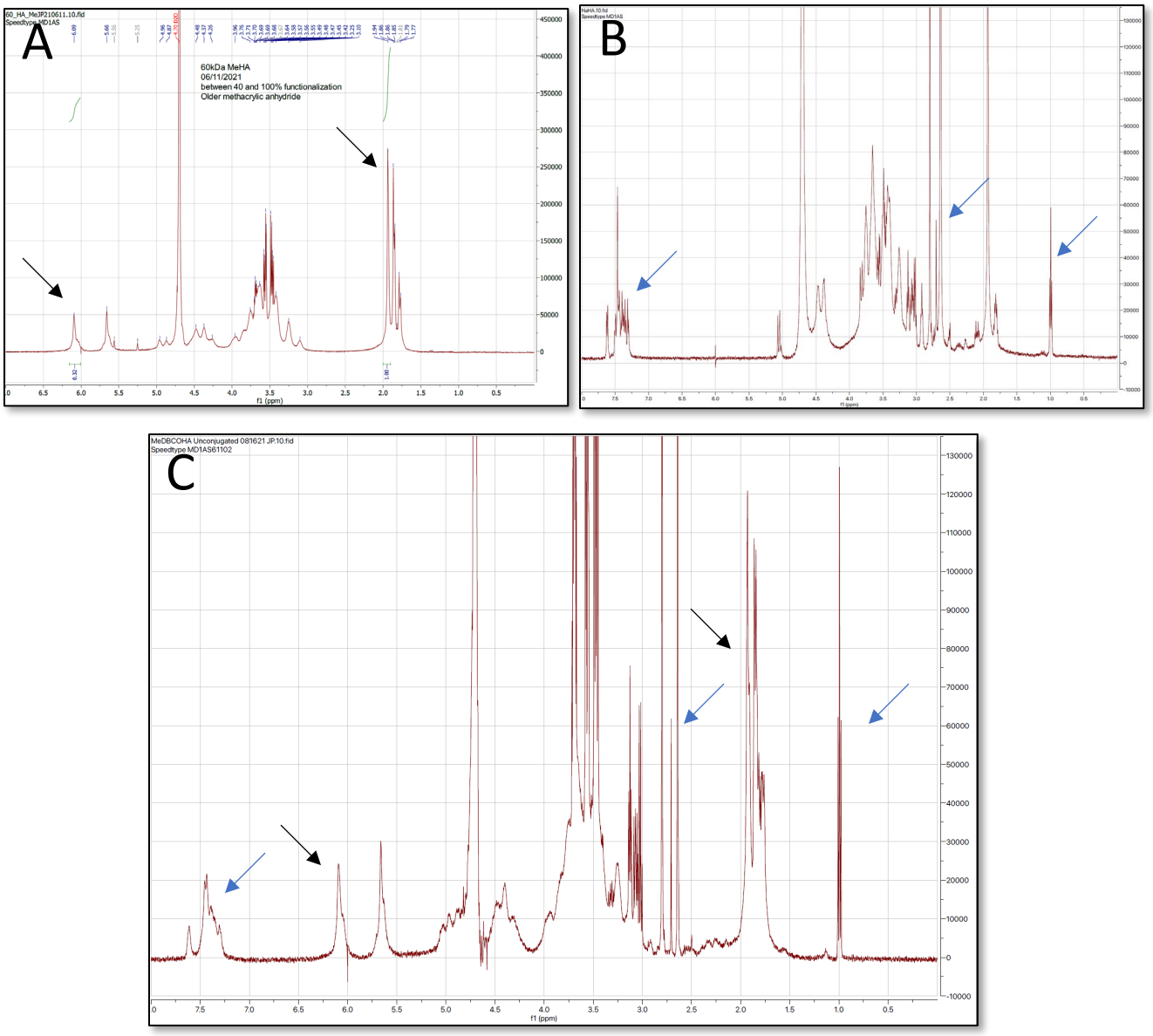

Figure 1-2: NMR spectra of the different HA hydrogels made: A) ^{1}H spectra of methacrylate functionalized HA. B) ^{1}H spectra of DBCO functionalized HA. C) ^{1}H spectra of methacrylate and DBCO functionalized HA.

Figure 1-3:

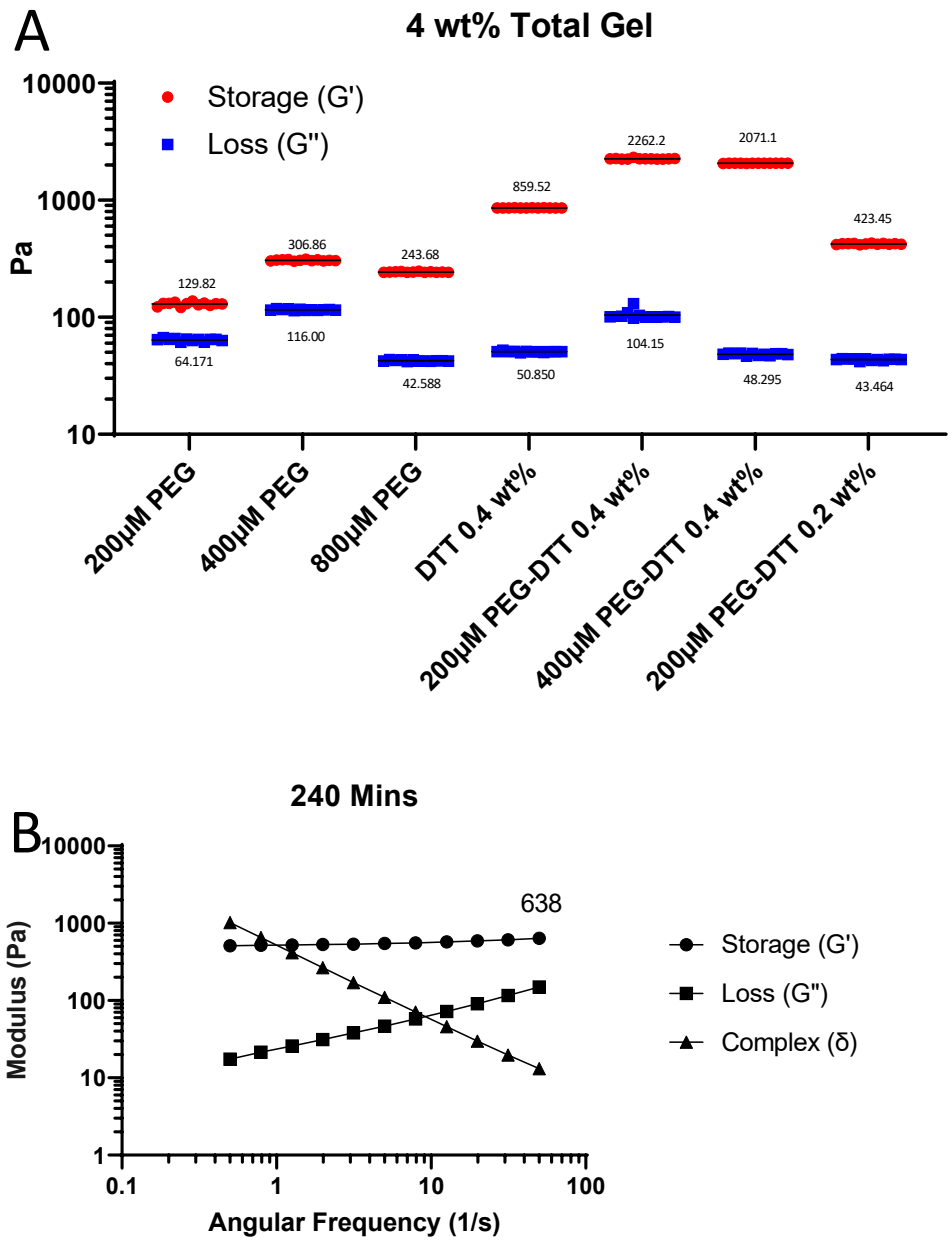

Figure 1-3: Crosslinking through MeHA and DBCO functional groups. A) Rheological measurements of MDHA crosslinked with a 4-arm Azido-PEG and/or DTT at different concentrations to determine the material outcomes of using heterogenous crosslinkers. B) Frequency sweep of a 3 wt% MDHA in PBS, crosslinked with 0.4 thiol to monomer ratio using DTT.

Figure 1-4

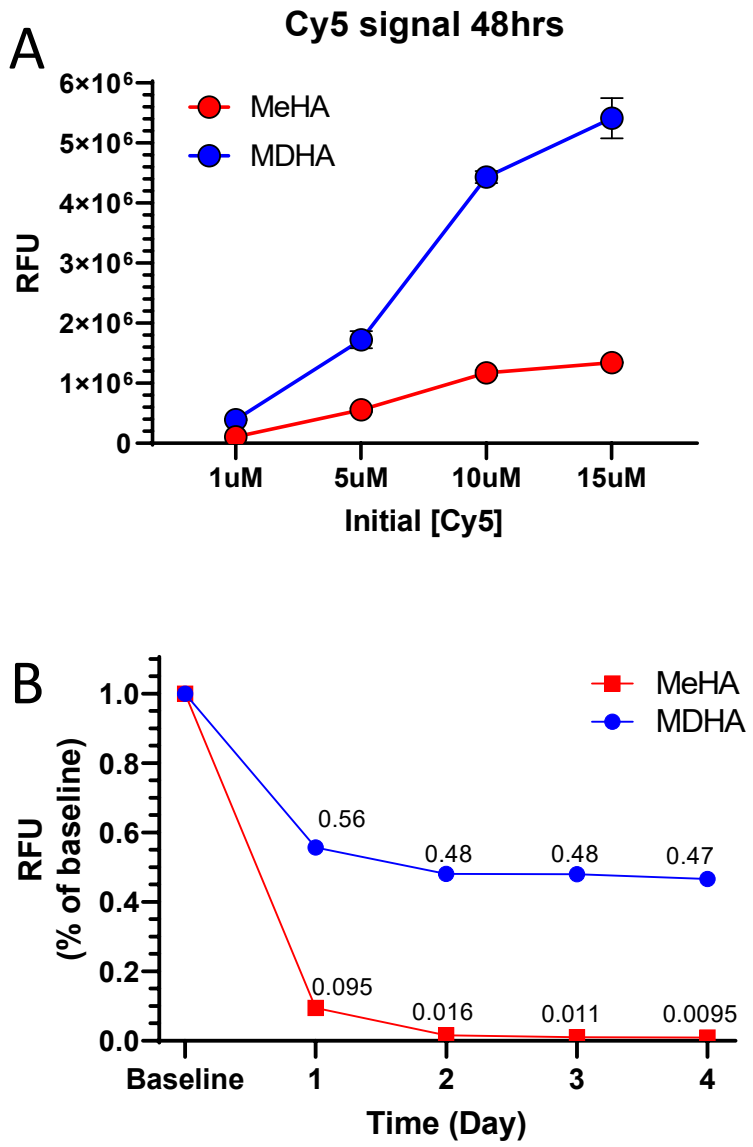

Figure 1-4: DBCO functionality testing using Azido-Cy5 washouts. A) Testing of hypothetical concentration range of Az-Cy5 sequestration to determine our functionalization efficiency. Washout occurred 4 times over 48 hours and then read on a plate reader. B) 2M excess, according to theoretical sequestration molar amount, loading of Az-Cy5 into MDHA or MeHA to show efficacy of difunctional HA.

Figure 1-5

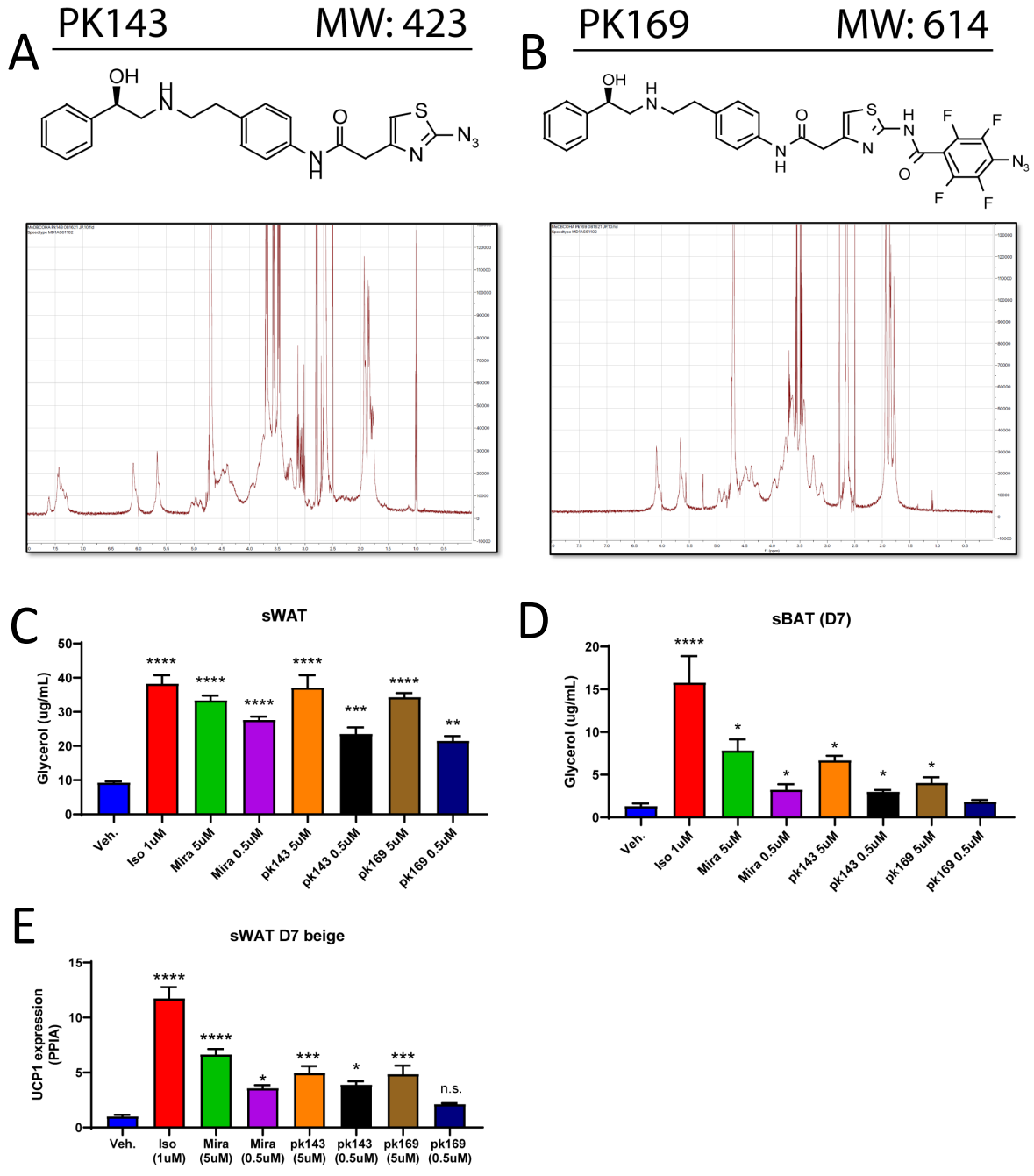

Figure 1-5: AzidoMirabegron structure and physiological effects while unconjugated. A, B Top) Azido-Mirabegron structures and molecular weights. (Bottom) ^{1}H spectra of MDHA conjugated with PK143 or PK169. C, D) Lipolysis stimulation comparisons of AzMira compounds to isoproterenol and non-modified Mirabegron in beige differentiated sWAT cells or sBAT cells. E) UCP1 gene expression levels (fold change) upon 4-hour treatment with listed compounds.

Figure 1-6

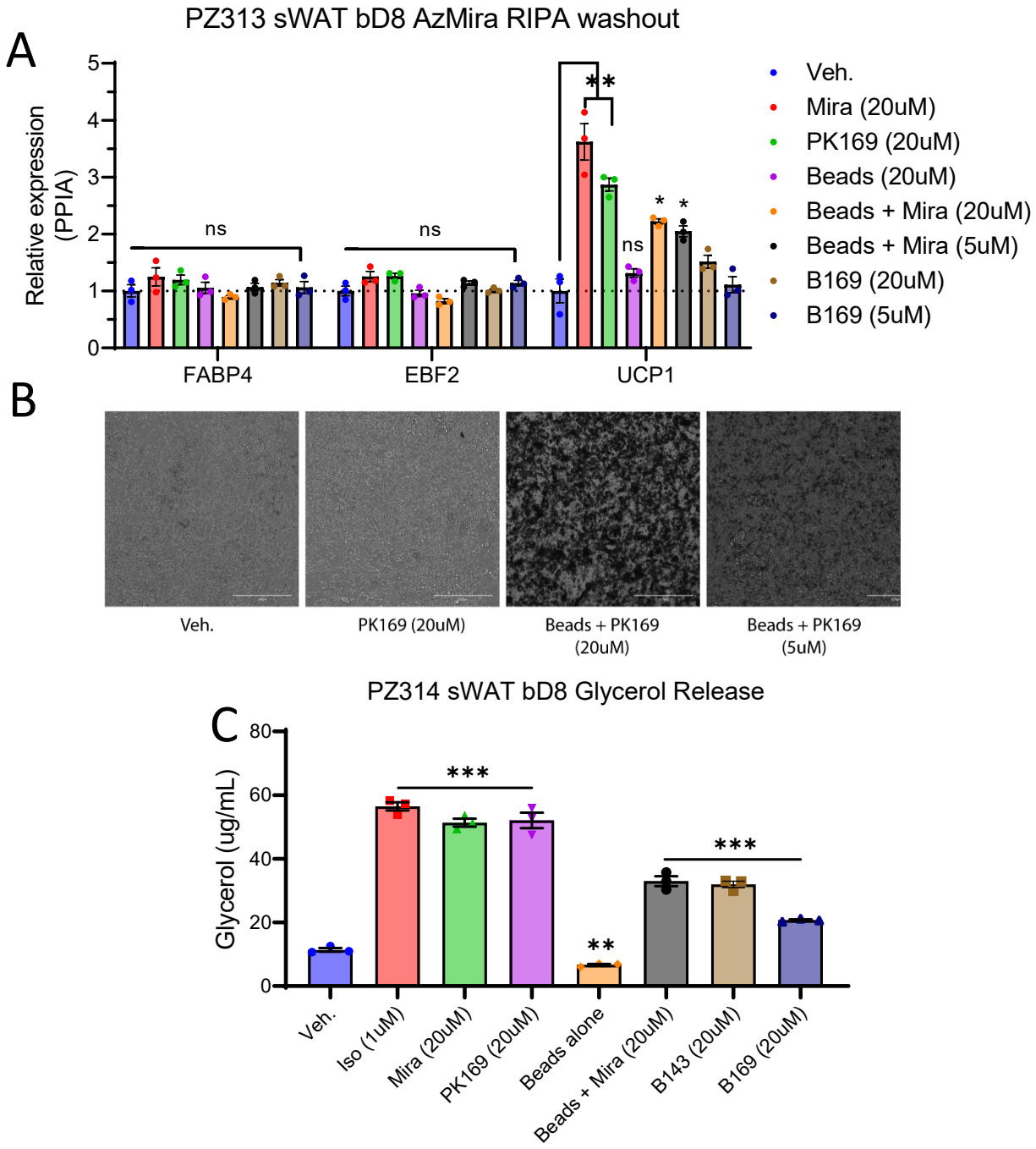

Figure 1-6: Cells physiology of AzMira conjugated magbeads. A) Beige sWAT differentiated cells gene expression after 4 hours treated with listed compounds. B) Brightfield images of cells after 4 hours treatment, showing no morphological changes due to toxicity. C) Lipolytic stimulation of sWAT cells using AzMira compounds conjugated to magnetic beads.

Figure 1-7

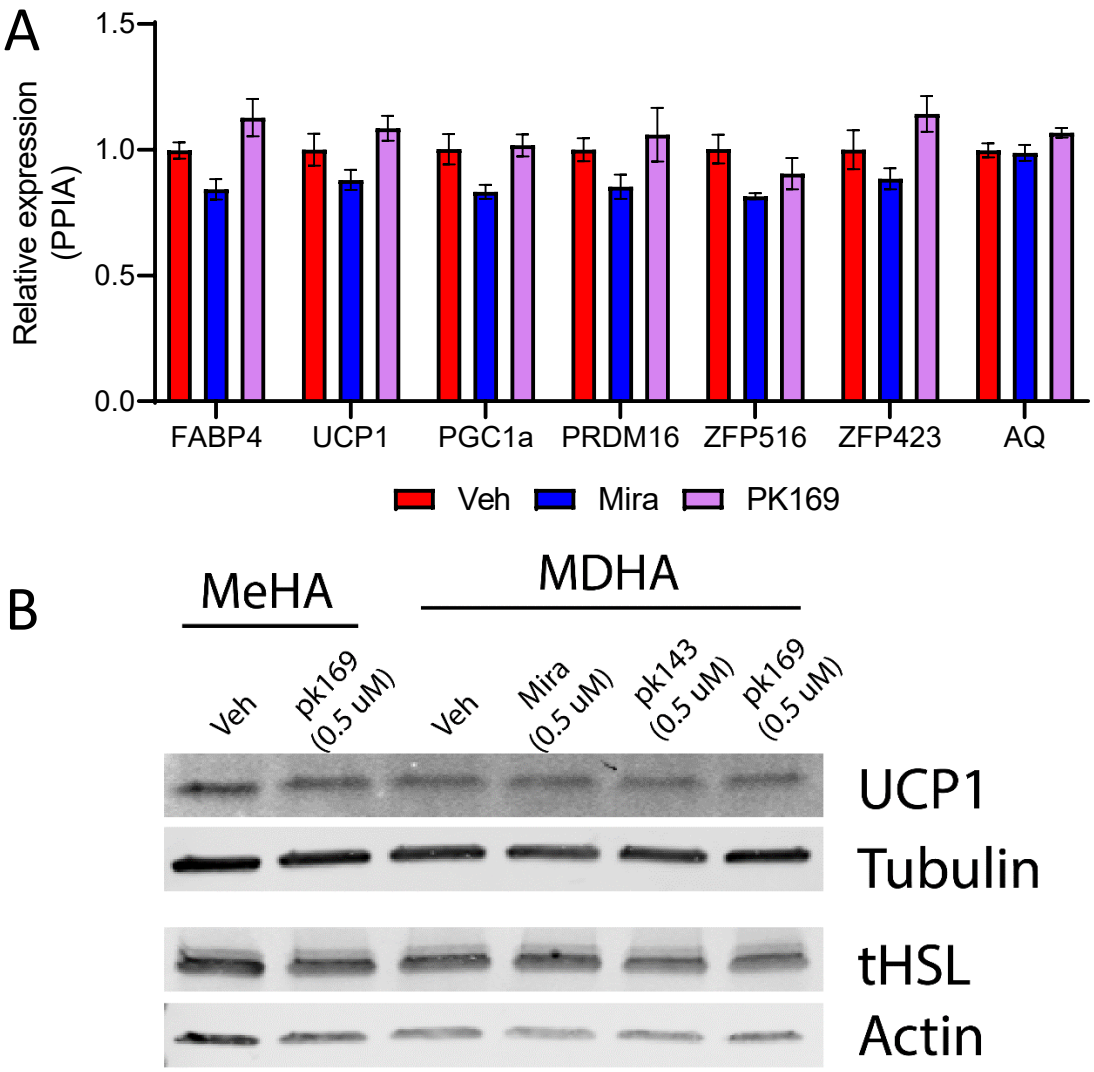

Figure 1-7: Beige adipocytes replated onto AzMira-conjugated MDHA. A) Gene expression of cells re-plated on veh containing, non-modified Mirabegron, and AzMira containing hydrogels. B) Immunoblot of beige adipocytes replated onto AzMira and control gels for 24 hours.

Chapter 2:
Modifying HA-Based Hydrogels for Improved Cell Ingression

Summary

Adipose tissue, in the past, has been the tissue that scientists have gone to as a source of differentiatable stem cells. As such, adipose tissue makes an ideal target for an implantable material that would recruit stem cells and differentiate them toward a desired fate for the benefit of disease amelioration, like beige adipocytes and obesity. Here we describe forays into bettering the recruitment aspects of our hydrogels. First, by using heparin-bound growth factors that are covalently attached to our scaffold and showing the stem cell populations that respond to those signals. Second, we investigate the role of loss modulus as an important material property to determine if modulation of this gel characteristic can improve cell differentiation, physiology, or morphology. Both methods show promise for creating a gel that will better support beige adipogenesis and hopefully provide input for others implementing similar therapeutics.

2.1 - Introduction

2.1.1 – Beige adipose tissue implant modifications for human use

In 2015, our lab published a series of experiments outlining the use of hyaluronic acid as a supportive matrix for the implantation of brown/beige adipocytes, resulting in the whole body increase in metabolic tone and amelioration of some aspects of high fat diet feeding[27]. While the results are promising, the brown adipose tissue matrix assisted transplant (BAT-MACT) is not a feasible product for use in humans due to the use of mesenchymal stem cells isolated from the stromovascular fraction that were then induced to differentiate toward a brown fate *ex vivo*, and subsequently suspended in the HA matrix and then injected into recipients. Therefore, we decided to improve upon the design of the material, making a beige adipose tissue matrix assisted *in situ* forming implant (BAT-MAISI) that would function by first recruiting beige adipocyte precursors, then differentiating those precursors to beige adipocytes, and finally maintaining the activation state of these cells over a long period of time.

Adipose tissue use as a source of stem cells is a common practice for those interested in utilizing a multipotent stem cell population for therapeutic investigations[28]. However, if a model could be introduced to recruit these same stem cells without removal from the body and also stimulate them toward a beige fate, that would remove many of the regulatory hurdles associated with this obesity therapeutic. Adipose tissue already undergoes significant remodeling during obesity and beige adipogenesis, so we propose to take advantage of the very same mechanisms to recruit beige stem cell populations to the implantable material to function as an energy substrate sink. In the following chapter we will focus on two different methods used to modify our hydrogel system to increase ingression into the hydrogels of target cell populations that are most likely to lead to beige adipocytes.

2.1.2 – Adipose tissue immune cell fluctuations during obesity are positive regulators of wound repair

During obesity, many different remodeling mechanisms occur that allows the adipose to first maintain its normal function, that then becomes maladaptive in the long run[29]. Interestingly, many of the same effectors of these early changes are also implicated in the wound healing process[30-32]. These cell populations, therefore, are attractive targets for some of the first responders to be recruited to the novel hydrogel niche.

Early on in obesity, neutrophils ingress into adipose tissue attracted to the site by inflammatory cytokines[33,34]. In addition, in mice given a neutrophil elastase inhibitor or mice with an inactive neutrophil elastase gene insulin resistance and tissue inflammation was ameliorated[35]. They have also been heavily implicated in both positive and negative aspects of wound healing, often leading the charge to sites of host perturbation[30]. Therefore, targeting neutrophil infiltration might be an attractive option for inducing the remodeling response *in vivo*.

Circulating monocytes are also increased in obesity [36]. Classical, intermediate and mature monocytes are all increased in obese individuals. Obese adipocytes secrete monocyte chemoattractant protein-1 (MCP-1) at a much higher level than lean adipocytes, which is the ligand for CCR2, a receptor expressed at high levels on classical monocytes. While expression of CCR2 decreases as a monocyte matures in the circulation normally[37], in obese patients receptor protein levels are still present much longer into maturation which may lead to greater numbers of monocytes ingressing into the adipose tissue and becoming macrophages[38]. However, their role in tissue injury repair is paramount[32], and their ability to enhance vascularization[39], stimulate stem cell pools[40], and provide a guiding role in the reformation of tissue structure[31] could improve the hydrogel niche to be more conducive to beige adipogenesis.

2.1.3 – Beige adipogenesis continued

As stated in Chapter 1, section 1.1.2, increased beige adipocyte number can occur through two different mechanisms. Transdifferentiation of white, or previously beige, adipocytes by increasing mitochondrial and lipid droplet number is one mechanism[41-43], though this process does not generate new adipocytes it may be an important route of action for the long term effects of our implants. Direct differentiation from a stem cell is more relevant to the initial design of the hydrogel system, so the focus of our experiments was mainly on this topic.

Beige adipocytes are inducible thermogenic adipocytes that are stimulated cold or β_3-adrenergic receptor agonists. These cells are *Myf5*$^-$ precursors[44], that arise from the stromovascular faction of adipose tissue and express PDGFRα, SCA1, CD81 and αSMA[3]. In humans, these cell types have been shown to reside in adipose tissue capillary walls and have been shown to differentiate in response to vasculogenic factors[45]. Cells that are capable of differentiation to a beige adipocyte fate are determined early, often prior to their final differentiation[46] due to their unique transcriptional profiles [47] owing to their expression of beige-specific transcription factors like PRDM16[44] and EBF2[48]. Targeting *de novo* beige adipogenesis therefore has a route through vascularization which will bring the ideal stem cell targets from the adipose tissue to the injected hydrogel, offering a proliferative, modifiable, space.

Adipose tissue stem cell residents have also been shown to prefer HA-based hydrogels, increasing proliferation and differentiation in comparison to other common matrices like MatriGel™ and decellularized placental matrix [49]. When autologous HA implants with preadipocytes were injected into the fat tissue of pigs, new vascularization was readily apparent after resection. In addition, islands of adipocytes were observed to have proliferated and differentiated during this time[50]. Taken together adipose tissue and HA-based hydrogels seems like a good match to create an *in situ*-forming beige adipose therapeutic to combat obesity and diabetes.

2.1.4 – Creation of tissue-like hydrogels

Novel biomaterials for tissue engineering are being created and described on a daily basis for therapeutic use. Hydrogels are a common variation and are water-swollen polymer networks that form via the use of crosslinking compounds, usually into a mold, well plate, or even *in vivo*. These hydrogels can be tunable in their physical properties based on the chemistries used, the amount of functionalization attained, and the crosslinkers used to solidify the hydrogel[51]. Often, these hydrogels contain one length of polymer and one length of crosslinker leading to a homogenous material that does not mimic tissue in the slightest, evoking a purely elastic behavior, with very little viscosity[52,53]. Across our formulations of HA-based hydrogels, we noticed this to be the case as well which led us to question if our hydrogels could be improved by altering the haptotactics of the implant, making it more tissue like, and seeing if that change led to more robust vascularization and stem cell ingression.

Tissue stiffness has often been reported in the past as just the elastic modulus[54], or storage modulus, however it has become increasingly evident that the ability to dissipate deformation energy, the loss modulus, can have just as important of a role in cell function[55]. *In vivo*, tissues like brain, liver, spinal cord and fat often have a loss modulus that is 10-20% of their storage modulus [56-59]. Deformation dissipation in these tissues can occur over a period of seconds[60,61] to minutes[62,63], which could be an ideal characteristic for a gel that is geared toward promoting vascularization.

One recent article[55] put a similar idea to the test, using polyacrylamide (PA) to make a crosslinkable version of the gel and then also mixing in a linearize non-crosslinkable at different percentages to produce a loss modulus tunable gel. Using different methods of protein modification on each of the two compartments within the gel they were able to discover that different ECM components preferably signal through each of the compartments, giving an idea of the importance that time-dependent mechanosensing may have on cell behaviors like differentiation, cell spreading and focal adhesion size[64].

Another method to alter the viscoelasticity is to alter the chain length and orientation of polymer used to create the hydrogel[65]. Previous work using different chain lengths of HA found that vascularization occurred best with a 60 or 500kDa HA at 3 wt%, but due to the persistence of the 500kDa HA in the presence of degrading factors like hyaluronidase, there is an argument for longer chain lengths to improve implant residency time[66]. Longer chain lengths of HA will probably be necessary in our implant as well as lower molecular weight HA has been implicated in the development of Type 2 Diabetes[67,19]. As such, modulation of HA molecular weight could also be a viable tissue-like gel permutation to investigate.

By modulating the haptotactics of our implant to become more tissue-like, we hope to be able to foster a niche that will support the site to improve vascularization and eventually beige preadipocyte ingression. In the following section, we show the effects of our endeavors into these modifications.

2.2 - Results

2.2.1 – Base implantable material recruits stems cells and immune cells

In order to determine the baseline effects of our hydrogels to recruit cells, we performed a fluorescently activated cell sorting experiment with the Malofsky lab at UCSF (Figure 2-1A). In this experiment we injected four animals bilaterally near the inguinal adipose depots, one implant containing isolated, and subsequently beige differentiated, SVF (a Matrix Assisted Cell Transplant, BAT-MACT) and the other an acellular hydrogel containing only short adhesion peptides and crosslinker (Matrix assisted *in situ* forming implant, BAT-MAISI). Interestingly, both types of implants showed similar effectiveness at recruiting PDGFRα$^+$ cells as well as dual positive PDGFRα$^+$/Sca1$^+$ cells which have been identified as potential precursors for beige adipocytes[68]. However, with the addition of cells into the implant there is a 2-fold increase in the number of resident CD4$^+$ T-cells, suggesting a general increase in the immune response, though CD8$^+$ cytotoxic T-cell numbers do not increase after 7 days *in vivo* (Figure 2-1B).

Next, we wanted to discover the amount of ingression into the hydrogel of immune cell components from the host. As seen in Figure 2-1C, cell ingression is varied throughout the hydrogel with F4/80$^+$ macrophages being present near the top of the implant close to the adipose tissue border (Orange line, above is adipose tissue, below is implant) and more mature CD11b$^+$ monocytes at the leading edge of the ingressing cell bulk. Upon closer inspection, these cells express Ly6C, a marker of hematopoietic-derived activated monocytes (Figure 2-1D). Finally, we looked at the effects of implant composition on the recruitment of neutrophils, another cell type that has been implicated in the remodeling of adipose tissue during early obesity[34,35] and found that by day 10, neutrophils are one of the furthest cell types ingressing into the hydrogel, potentially laying down ECM as they go to help other cell types following behind.

2.2.2 – Stem cells and vasculature are recruited to the hydrogels

To continue our investigations into the effects of including thiolated heparin-bound growth factors, we added PDGFaa or VEGFa into the gels. Both are potent chemoattractants that will recruit stem cells and vasculature. In Figure 2-2A Top panel we see the results of have a fully functionalized implant on the right (Growth factor and SAPs Ag73+C16) compared to an HA-alone implant on the left. The bottom panel illustrates a gross cross section of the implant where the AcHyA alone is completely transparent all the way through. No cell ingression is apparent using microscopy either, even after 10 days (Figure 2-1E, top right panel).

The implants also exhibit a location dependent morphology. Due to the implant site, near the inguinal adipose tissue, we have a unique look at the effects adipose tissue, skin, and muscle all have on the implant; namely, where are the cells coming from? In all three versions we can see ingression of vasculature (Endomucin, red) as well as DAPI labeled cells mostly on the side of

the implant next to the adipose tissue. No differences were noticed when looking at how far the vasculature had ingressed into the hydrogel across any of the different growth factors. No data was obtained for the VEGFa containing implant near the muscle border.

To determine the effects of implant residency, we placed PDGFaa and VEGFa containing hydrogels near the inguinal adipose depot again and removed them after 1 day and 5 days. While there is a time component to this, more cells have ingressed into the hydrogel after 5 days than one day, no other differences in cell number between the two growth factor types was able to be found. However, when these hydrogels were RNA extracted and gene expression analysis was performed, we can see an almost 1.5-fold increase in CD137 expression in PDGFaa implants and an over 2-fold increase in VEGFa implants suggesting recruitment of potential beige adipocyte precursors in the VEGFa implants.

2.2.3 – PDGFRα$^+$ stem cell ingression into the hydrogels

In another growth factor-based experiment, we looked at the vascularization and stem cell ingression over a 10-day period. To measure both aspects of the implants, we performed cryosectioning of the gels and stained for vasculature (Endomucin, Green) and PDGFRα$^+$ (Red). In any hydrogel containing Ag73 and C16 SAPs we saw a large amount of microvasculature ingression by day 10 regardless of the growth factor included (Figure 2-3A) compared to the AcHyA with heparin alone. PDGFRα$^+$ cell populations also increase over the 10-day period, though again, there was no noticeable difference between the different formulations.

To better quantify the presence of certain cell types, we took portions of the injected hydrogels from the above experiment and extracted RNA. By Day 10 all formulations of implant had significant increase of PDGFRα$^+$ gene expression. The highest expression levels were unsurprisingly the gel containing the PDGFRα ligand, PDGFaa, follow by VEGFa. Beige adipocyte precursors genes TMEM26 (Bottom) and CD137 (Middle) were also up by day 10 in the PDGFaa containing hydrogel, suggesting this might be the best way for in the future when considering which growth factors to use in our BAT-MAISI.

2.2.4 – Modifying HA Molecular weight to induce better cell physiology and behavior

Our next goal was to improve the haptotactic attributes of the hydrogels to improve movement and ingression. Various molecular weight HAs were modified to allow for Michael addition-based click reactions. First, we wanted to make sure the different HAs were tunable in their stiffness in order to achieve an adipose tissue-like storage modulus of around 1kPa (Figure 2-4A). All gels were able to be tuned to this level by modulating the concentration of the crosslinker, an MMP13 sensitive peptide, where 1x is the concentration published in Tharp *et al.* 2015. These gels were then used to perform various metabolic assays using hMSC from an n=8 pooled sample of female liposuction aspirants. Cells differentiated on top of the hydrogels for 14 days showed no changes in gene expression relative to TCPS controls (Figure 2-4B). To verify that the gene expression translated to protein levels we performed a western blot on n=3 pooled samples of cells differentiated toward a white or beige fate (Figure 2-4C). No alterations in UCP1 or Leptin protein levels were observed. Finally, we tested out the lipolytic and insulin sensitivity capabilities of the cells by stimulating them with isoproterenol followed by a full media change

into media with isoproterenol and insulin (Figure 2-4D). HA MW did not play a role in any significant changes in the stimulation of glycerol release with 2μM isoproterenol or in the inhibition of the lipolytic signal through the addition of Insulin. All of these data suggest that HA MW does not play a role in adipocyte differentiation.

2.2.5 – Addition of longer unmodified HA increases loss modulus and changes gel morphology

Another haptotactic change we introduced into the hydrogels was based off of a publication that added in a "linearized" or unmodified version of their base hydrogel, with the result of an increased loss modulus that approached the storage:loss modulus ratio that stiffer tissue often have[55]. Applying the same ideas to our gel we attempted to recreate this material phenomenon. In Figure 2-5A we crosslinked a 60kDa MeHA hydrogel with varying amounts of 60 kDa non-modified HA which resulted in no increases in loss modulus and also decreased the storage modulus at the same time. Substituting the molecular weight of the HA with a 500 kDa of each resulted in a slight increase in loss modulus (G") initially, but no further increase with increasing unmodified HA (Figure 2-5B). Next, we combined a 60kDa MeHA with different amounts of non-modified 500kDa HA. A 3 wt% alone MeHA gel obtained a storage modulus of 547 Pa with a loss of 26, resulting in a 5% loss modulus to storage percent. Increasing the non-modified HA up to an equal amount, 3 wt% in addition to the 3 wt% of the MeHA, result in a gel with 40% loss to storage, where the storage modulus was the same as the 3 wt% MeHA alone (Figure 2-5C). To increase the storage modulus(G') to a more adipose tissue like amount, we increased the amount of MeHA to 4 wt%, resulting in a G' of 1299 Pa and G" of 83. When an equal amount of non-modified 500 kDa HA was added we were able to achieve a G" of almost 74% of the G', a supraphysiological amount (Figure 2-5D). These gels with increased loss moduli are referred to as iGDP gels (increased G" gels).

We next wanted to compare the hydrogel morphology of three select gels from panel D. Porosity was imaged using a SEM (Figure 2-5E Left panels), at two magnifications showing the difference in the pore size between the 4:0, 4:2, and 4:4 gels. Pore area was quantified using FIJI (n=100) (Figure 2-5E, right panels) where the media 4:0 pore size was 825μm, 4:2 was 18.3, and 4:4 was 6.8. The minimum and maximum numbers were also drastically decreased as more unmodified 500kDa HA was added to the gel. All of this shows the importance of using various chain length polymers to create a hydrogel that has a dynamic G", the generation of which decreases the pore size of the gels drastically and may allow faster migration through the gel as a result.

2.2.6 – Gene expression of adipocytes on iGDP gels

To determine the effects of the iGDP gels on adipocyte differentiation, we plated sWAT cells at confluence overnight and differentiated them the next morning using a beige differentiation medium. After 8 days of differentiation, gene expression was analyzed using qPCR (Figure 2-6A). No significant difference was seen between cells grown on 4:2 or 4:4 gels in comparison to 4:0, though trending significance are evident in PGC1α, a mitochondrial biogenesis transcription cofactor, and Myoz3, a calcineurin-interacting protein that helps tether calcineurin to the sarcomere of skeletal muscle along with α-actinin.

We also wanted to test how differentiated cells respond to the iGDP gel. To accomplish this, we differentiated the cells for 7 days in a 10cm tissue culture plate and then replated at confluence on the hydrogels. Gene expression of UCP1 and CTGF, a gene that is transcribed when YAP is functional in the nucleus, trended down when plated on the 4:0 MeHA, but then seemed to increase with 4:2 and 4:4 (Figure 2-6B). This gene expression trend was more apparent in the isoproterenol-stimulated cells (Figure 2-6C) where CTGF, but not UCP1 is down in the gels plated on the gel pad. CYR61, another gene transcribed when YAP is active and has been implicated in cell proliferation and cell adhesion[69], is significantly upregulated in the 4:2 and 4:4 gels in comparison to the 4:0 gel as are adiponectin and FABP4 suggesting a positive role being played by the iGDP gels in cells going from a stiff substrate to a more tissue-like one.

We next wanted to test if this change in substrate viscoelasticity would affect a physiological outcome like lipolysis[70]. sWAT cells were replated as outlined above and then stimulated with 1μM isoproterenol for 6 hours. Media was then sampled, and free glycerol was measured. No alterations in lipolytic ability were observed across the iGDP gel formulations (Figure 2-6D).

2.2.7 – Adipocyte stability on iGDP gels is increased

One noticeable difference in the iGDP hydrogels was their ability to keep cells from lifting off during differentiation. As seen in Figure 2-7A, cells remained in a confluent arrangement in TCPS after 8 days of beige differentiation but lifted off the hydrogel in the 4:0 formulation. The 4:2 and 4:4 formulations allowed the cells to adhere better over the course of differentiation, though not to the same degree as the TCPS only well.

To determine if there were any differences in focal adhesion protein expression at the end of differentiation, cell wells were lysed in ice-cold RIPA buffer with protease and phosphatase inhibitors and pooled before immunoblotting for various proteins of interest (Figure 2-7B). Isoproterenol was able to reliable stimulate UCP1 and HSL protein increases, showing the cells can respond to these stimuli. Total YAP levels do not decrease, though phosphorylation at ser127 does decrease suggesting YAP cytosolic localization should increase, effectively decreasing its transcriptional activity. Vinculin levels also seem to be increased in the 4:2 formulation over both 4:0 and 4:4 where FAK does not significantly change in a reliable manner (Figure 2-7C).

2.2.8 – iGDP gels have different YAP localization patterns in preadipocytes

Based on the CTGF gene expression and phosphorylated YAP protein expression data, we wanted to determine if YAP localization was indeed altered. Preadipocytes were plated sparsely overnight and allowed to adhere to the various tissue culture or iGDP hydrogel substrates. They were then fixed and immunostained with YAP and Tomm20 antibodies (Figure 2-8A). We used the Tomm20 signal to localize the YAP cytoplasmic average intensity and DAPI for the nuclear intensity to obtain a nucleus to cytoplasm intensity ratio (Figure 2-8B). YAP localization was indeed altered across the iGDP gels in a manner that replicated the gene expression data for the 4:0 and 4:4 gels, though not for the 4:2.

2.2.9 – Cell spreading and focal adhesions of preadipocytes on iGDP gels

Because of the YAP localization differences, we decided to look at cell spreading and focal adhesion formation in the preadipocytes plated on the different iGDP gels. Cells were stained with Phalloidin, an f-actin stain (red), and DAPI. In addition, we fluorescently labeled Vinculin, an integral protein for focal adhesion formation (Figure 2-9A). F-Actin was then used to determine the overall cell area (Figure 2-9B), where a significant decrease in cell area was observed in the 4:2 iGDP gel only in this experiment.

2.2.10 – Preadipocyte migration on iGDP hydrogels is increased

Lastly, due to the alterations in cell spreading and YAP localization, we decided to test the ability of preadipocytes to migrate on the surface of iGDP hydrogels. Cells were sparsely plated and stained with Hoescht for one hour before washing and imaging overnight on an inverted confocal microscope (Figure 2-10A). There was no difference observed between cells on TCPS vs. the 4:0 MeHA gel. However, there was a significant increase in cell distance traveled in the 4:2 and a trending significance in the 4:4 gels. Suggesting that the elasticity and viscosity of the gel play an interconnected role in how quickly the cells can move on the substrate as the 4:2 gels also have a much higher elastic modulus in addition to the more tissue like loss modulus.

2.3 - Discussion

In this chapter, we have shown the ability of different MeHA-based hydrogels to promote the recruitment or change the behavior of cells depending on a handful of different changes to the hydrogel recipe. HA is already an ideal medium for creating a hydrogel to work with adipose tissue[71]. HA-based therapeutics within adipose tissue in the past have shown that our HA base for the implant would more than likely be beneficial[72]. In this study they used non-functionalized HA nanoparticles injected into epididymal WAT and noticed that the injected WAT have less macrophages as a result, possibly due to the nanoparticles competing with Low molecular weight HA-CD44 interactions. Our HA hydrogels are biologically degradable through two mechanisms; hyaluronidase as well as MMP13. Both methods of degradation are present in adipose tissue suggesting our implants may play a similar role as they break down over time.

Initial investigations into the ability of our MACT vs MAISI implants were surprising as the experiments used to optimize them as a cell transplant scaffold had been centered around inducing UCP1 expression and increasing lipid uptake[27]. The BAT-MACT saw a trending increase in $PDFGR\alpha^+/SCA1^+$ cells during the seven days the implants were *in vivo*. This might be due to the increased energy substrate demand in these implants, potentially resulting in the recruitment of greater neovascularization and therefore recruitment of these beige adipocyte precursors. Additionally, $CD4^+$ T-helper cells were decreased in the BAT-MAISI, though $CD8^+$ Cytotoxic T-cells showed no difference in number, suggesting that the host immune system is at the very least recognizing the non-self cells within the MACT (Figure 2-1A,B). Both of these are promising questions to answer to better understand potential methods that could be used to better form the beige synthetic tissue.

Addition of growth factors PDGFaa and VEGFa bound to a thiolated heparin that was conjugated to the HA backbone both induced robust recruitment of PDFGRα^{+} cells within the implant after 10 days. As the HA breaks down, these growth factors can get released and then spread to the general area and induce recruitment of their respective cell types. Unsurprisingly, PDGFaa recruited these cells at a much higher rate, increase the fold expression level changes in PDGFRα immensely while in VEGFa-containing implants there was only a modest increase (Figure 2-3B). CD137 and TMEM26, purported beige preadipocyte markers[73], gene expression were only up in the PDGFaa implants. While we cannot answer if all of the cells within the PDGFaa-bound HA are all beige preadipocyte precursors, we can say that the vascularization apparent in both should carry the cells that we are targeting along with them. It will be interesting to see if a mix of growth factors is better for beige adipocyte precursor recruitment.

Of the two recipe modification we performed aimed at improving the tissue-like feel of the hydrogels, various HA MW or mixing in non-modified HA, it turns out both were needed in order to obtain a gel that had a dynamically modifiable loss modulus. Changing the molecular weight and titrating in different concentrations of crosslinker altered primarily the storage modulus at the weight percents we reconstituted the gels at with no relative change in loss modulus across those crosslinker concentrations (Figure 2-4). However, adding non-modified HA at a longer chain length, 500kDa added to a crosslinkable 60kDa, seemed to not only increase the storage modulus, but also increase the loss modulus at the same time up to a final ratio of close to 74% of the storage modulus (Figure 2-5D). This change in loss modulus is accompanied by an alteration in the bulk structure of the hydrogels, increasing the overall porosity (Figure 2-5E,F) which might lead to better ingression mechanics over the lifetime of the hydrogel *in vivo*.

Unfortunately, on our various loss modulus hydrogels, we found no improvement of differentiation or proliferation over TCPS controls. However, replating the cells on to the gels overnight resulted in significant alterations in gene profile, specifically tension related genes, in a trend that was not related to elastic modulus, suggesting that genes like CTGF and CYR61 can be controlled through loss modulus alone (Figure 2-6B, C). When looking at YAP protein specifically, phosphorylation at residue ser127 was decreased suggesting a decrease in YAP nuclear localization and therefore transcriptional activity (Figure 2-7 B, C). Interestingly, while total HSL is increased when plated on our hydrogels phospho-HSL ser563, and indicator of increased activity due to AMPK phosphorylation, levels decreased suggesting an impair of lipolysis on the hydrogels. Unfortunately, this was not able to be verified with a physiological test due to our gel's cross-reactivity with our free glycerol testing reagent leading to false increases in signal.

Upon further investigation we found that YAP localization is indeed altered on our hydrogels, though not in a loss modulus-specific manner. Compared to TCPS, cells plated on our 4:0 and 4:4 gels showed a decreased localization of YAP. Both of these gels have the same storage modulus, but drastically different loss moduli. Our 4:2 gels have an increased storage modulus to accompany an increased loss modulus. The loss modulus is almost 3-fold higher than the 4:0 gels and equates to roughly 14.5% of the storage modulus. As reported previously, having an increased loss modulus allows better traction on the hydrogels and therefore more robust transmission of the storage modulus [74]. This could also conceivably lead to the stabilization of the cells as they differentiate on the hydrogels as seen in Figure 2-7A.

When we attempted a closer look at the size and shape of the focal adhesions, vinculin unfortunately was not able to be measured quantitatively due to issues in the labeling, creating an excessive number of artifacts, as well as the decreased transparency resulting from the 4:2 and 4:4 iGDP formulations. However we were able to verify that cell area is indeed decreased on the 4:2 gels based on the f-Actin staining, suggesting a increased YAP/low cell area phenotype that may be representative of a motor/clutch model of mechanosensation by the cells on the hydrogel [75,76].

Finally, we found that our iGDP hydrogels were capable of increasing the median and average distance traveled by preadipocytes compared to both TCPS and the 4:0 gel. The 4:2 iGDP gel on average significantly increased the distance traveled by a preadipocyte by 60μm, with a trending increase in the 4:4 gel. This potentially suggests that there is a fine-tuned ratio of storage to loss modulus required for optimum migration characteristics of preadipocytes and that a loss to storage modulus percent greater than the 6.4% seen in the 4:0 gel is ideal. Further titration of the hydrogel's loss modulus characteristic would be required to find that tipping point.

In this chapter we have shown that adipose tissue is a rich resource for stem cells and immune cells that are usually targeted for therapeutic purposes in the bioengineering field. With the addition of heparin-bound growth factors we can improve the ingression of stem cells and vasculature that carry the mural and preadipocyte precursors necessary for the BAT-MAISI development. We have also shown that ingression could conceivably be improved by tuning the hydrogels haptotactic traits, increasing the loss modulus, and making the synthetic tissue behave in a more tissue-like way. In all we have made strides at improving cell ingression and movement on this modified HA substrate in ways that will hopefully be useful for others to build upon.

2.4 – Figures

Figure 2-1

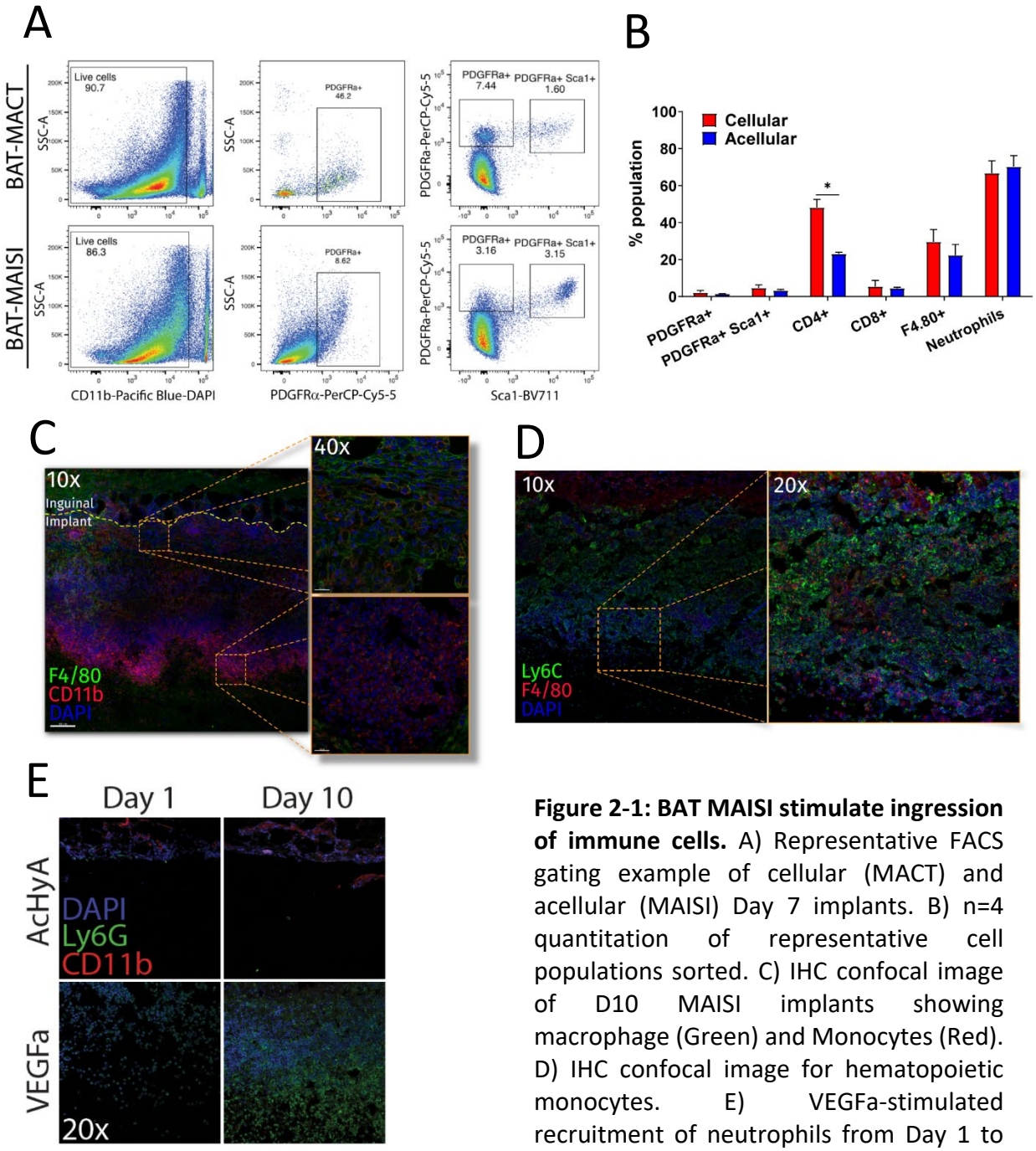

Figure 2-1: BAT MAISI stimulate ingression of immune cells. A) Representative FACS gating example of cellular (MACT) and acellular (MAISI) Day 7 implants. B) n=4 quantitation of representative cell populations sorted. C) IHC confocal image of D10 MAISI implants showing macrophage (Green) and Monocytes (Red). D) IHC confocal image for hematopoietic monocytes. E) VEGFa-stimulated recruitment of neutrophils from Day 1 to Day 10 of implant.

Figure 2-2

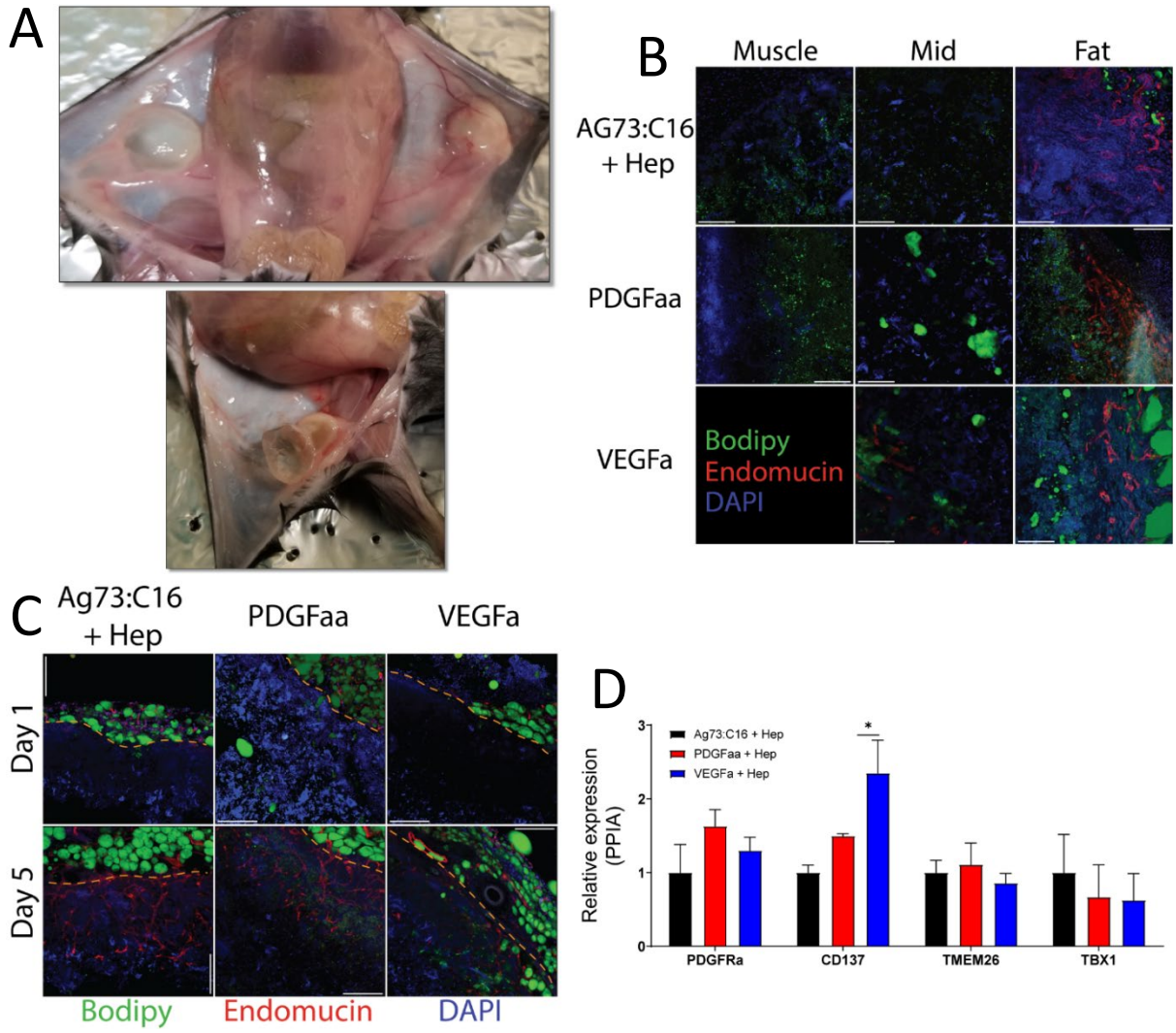

Figure 2-2: Recruitment of stem cells and vasculature are signal and placement dependent. A) Representative pictures of non-functionalized (Left) vs functionalized with Ag73/C16 and heparin bound VEGFa (Right). B) Localization of cell and vasculature ingression in functionalized implants based on implant composition. C) Growth factors improve cell and vasculature ingression. D) Gene expression analysis of Day 5 implants containing PDGFaa or VEGFa bound to heparin.

Figure 2-3

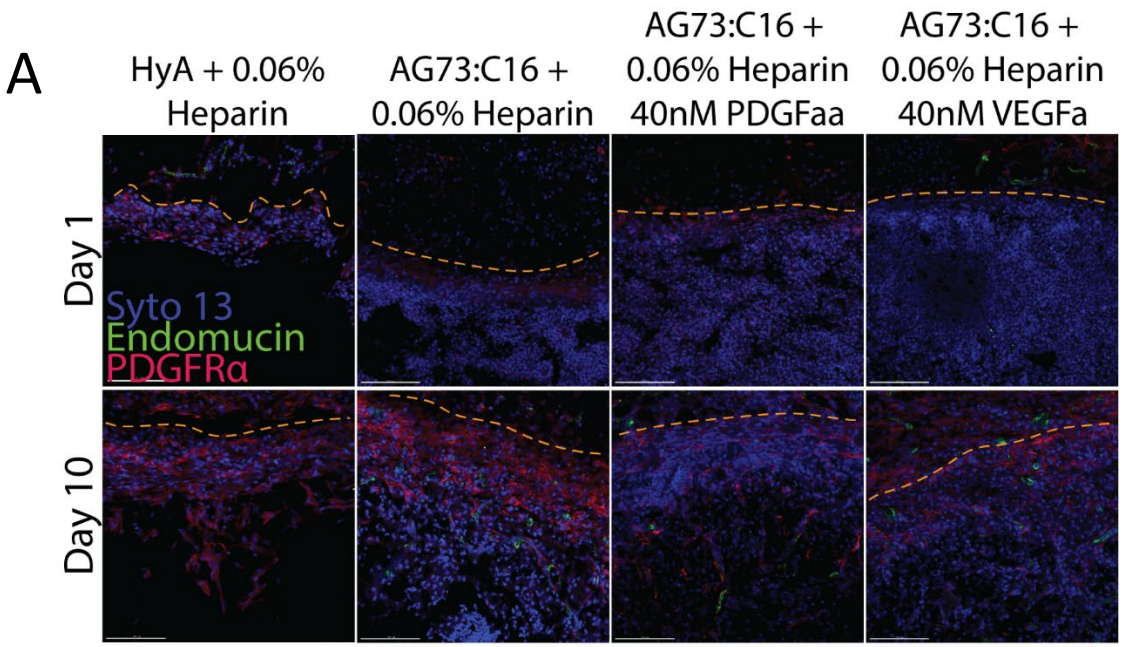

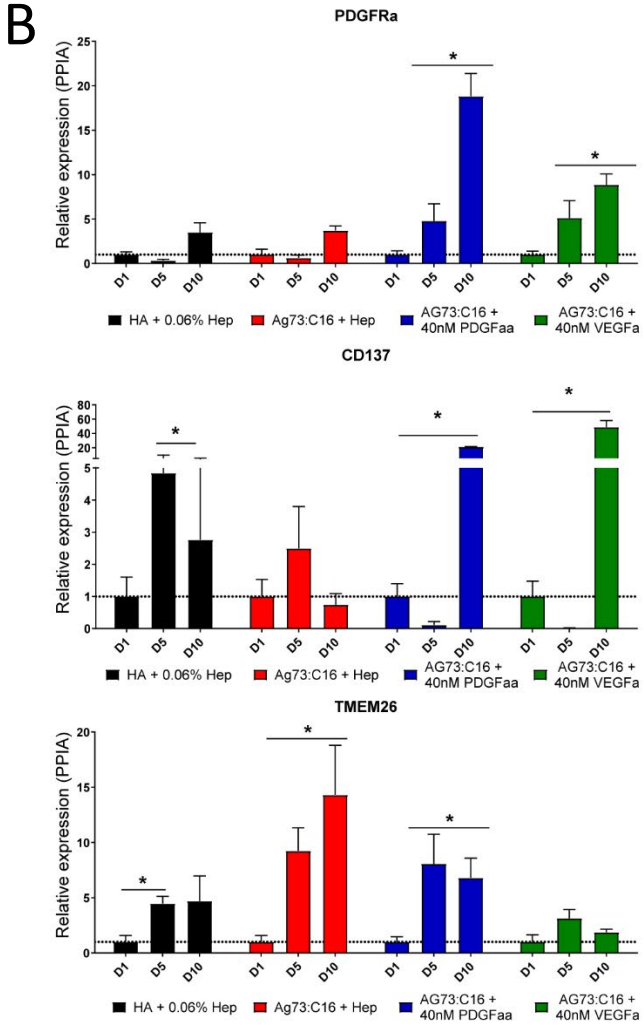

Figure 2-3: Stem cell recruitment can be tailored by growth factor type. A) IHC confocal images for stem cells (Red) and microvasculature (Green). B) Gene expression analysis of the different implants over 1, 5 and 10 days within the animal comparing their respective abilities to target appropriate cells types.

Figure 2-4

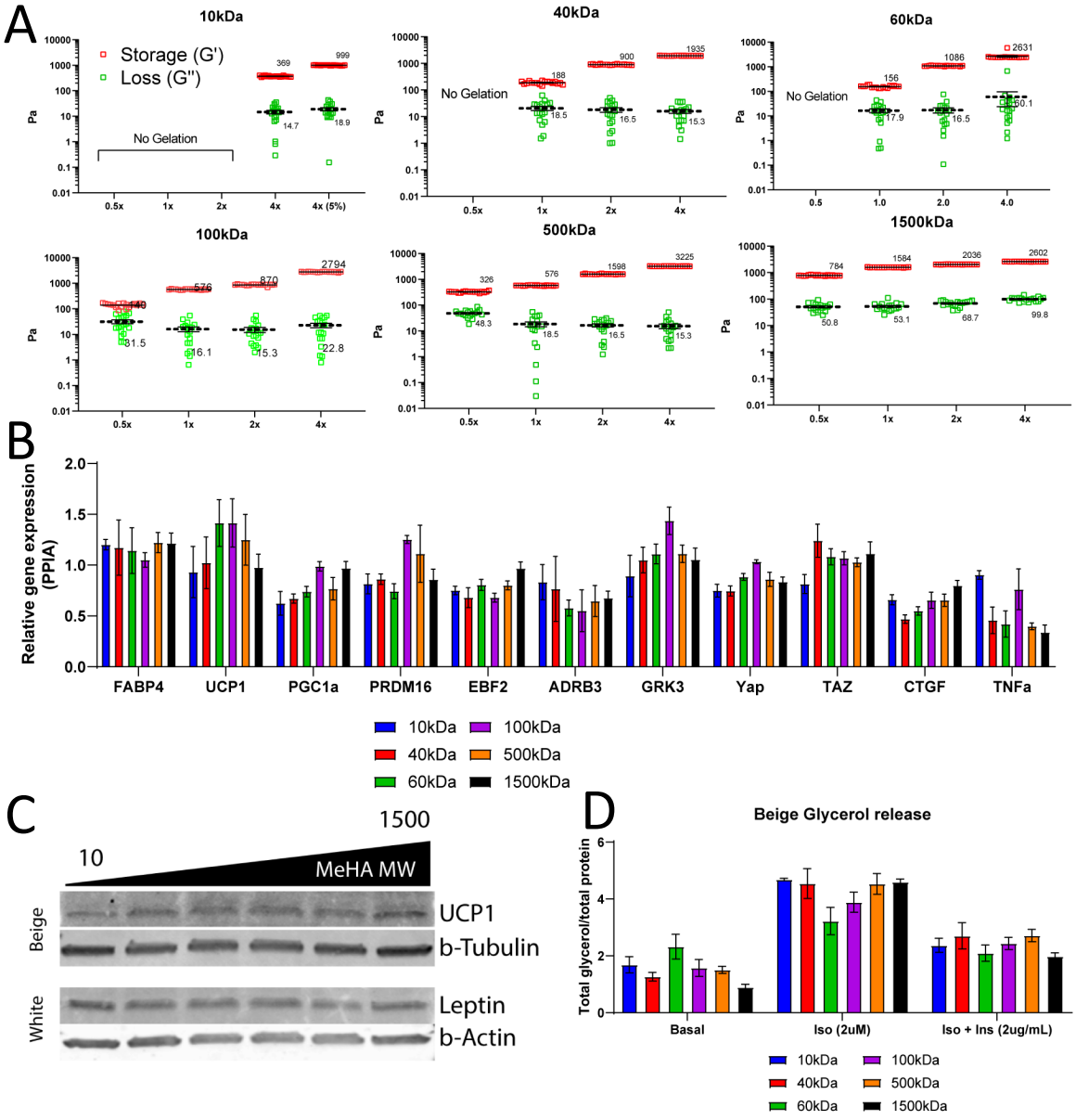

Figure 2-4: HA molecular weight varied hydrogels are elastically tunable. A) Parallel plate rheometry on MeHA hydrogels with differing concentrations of crosslinker. B) Gene expression of hMSCs differentiated on the hydrogels for 14 days. C) Western blot of 3x pooled samples from day 14 differentiated hMSCs and increasing in HA molecular weight from left to right. D) Glycerol release from Day 14 differentiated cell upon 2µM isoproterenol stimulation for 6 hours and then Insulin stimulation for 6 hours.

Figure 2-5

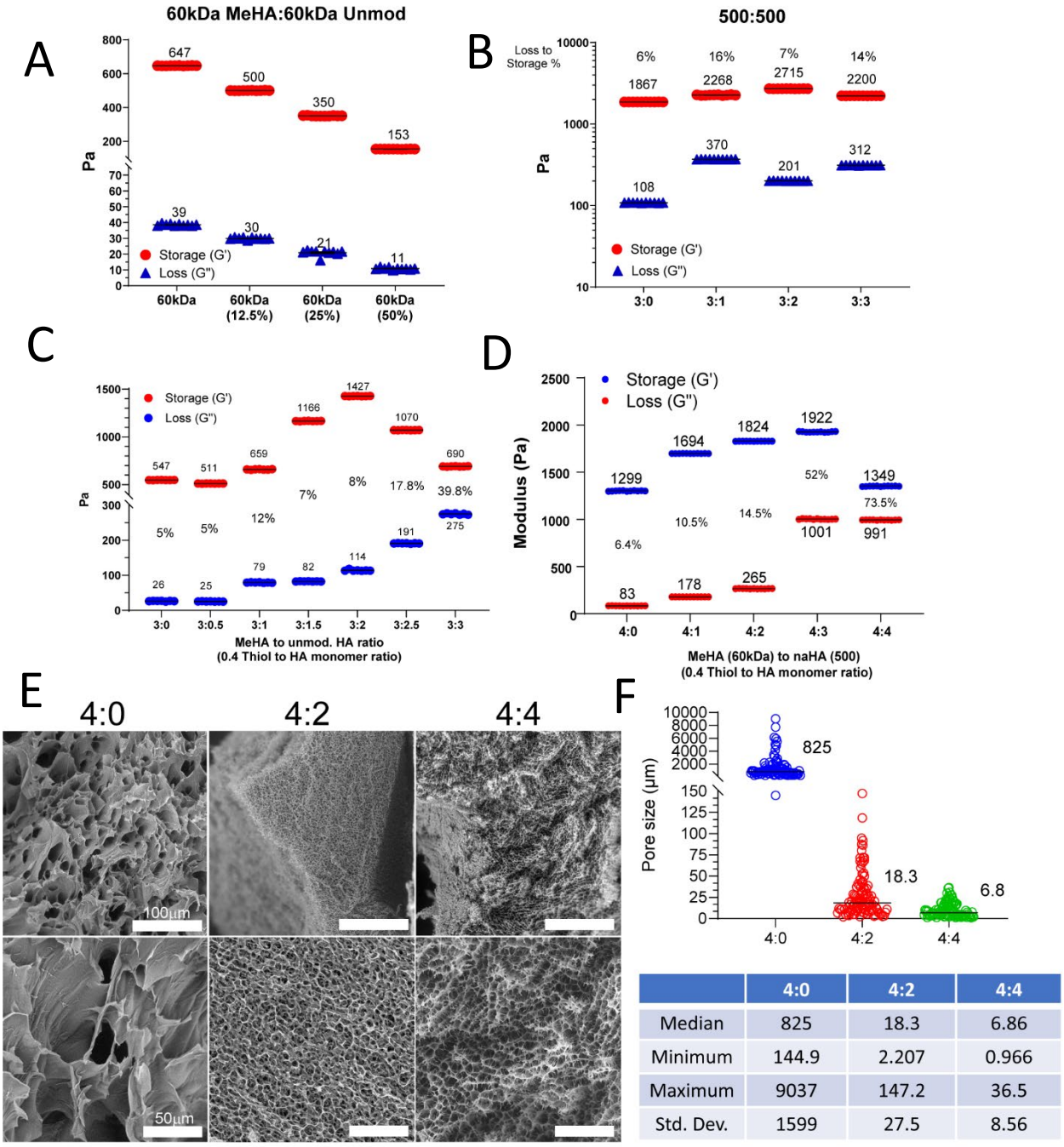

	4:0	4:2	4:4
Median	825	18.3	6.86
Minimum	144.9	2.207	0.966
Maximum	9037	147.2	36.5
Std. Dev.	1599	27.5	8.56

Figure 2-5: Mixing of modified and non-modified HA results in highly viscoelastic gels. A) 60kDa MeHA with varying concentrations of unmodified 60 kDa HA. B) 500kDa MeHA with varying ratios of unmodified 500kDa HA. C, D) 60kDa MeHA with varying ratios of unmodified 500kDa HA. E) SEM images of hydrogels listed in D, illustrating pore size. F) Pore sizes from each of the different hydrogels, bars are the median size. n=100.

Figure 2-6

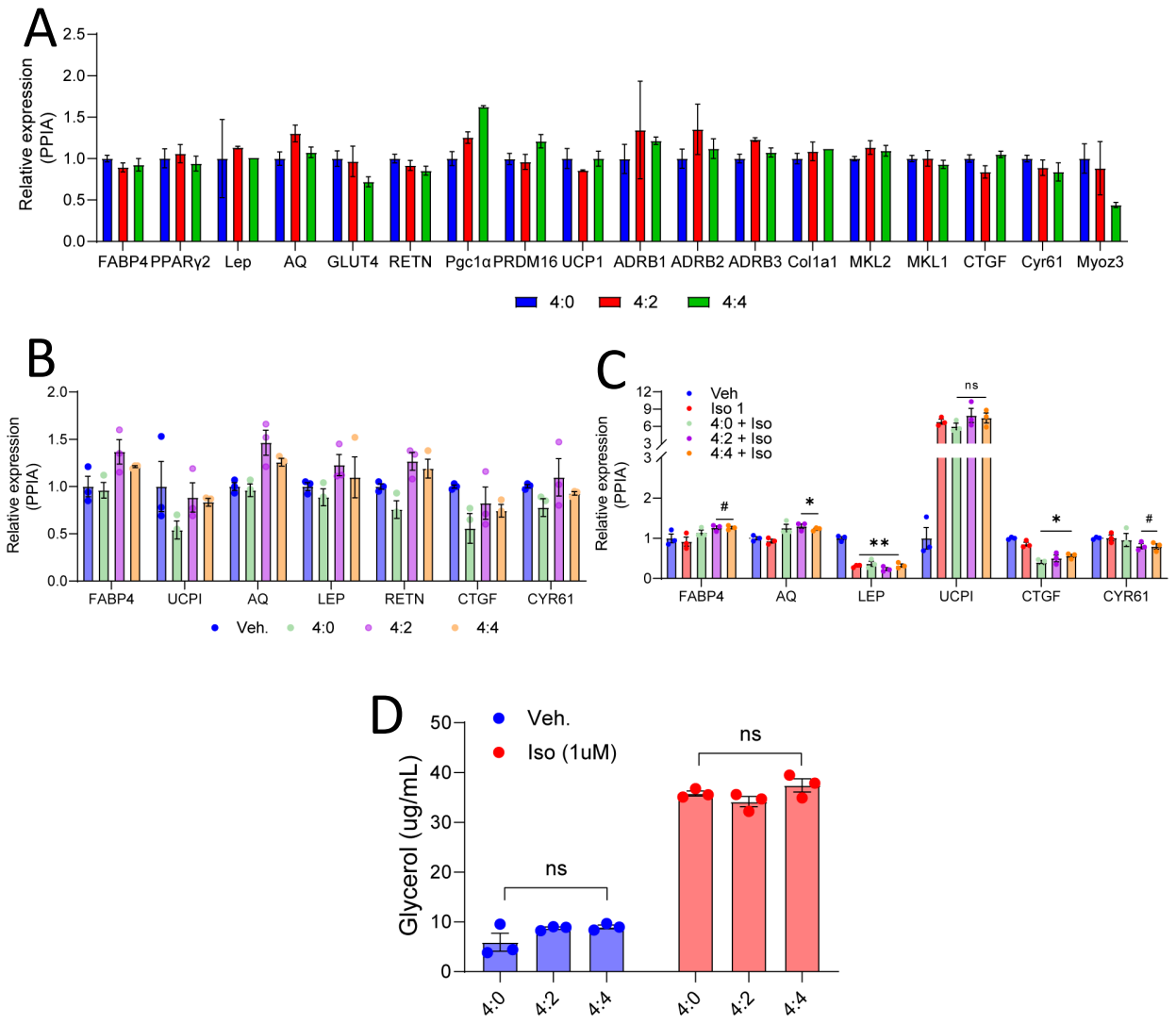

Figure 2-6: iGDP gels do not change differentiation outcome but do alter gene expression if re-plated. A) Gene expression of sWAT cells differentiated towards a beige fate for 8 days on the three different hydrogels. B) Gene expression of cells differentiated for 7 days with beige differentiation media, then replated on iGDP gels. C) Same cells as B, but with isoproterenol stimulation. D) Lipolysis stimulation of cells replated on iGDP gels, same as B and C.

Figure 2-7

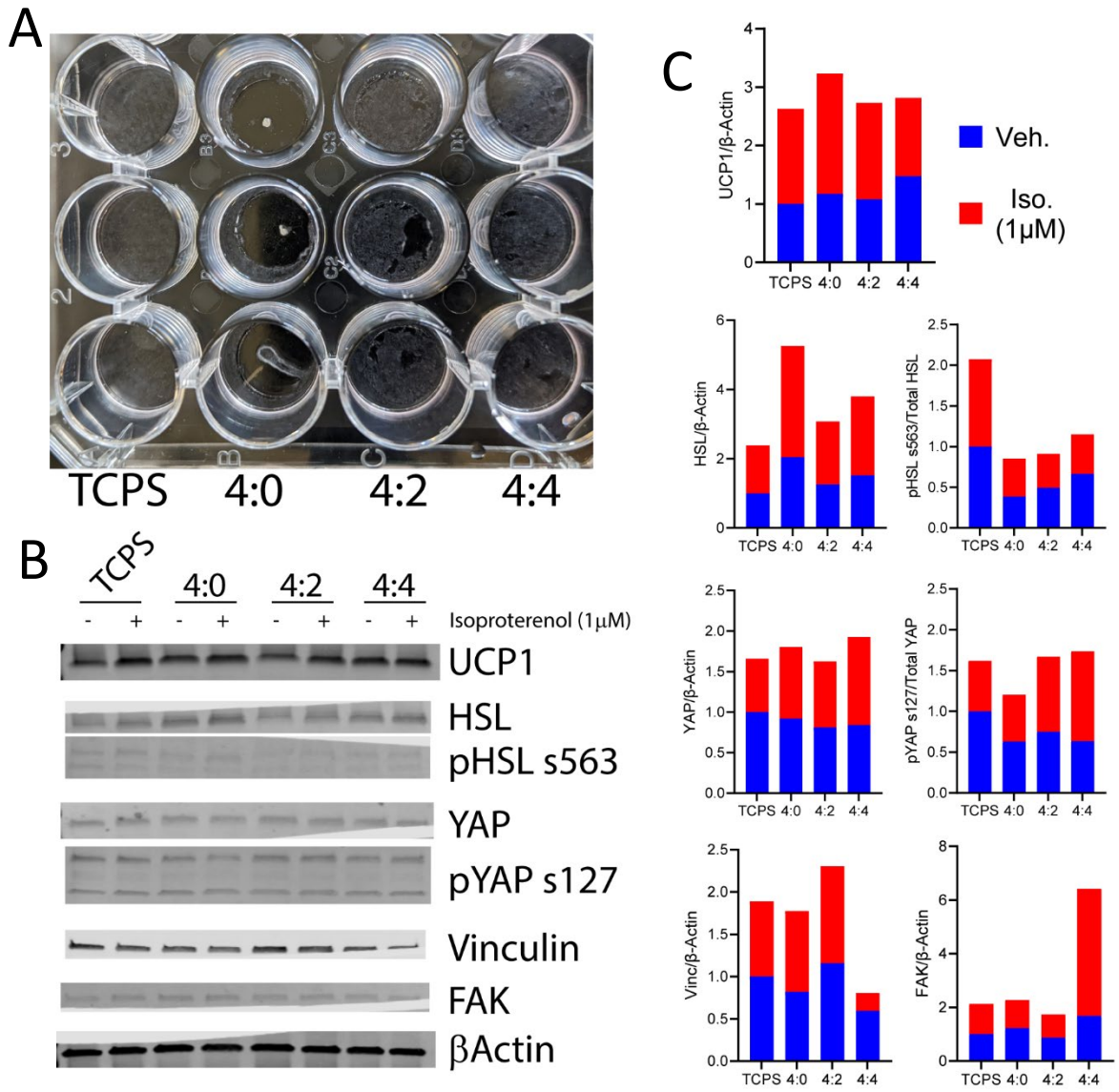

Figure 2-7: Preadipocytes are more stable on iGDP gels. A) Beige differentiated sWAT cells after 8 days of differentiation. B) Western blot of the cells in A, with and without 6 hours of isoproterenol stimulation. N=3 pooled samples for each lane. C) Band quantitation of western blots in B.

Figure 2-8

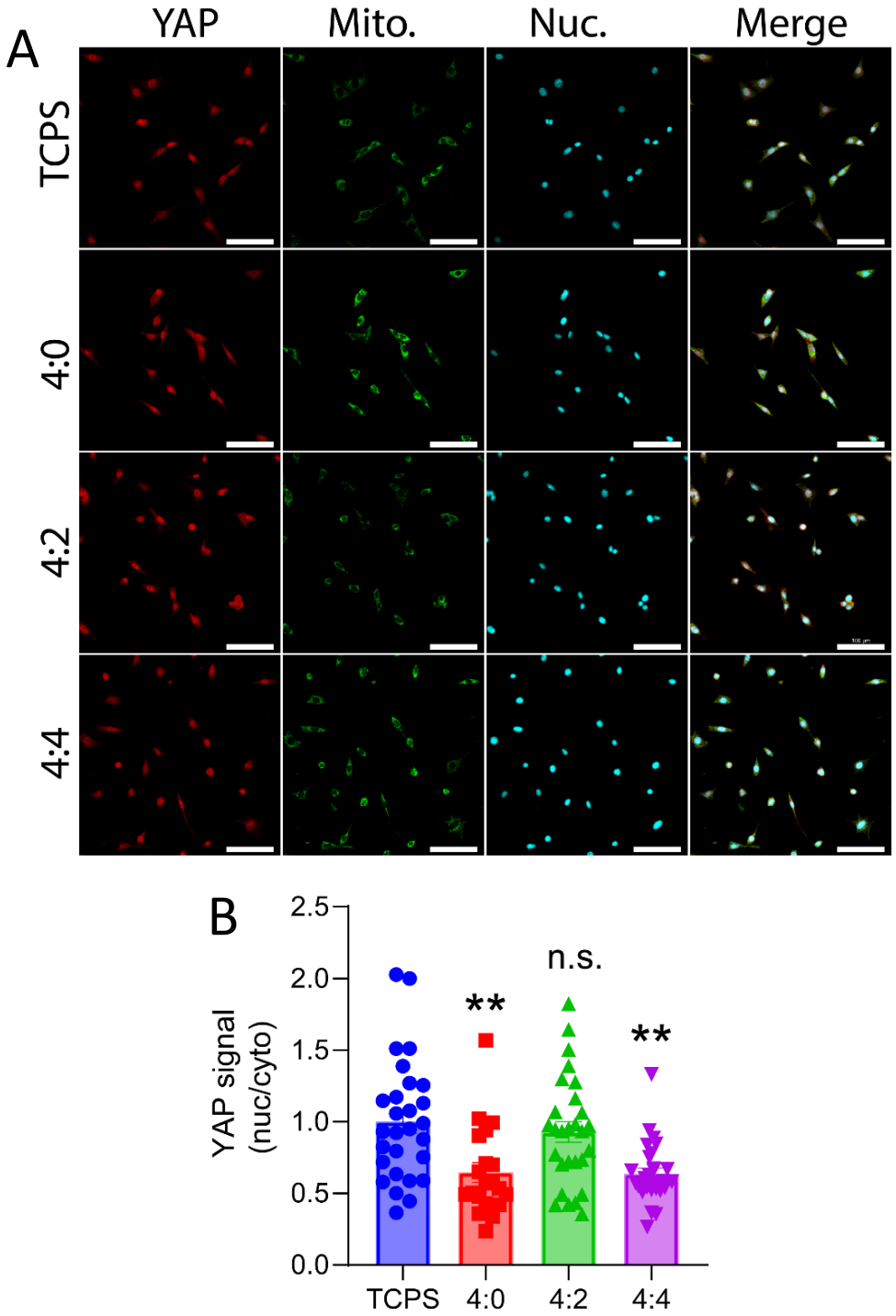

Figure 2-8: Preadipocyte YAP localization is dependent on storage modulus. A) ICC of undifferentiated sWAT cells plated overnight on iGDP gels. B) YAP intensity was calculated using the nuclei signal or mito signal to localize and calculate the signal. Normalized to TCPS.

Figure 2-9

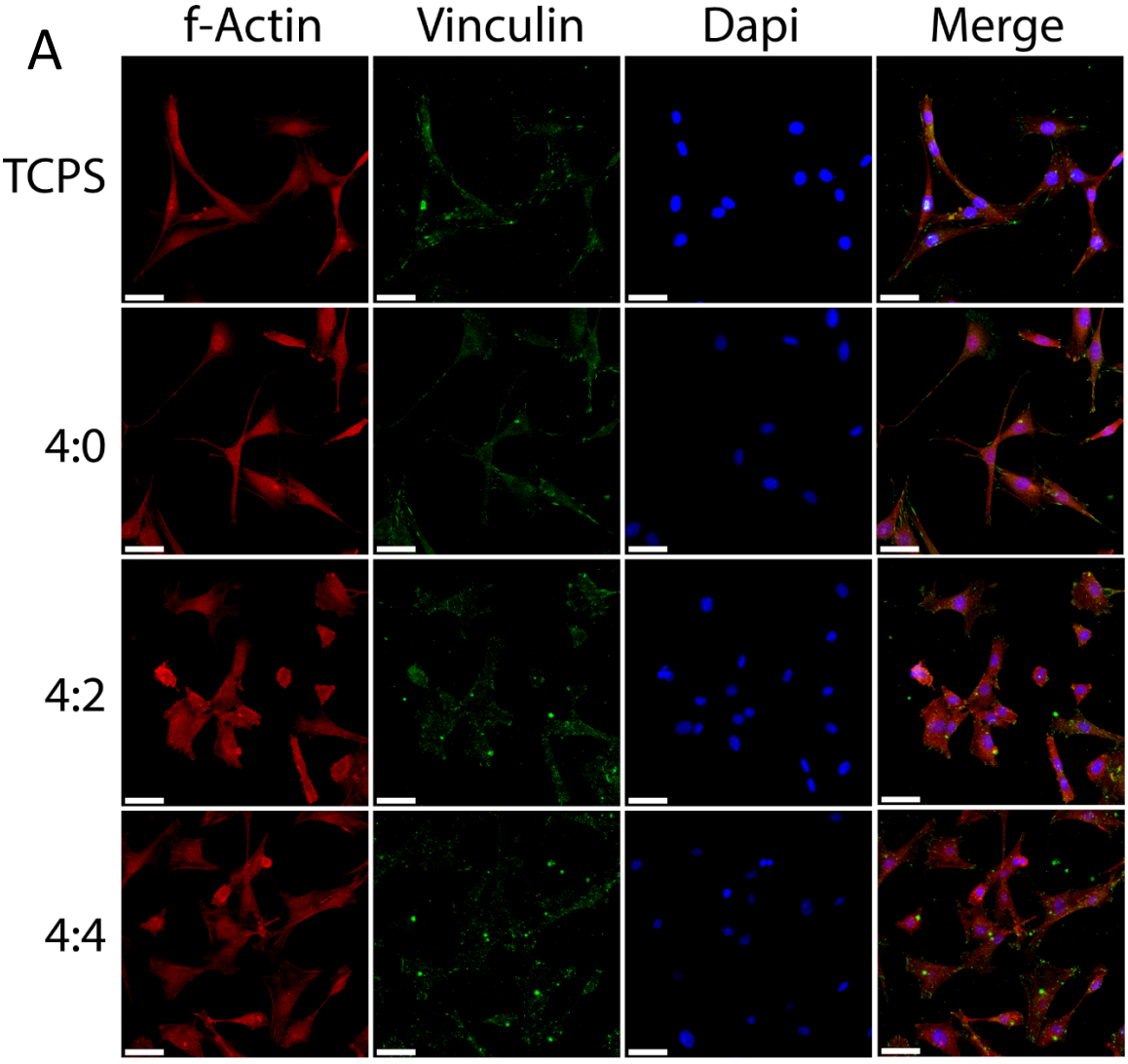

Figure 2-9: Preadipocyte cell morphology is determine by stiffness and loss modulus. A) ICC of undifferentiated sWAT cells stained for focal adhesions and cytoskeleton. B) Cell area quantitation based off of f-Actin signal. n≥30.

Figure 2-10

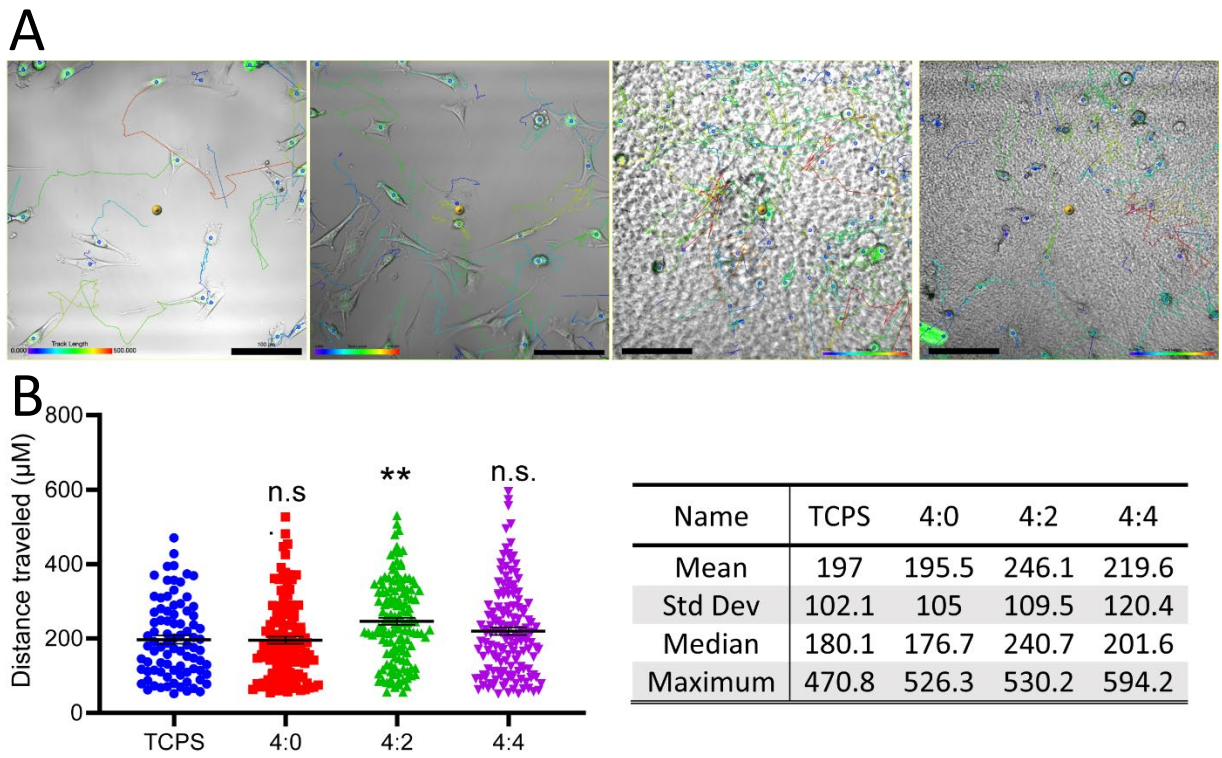

Name	TCPS	4:0	4:2	4:4
Mean	197	195.5	246.1	219.6
Std Dev	102.1	105	109.5	120.4
Median	180.1	176.7	240.7	201.6
Maximum	470.8	526.3	530.2	594.2

Figure 2-10: Undifferentiated preadipocytes migrate faster on iGDP gels. Undifferentiated sWAT cells were plated onto iGDP hydrogels, stained weakly with Hoescht, and then imaged overnight every 15 minutes. A) Representative images of cell tracking on each of the different hydrogels. (Left to right: TCPS, 4:0, 4:2, 4:4). B) Quantitation of length of tracks over 8 hours of imaging.

Chapter 3:
Adipose Tissue-like Microphysiological Device for the Investigation of Insulin Resistance

Summary

Insulin resistance is a common early metabolic dysfunction that occurs in adipocytes that have been subjected to chronic energy substrate excess. This results from aberrant differentiation of mature adipocytes as well as localized inflammation resulting from a positive feedback loop with M1 polarized macrophages. Here we describe a system that is modeled around the pluripotency of iPSCs to create adipocytes and macrophages, all from the same donor and within an adipocyte-tailored 3D microenvironment, to investigate the role PPARγ plays in human adipocyte differentiation as well as the effects of co-culture with M1 macrophages and the resulting insulin resistance they induce. Finally, we show that these insulin resistance models are in fact druggable using clinically relevant methods, illustrating the feasibility of the MPS as a model system for drug screening on a patient-by-patient basis.

3.1 – Introduction

3.1.1 Obesity is a worldwide epidemic

Obesity is a worldwide epidemic with many, varied, health defects that can wreak havoc on a person's healthy life span. Diseases that emerge from this chronic caloric excess like diabetes[77,78], cardiovascular disease[79], fatty liver disease and cirrhosis[80], and ultimately cancer are on the rise as a result. Diet and exercise are often the clinical recommended method for getting back to a healthy weight, but novel methods might be required to better understand and combat the epidemic from a patient specific level. However, it is expensive and difficult to do experiments in at the patient level due to their highly heterogeneous genetic nature, so generalizing drug effectiveness from one person to the next is challenging at best and deadly at worst. To meet this need head on, we have developed a metabolically relevant platform that allows for the physiological testing of two types of human cells from a single donor in order to illustrate the power this type of investigation can have on elucidating biology from a patient-specific perspective.

3.1.2 – WAT is an important regulator of metabolism

White adipose tissue plays a central role in whole body energy homeostasis, and its dysfunction can lead to a myriad of health complications. It was not long ago that this dynamic and broadly acting metabolic organ was only seen as a place for excess energy storage. We now know these disparate depots not only act to influence food intake, energy substrate utilization, insulin signaling and immune function[2], but also in depot specific ways like thermogenesis[3]. As such, adipose tissue health and overall physiology can behave like a "canary in the coal mine," acting as the first warning sign of excessive chronic energy intake.

Dysregulation of these interconnected functions during the obese state illustrates the importance of adipose tissue health. However, examining the role adipose tissue plays in an

individual's health is problematic due to the difficulty of performing clinical assays on humans, even in the face of persistent health threats, that studies in mice cannot resolve due to their metabolic differences[81]. New methods to better understand the function of adipose tissue from a single patient in emergent disease states would be ideal to push back the rate of obesity, give better clinical-like data sets as induced pluripotent cell technology is easily accessible by most labs, and allow the targeted testing of cell-cell behaviors in adipose tissue.

3.1.3 – WAT sequesters excess energy for later

Adipocytes are integral to the clearance and sequestration of excess energy metabolites. This is especially true after a large meal when energy substrate is abundant. After being taken up in the small intestines, glucose is taken up from circulating blood through insulin signaling which results in translocation of GLUT4 to the plasma membrane. Glucose is then phosphorylated by glucokinase, which prevents it from moving back across the plasma membrane effectively trapping it there. After proceeding through glycolysis, pyruvate is formed which then enters the mitochondria and is converted to acetyl-CoA to enter the Krebs cycle. If mitochondrial citrate concentrations are high as a result of glycolysis outpacing the Krebs cycle, citrate can be pumped from the mitochondria to the cytosol again where ATP-citrate lyase and acyl CoA carboxylase (ACC)[82,83] can drive the fixation of these excess carbons into lipid species with other companion proteins like Fatty Acid Synthase (FASN)[84] which is the end step of De Novo Lipogenesis (DNL).

Alternatively, lipids can be removed from circulating chylomicrons (postprandial) or Very Low-Density Lipoproteins (VLDL) (Fed state) after being hydrolyzed from triacylglycerol and added directly to the adipocytes themselves through cell membrane proteins like Lipoprotein Lipase[85] and CD36 respectively.[86] Regardless of how the fatty acid gets into the cell, either through DNL or fatty acid uptake, these lipid species need to be re-esterified back into triacylglycerol before being capable of entering a lipid droplet for storage.

3.1.4 – WAT is dynamically regulated during early obesity

WAT is highly dynamic when faced with excessive caloric intake, increasing its size and body proportions over long periods of time. Tissue mass can be increased through two mechanisms, the first is hypertrophy (increased cell size), the second is hyperplasia (increased cell number). In humans, cell number seems to be the primary determinant of overall WAT mass which is set in childhood, and maintained into adulthood[87]. In mice, and assumingly in humans, Males and females on an obesogenic diet exhibit different levels of each of these types of expansion, often in a depot-specific manner[88].

Visceral WAT depots showcase the ability of certain WAT to increase in size through hypertrophy[89] as well as hyperplasia[90] with an increase in the amount of supporting vasculature to ensure proper oxygen saturation[88] and precursor cell populations. These pericyte populations actively proliferate during the first week of high fat diet, and often express ZFP423 and PDGFRβ[90]. Inguinal adipose tissue, or subcutaneous adipose tissue, on the other hand illustrates the sexual dimorphic aspect of WAT. In male mice, this depot enlarges primarily due to hypertrophy on any diet. In females it is similar to visceral adipose tissue with a mix of both[91].

While hyperplasia within the first week of an obesogenic diet is common, hypertrophy is also a key part of maintaining a healthy adipose tissue. In lean patients, adipocyte hypertrophy is associated with greater insulin sensitivity [92] at the start of a high fat diet. However, a size limit exists for adipocytes, roughly around 100μm, that once bypassed results in a conversion to an unhealthy physiology thought to revolve around the diffusion distance of oxygen resulting in a hypoxic environment[93]. This new environmental stress induces the expression of transcription factor Hif1α, leading to the expression of pro-fibrotic genes in adipose tissues[94] as well as decreases in healthy adipocyte indicators like adiponectin[95]. This can continue until adipocyte apoptosis begins, which usually induces an inflammatory response that triggers the recruitment of macrophages[96] and other immune cells to start cleaning up the dead and dying adipocytes. Many of these cells, once they arrive on site, begin secreting factors that limit nutrient uptake in the surviving adipocytes giving way to the beginnings of insulin resistance in the tissue[97].

3.1.5 - Insulin resistance is driven by adipocyte dysfunction

Insulin resistance is an obesity-driven metabolic dysregulation that affects WAT, liver, and skeletal muscle primarily, and results in a decreased response to insulin signaling. This change affects glucose uptake[98-100] and fatty acid uptake[101,102], and are the methods through which we commonly diagnose and describe the disease due to dedicated proteins like GLUT4 and FATP1 undergoing trafficking to the plasma membrane, but there are noticeable changes to how adipocytes function intercellularly as well[103]. Interestingly, lipolysis is also increases in insulin resistant adipose tissue and is potentially a more reliable method for the quantitation of insulin resistance in adipocytes[104-106]. As such, it is now generally viewed as the best indicator for measuring insulin resistance in humans[107]. Through the use of a multistep pancreatic clamp technique it is possible to calculate the adipose tissue insulin resistance index which measures plasma levels of fasting insulin and free fatty acids[108] which determines the IC50 (50% lipolysis suppression) of insulin action[109-111]. This excess secretion of lipids, on top of the increased uptake in fatty acids normally seen in a western diet, leads to ectopic lipid deposition in other tissue which can then lead to further insulin resistance[103]. While Insulin-Clamp studies can lead to better understanding of and individual's adipocytes and their current insulin sensitive state, a more cost effective and efficient study should be investigated to test more human samples, in a higher throughput mechanism.

3.1.6 – human Induced Pluripotent Stem Cells for the investigation of adipocyte insulin resistance

iPSCs are cells that have been reprogrammed from their terminal cell fate to one that resembles pluripotency. This is performed through the introduction of four transcription factors, dubbed Yamanaka factors, OCT4, SOX2, KLF4 and MYC[112]. Over the past 15 years this technology has driven a significant portion of our understanding of human cell-autonomous biology, and promises advances in human disease modelling, drug discovery and stem cell-based therapies [113]. Many cell types have thus far been differentiated[114], including adipocytes[115,116]. The benefits of iPSC models lie in their ability to be made from any tissue, from any person, creating a patient-specific model that is able to assayed *in vitro*, allowing for the modeling of the origins and development of diseases from a purely human perspective[114,116,117]. This makes the use of these

cells all the more intriguing in an insulin resistance model, especially when paired with a high throughput testing method.

3.1.7 – Microphysiological devices are a powerful *in vitro* drug screening tool

Standard tissue culture techniques require the plating of millions of cells in relatively large formats with even larger volumes of nutrient and growth factor-containing media. As such, these studies in these architectures often require large amounts of space and reagents. This process is usually one of the first steps in screening clinical compounds for use in humans, a step that can take up to a decade, cost millions of dollars, and 95% of the time result in failure[118]. It is no wonder that these formats do not replicate once tested in humans as they are semistatic environments that lack the 3D tissue microenvironment[119]. Current generation microphysiological devices are geared toward solving these *in vitro* deficiencies to better replicate human cell physiology *in vitro* and push back against the high failure rate currently seen in drug discovery[120].

Combining these different methods in the face of a challenging, inter-organ, disease like insulin resistance is an ideal space to make scientific progress to better understand the disease and treat the various negative clinical outcomes that compound the obesity. It is our goal to test an adipose tissue-based microphysiological device that accurately models insulin resistance through drug-based mechanisms, as well as cell influenced mechanisms like those seen in early macrophage infiltration into hypertrophically expanded WAT during the obese state.

3.2 – Results

3.2.1 - Generation of the iPSC line

WTC11 iPSCs were first differentiated to a mesenchymal cell (hMSC) fate following the kit-based method from Stem Cell technologies. These cells were verified as being similar to mesenchymal in origin by comparing them readily available hMSC stocks from ZenBio (Catalog#: SP-F-SL, Lot#: SL0060 and 0064, pooled donors with BMI 25.0-29.99) by flow cytometry for positive expression of CD73, 90, and 105 with concomitant negative expression of CD45.[121] After validation of hMSC lineage, a doxycycline inducible PPARγ construct was transduced into the cells to help drive differentiation as previous attempts at differentiation with our normally used differentiation cocktail had failed.

Due to the inducible nature of PPARγ in the iPSC-MSCs, and since a PPARγ agonist was used in the differentiation cocktail, a rosiglitazone titration was performed. As seen in Figure 3-1a, the dose of rosiglitazone had a dose dependent increase on all adipogenic genes measured. This is in addition to the increases in glucose uptake in both 100 and 1000nM groups as in Figure 3-1b, but not fatty acid uptake (Figure 3-1c). In this assay we can see a pronounced increase only at 10 and 100nM, illustrating the bimodal effectiveness of rosiglitazone use during differentiation on insulin sensitivity. iPSC-MSCs differentiated in this fashion are also capable of performing lipolysis at a high level upon Isoproterenol stimulation (Figure 3-1d) as measured by glycerol released into the media that can be decreased almost back to baseline with insulin treatment, demonstrating the insulin sensitivity of these cells.

3.2.2 - Validation of the iPSC line and how it performs relative to other cells

Next, we compared the adipocyte differentiated iPSC-MSC line to other available pre and post differentiated cells. Notably PPARγ gene expression was almost 20-fold higher in the iPSC-MSC line after 14 days of differentiation, illustrating the effects of the dox-inducible construct within the line (Figure 3-2a). However, other canonical differentiation markers like FABP4, HSL, and LPL showed little to no change in this cell line in comparison to commercially differentiated adipocytes or even hMSCs that were differentiated here in our lab. RNA from human adipocytes from biopsies did exhibit a much higher HSL signature, and lower UCP1 signature illustrating that the iPSC-MSC line has some room for differentiation optimization.

In addition, the lipolytic capabilities of the iPSC-MSC cells were the highest of the *in vitro* cells we tested, exhibiting an almost 2-fold higher glycerol release with 1µM isoproterenol than commercially differentiated stocks that was able to return to basal levels of secretion with 500nM insulin added to the media (Figure 3-2b). This is in contrast to the glucose uptake experiments however, as the same dose of insulin was over twice as effective at inducing the iPSC-MSCs to remove glucose from the media compared to the commercial cells but not as effective as the hMSC primary cells (Figure 3-2c). These data show that the iPSC-MSCs represents most reliable *in vitro* tissue culture compatible cell in our hands and are more able to reproduce human adipocyte physiology than other available methods.

3.2.3 – Cell viability in the MPS

To accomplish our goal of a small form-factor adipocyte-containing device, we used common photolithographic methods to produce a two-chambered system separated by and isoporous membrane. As seen in Figure 3-3a, the top channel circulates medium while the bottom channel contains the cell wells that hold the adipocytes. Pre-differentiated adipocytes are loaded into the MPS first along with a supportive matrix that is hyaluronic acid-based, MMP degradable, hydrogel containing a short adhesion peptide. Because adipocyte differentiation is dependent on cell-cell contact, and since a supporting matrix was being used, cell number titration experiments were required to ensure optimally differentiated cells. In Figure 3-3b we loaded the notated numbers of cells into the MPS and observed their morphology after six days in the MPS with differentiation media flowing. 8×10^7 cells seemed optimal to allow for the most robust differentiation and was used going forward. After 30 days, the cells were stained using a Live/Dead assay from Thermofisher that stains the cell membrane of live cells with Calcein AM, a dye that is visible upon esterase activity, and dead cells with ethidium homodimer, a nuclear dye that is present in dead cells. There was no notable difference in the number of dead cells in the iPSC-MSC cells in comparison to comparably differentiated hMSCs (Figure 3-3b). When compared to cells differentiated only in a well plate format, iPSC-MSC viability is drastically increased (Figure 3-3d) when place in the 3D environment within the MPS showing an optimal niche for these cells to behave in a physiological manner.

3.2.4 – iADIPO-MPS Physiological Assay Validation

To determine if this system is viable as an alternative to standard tissue culture techniques, as well as judge the overall potential effectiveness as a patient-specific drug screening platform, MPS loaded with day 14 differentiated were assayed with common metabolic tests. Figure 3-4a and b illustrate the lipid droplet development, cytoskeleton, and nuclei of these adipocytes, and show how the overall structure of these pseudotissues form after 14 days. Analyzing these images, we can see that lipid droplet size increases in cells cultured in the MPS compared to tissue culture well plates (Figure 3-4c). Locularity, or the number of lipid droplets per cell, shows a concomitant decrease as well supporting the idea that these adipocytes are achieving a whiter adipocyte-like phenotype. Cells cultured in the MPS also show similar levels of glycerol release upon administration of isoproterenol, which is inhibited upon insulin administration (Figure 3-4d). Similarly, glucose uptake (Figure 3-4e) and fatty acid uptake (Figure 3-4f) are both increased upon insulin stimulation. Taken together these data suggest that the iADIPO-MPS model is a valid one that accurately reproduces, at the very least, a tissue-culture phenotype.

3.2.5 – iADIPO-MPS can be drug treated to manipulate adipocyte physiological function

Final testing of the iADIPO-MPS was performed to see if common diabetic treatment methods from the clinic could be employed to influence the performance of the cells in chip. Two different methods of compound administration can be used to assay the 4-way final chips. The first, illustrated in figure 3-5a, shows a parallel dosing where media is circulated through each set of 8 wells in one MPS which then goes immediately on to the next in line. This sequential dosing might be a possible way to determine adipocyte/drug sequestration ability. For our experiments, the dosing in Figure 3-5b was used. One module of a 4-way chip was tested with metformin, and insulin sensitizer, hydrocortisone, a glucocorticoid receptor agonist that forces development of insulin resistance over time, and finally atorvastatin, and HMG-CoA reductase inhibitor with previously reported insulin resistance phenotypes. As expected, three-day pre-treatment with metformin increased the cell's sensitivity to insulin illustrated by the increased fatty acid uptake rates as well as total uptake amounts (Figure 3-5c, d). The reverse was seen in hydrocortisone and atorvastatin, both of which potently inhibited the insulin stimulated uptake of fatty acids (Figure 3-5c, d). These data illustrate the drug discovery possibilities the iADIPO-MPS provides, showing cells cultured in this method as physiologically tunable and drug responsive creating a novel method to test a single patient's responsiveness to a battery of common drugs.

3.2.6 - Isogeneic Coculture of Different Cell Types to Model Cell Interactions

The iADIPO-MPS can also be modified to assay cell-cell interactions. In Figure 3-6a and b we illustrate a method to include macrophages in the MPS by first loading pre-differentiated adipocytes into the cell chambers, allowing them to condense over a period of 10 days, washing out the adipocytes forming in the cell loading channel and back-filling with pre-differentiated and pre-activated macrophages from the same iPSC source as the adipocytes. The ratio of iMACs:iADIPOs was tuned to 1:5-1:10 based on our preliminary effectiveness tests and the

reported physiological ratios of both cell types in human WAT[122,123]Macrophages were then given time to ingress into the iADIPO cell mass and influence their function. Figure 3-6 c and d show this movement over a period of 12 hours, where the blue stained iMACs are around the periphery of the iADIPO cell mass in the MPS well at 30 minutes post loading but have ingressed fully into the iADIPO by 12 hours. This can be seen in greater detail with confocal imaging which more cells around the periphery and bottom of the cell well (Figure 3-6e, f) at 6 hours compared to 12 hours. After three days within the chip, we can see macrophages surrounding adipocytes forming canonical crown-like structures that have been so well described in the literature (Figure 3-6 g, h).

3.2.7 - Bimodal Modeling of Unhealthy Adipose Tissue in MA-MPS

To better understand the iMAC and iADIPO cell interaction within the MPS (MA-MPS), we developed an age as well as an obese model. Figure 3-7a illustrates BODIPY stained iADIPOs with blue nuclear stained iMACs in a standard (Day 14) differentiated MPS well. The 74-day aged samples seen in panel b show drastically increased lipid droplet size (Figure 3-7e), while the obese model wells that were preloaded with 0.5mM palmitic acid during differentiation show a very similar distribution of lipid droplet size (Figure 3-7c). Figure 3-4d shows a confocal image of CLS in the obese phenotype wells as well as iMACs that seem to present with a foam cell-like morphology (arrows). CLS are quantified with obese iADIPOs having over two-fold more than control wells, and 50% more than the aged wells (Figure 3-7f).

In addition, these MPS are functional for long periods of time. Figure 3-9a shows cell viability at 1 month, and 6 months (Figure 3-9b). In comparison to 1 month in tissue culture, the MPS-based culture method seems ideal to move for with. These results show the feasibility of age-related and obesity-related modeling of the MA-MPS system.

3.2.8 - Altering Macrophage Polarity alters MA-MPS Physiological Responses

Next, we tested the effectiveness of altering the polarity of the iMACs in the MPS to directly test if the role being played by them replicates what has been published in the past, namely do M1 polarized macrophages induce insulin resistance? iMACs were polarized to an M1 fate before pre-loading with 10ng/mL LPS and 20 ng/mL IFNg for one day. This method of iMAC differentiation has previously been shown to result in M2 polarized cells[124], so those were used for an M2-like comparison. As seen in Figure 3.2.9a-c, M1 coculture but not M2 coculture resulted in MPS that did not respond to insulin presentation as fatty acid uptake, glucose uptake, and glycerol release were all at or below baseline levels. Using western blots, these cells were co-cultured in tissue culture plates to look at insulin signaling pathways. In Figure 3.2.9d phospho-AKT ser473 levels are induced in no co-culture and M2 wells but are decreased to almost baseline levels in M1 wells. To further supplement this phenotype, we looked at JNK activation states (Figure 3.2.9e). The phosphorylation of JNK at p46 and p46+p54 was significantly increased in iADIPOs after M1 macrophage coculture compared to no coculture conditions. These data show a very similar outcome to the well reported behavior of M1 macrophages in adipose tissue, inducing inflammation as well as promoting a prediabetic phenotype, and created a suitable model to study the effects of inflammation and insulin resistance.

3.2.9 - Co-culture alters transcriptional changes in both populations

In order to better understand the pericrine effects the two cell types had on one another, a transwell co-culture was setup, after which cells were prepared for RNAseq analysis. Using the Database for Annotation, Visualization, and Integrated Discovery (DAVID), genes from the cluster with the highest enrichment score, and with a FDR < 0.05, were reviewed. As shown in Figure 3-10a, iADIPOs cocultured with M1 macrophages significantly upregulated genes associated with immune/inflammatory responses, interactions with intracellular space cells, and chemotaxis cytokines. Interestingly, the most enriched pathways measured were all chemokine related (Figure 3-10b). Others include TNFα signaling (11-fold) and extracellular matrix remodeling (3.6-fold), all of which suggest that the adipocytes in culture with M1 macrophages are secreting signals to attract other immune cells, inducing angiogenesis[125], and altering the ECM.

While the transcriptional changes measured in M1 macrophages as a result of co-culture with the iADIPOs was less pronounced, noticeable changes to cytokine/cytokine receptor interactions and inflammatory immune responses were the top GO enrichment categories (Figure 3 -10c,d).

Figure 10e is a direct measurement of cytokines in media collected from these co-culture experiments. Baseline measurements were made in monoculture, illustrating the proinflammatory role that M1 macrophages play in their secretion of chemokines like TNFα, IL6, and IL1β. iADIPOs secreted few cytokines and quite a few known adipokines. Co-culture of the two cell types resulted in the production of many known cytokines illustrating the effectiveness of the co-culture method at inducing an inflammatory state in the MA-MPS.

3.2.10 - Secreted chemokines alone enough to alter iADIPO function

To verify the previous data of the transwell co-culture, iADIPOs were differentiated in a 96-well plate and treated for 3 days with TNFα, IL4, and IL1b before measuring their adipocyte physiology. TNFα and IL6 treatment decreased the fatty acid uptake of cells where IL4 and IL1b showed similar behavior to controls with insulin treatment (Figure 3-11a). However, only TNFα decreased the effectiveness of insulin stimulated glucose uptake as well as sensitivity to isoproterenol (Figure 3-11b,c). To determine if TNFα was the sole contributor to this phenotype, a blocking antibody at different concentrations was used while TNFα was administered (Figure 3-11d). With increasing doses of the antibody, greater fatty acid uptake was achieve by the iADIPOs. This effect wasn't seen in the IL6, another well-known M1 macrophage secreted cytokine, antibody treated media. When these two antibodies were combined in the MA-MPS, they robustly inhibited the effects of M1 polarized iMACs on the iADIPO stimulation with insulin and isoproterenol showing fatty acid uptake, glucose uptake and glycerol release at levels similar to the no co-culture controls. These data illustrate the effectiveness of the MA-MPS system to interrogate cell-cell interactions arising from a diabetic model phenotype.

3.2.11 - Chemical Interventions in MPS have similar effects as those published

Finally, M1 MA-MPS were utilized to show the model's effectiveness as a drug discovery model. M1 MA-MPS were treated with dexamethasone, a well characterized glucocorticoid

receptor agonist, and metformin, a prediabetic drug that is used heavily in the clinic. Metformin treatment was able to ameliorate the effects of M1 co-culture in MA-MPS by increasing fatty acid up take rates as well as fold amount almost back to the same levels as the no co-culture control (Figure 3-12a,b). Similarly, metformin, but not dexamethasone, increased the total amount of glucose uptake when cells were perfused with insulin containing media (Figure 3-12c). These data show the MA-MPS system as a valid model to study drug effects in complex tissues that contain multiple cell types.

3.3 Discussion

Adipose tissue is a highly dynamic organ system that is often the first to become dysfunctional as a result of chronic nutrient excess [105]. This dysfunction results in localized inflammation that often precedes insulin resistance[106], so investigations into how human adipocytes develop at this early stage are necessary. In Chapter 3 I have outlined experiments aimed at elucidating adipocyte physiology and function through the use of an isogeneic system embedded in a microphysiological device. The evidence reveals a robust reproduction of many well-known cell autonomous behaviors like decreased fatty acid and glucose uptake as well as a cell-cell interaction aspect that models the morphological changes that occur in adipose tissue during obesity. As such, this model can be a powerful method to better understand obesity and drug interactions on a patient-by-patient basis.

Human induced pluripotent stem cells offer a way to meaningfully investigate a person's response to drug treatment. Here, we show that hiPSCs are capable of being differentiated into WAT resulting in a 3D tissue that behaves similarly to human mesenchymal stem cells partially due to the hyaluronic acid-based matrix that we use to embed the adipocytes in. These iPSCs have tunable insulin resistance with increasing amounts of the PPARγ agonist rosiglitazone. Since these cells are transduced with a doxycycline-inducible PPARγ construct there is a worry that even higher amounts of dox could induce insulin resistance, however the fatty acid uptake rates in response to insulin are similar to the hMSCs meaning that the dox-induced PPARγ is not over stimulating the cells to insulin resistance at 100nM rosi. We were also interested in the ability of the hMSC and iPSC cells to outperform commercially available adipocytes with our standard insulin resistance assays.

Previous endeavors to model WAT in microphysiological systems have been extensive[126,127]. However, these systems have all used murine cells, preadipocytes, and whole even isolated human adipocytes [128] to test the efficacy of the MPS. To build off of these other versions we adjusted the MPS geometry to allow for a 3D arrangement of cells to simulate the environment these differentiating adipocytes would see *in vivo*, with the added benefit of a supporting scaffold of degradable acrylated HA as outlined in Chapters 1 and 2. The result is a differentiation capability, and overall ability to survive over a period of 14 days, that matches those seen in hMSC versions of the MPS. iADIPOs cultured in this way have larger lipid droplets on average with decreased locularity suggesting this is an ideal environment for adipocytes to finish their differentiation in.

The iADIPO-MPS platform was also able to be used to model macrophage infiltration and action in an obese state. Here we preloaded MPS with palmitic acid before subjecting them to an isogeneically-derived iPSC macrophage bolus. These macrophages homed in on the adipocytes

quickly and had ingressed into the 3D structure in 12 hours forming crown-like structures. These are morphological features that are highly apparent in obese WAT take from humans and are a hallmark of inflamed WAT. These MPS exhibited Insulin resistance-like physiological tests with a blunting of the effects of insulin on glucose uptake as well as fatty acid uptake rate. This is in stark contrast to previous studies that placed macrophages in coculture often either placing them on top [129-131] of a monolayer of adipocytes, or side-by-side [132]. This allowed our system to work with both M1 and M2 polarized macrophages, which created structures like those seen *in vivo* depending on the disease model chosen.

Finally, the iMACS and iADIPOs in co-culture behaved in previously characterized ways, stimulating one another along TNFα and IL-6 dependent pathways that induced inflammation and stress. These results were readily blocked with antibodies, and as a result insulin resistance measurements were returned to normal levels this shows that the insulin resistance seen in the co-culture method is a result of the crosstalk and feedforward signaling occurring between the two cell types. Lastly, we showed the drugability of this co-culture MPS with insulin resistance by treating with common drugs used to treat insulin resistance like Metformin. These treatments completely insulin sensitized the M1 co-culture, illustrating the MPS ability to act as a insulin resistance drug testing platform.

3.4 Figures

Figure 3-1

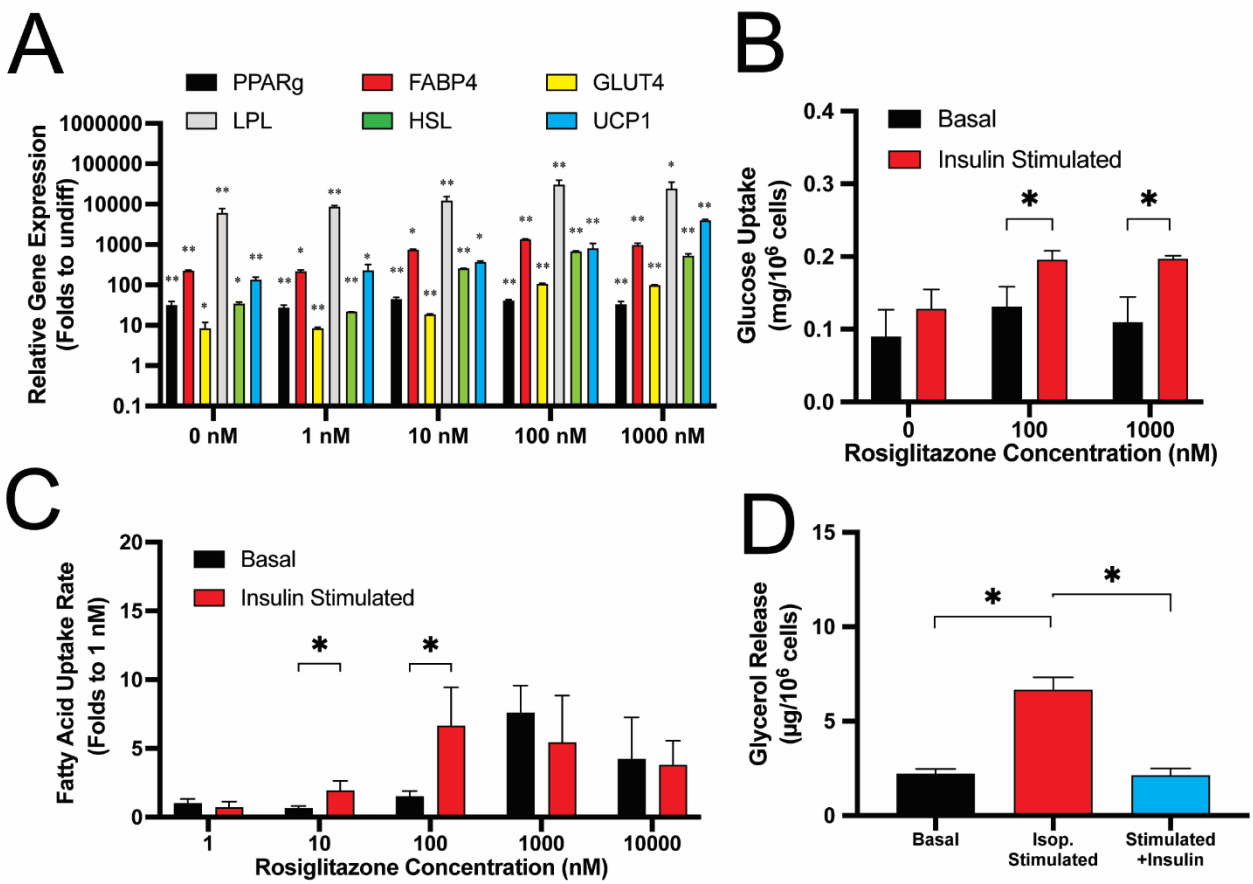

Figure 3-1. Optimization of iPSC-MSC adipocyte differentiation. A) Gene expression of differentiated cells in with altered concentrations of rosiglitazone. B) Glucose uptake ability of differentiated cells with 100nM or 1µM rosiglitazone. C) Dose response of rosiglitazone during differentiation and the effect on fatty acid uptake in day 14 differentiated cells. D) Lipolytic ability of cells differentiated with 100nM rosiglitazone. Stars are used to label a significant difference compared to undifferentiated iPSC-MSCs. In A), expression values are presented as values relative to the calculated mean of undifferentiated iPSC-MSCs.

Figure 3-2

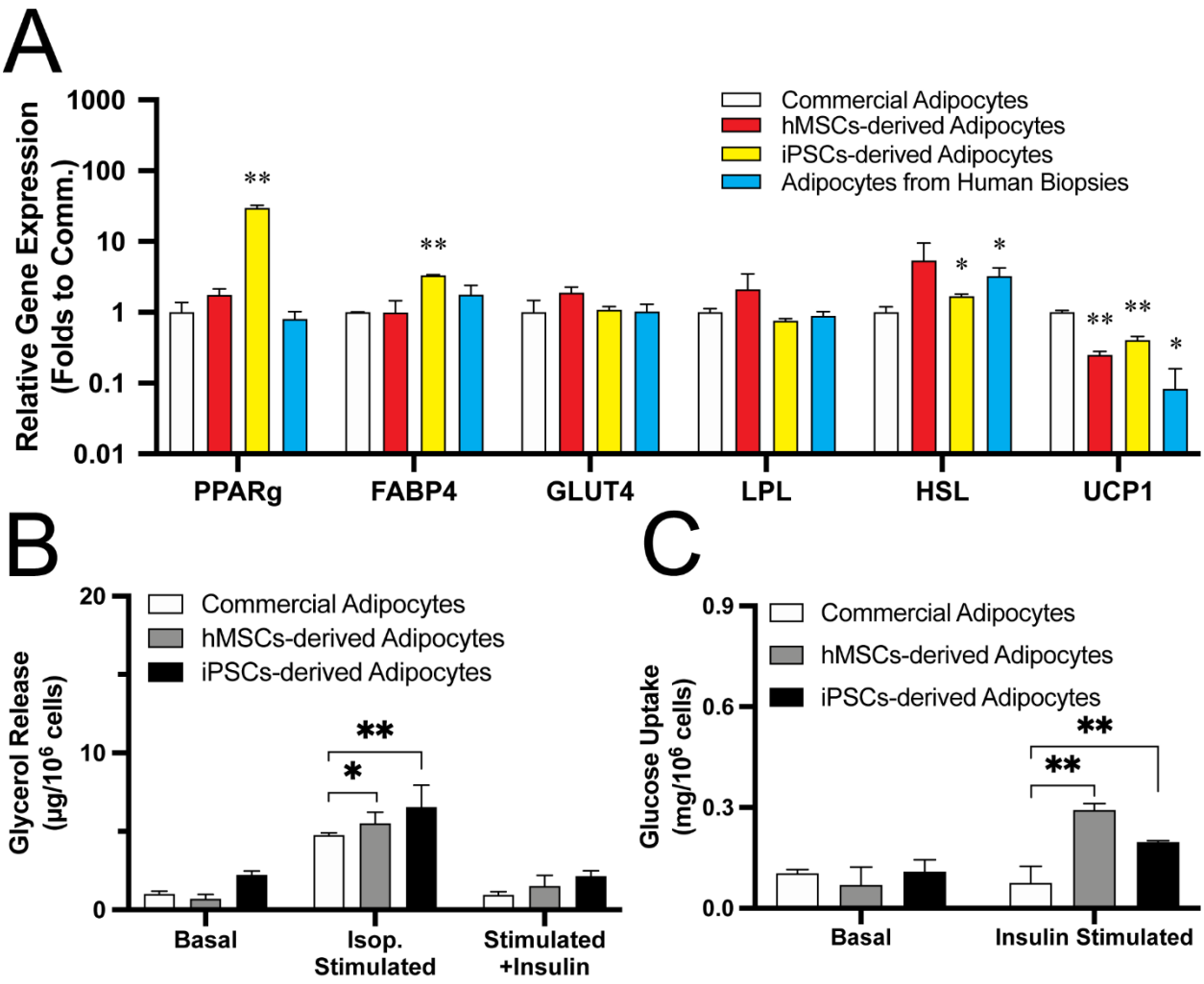

Figure 3-2. Optimization of iPSC-MSC adipocyte differentiation. A) gene expression comparison of iPCS-MCS differentiation to other sources. Genes were normalized to the commercial adipocytes. B) Lipolytic capabilities of the different differentiated cell types. C) Glucose uptake capabilities of the different differentiated cell types.

Figure 3-3

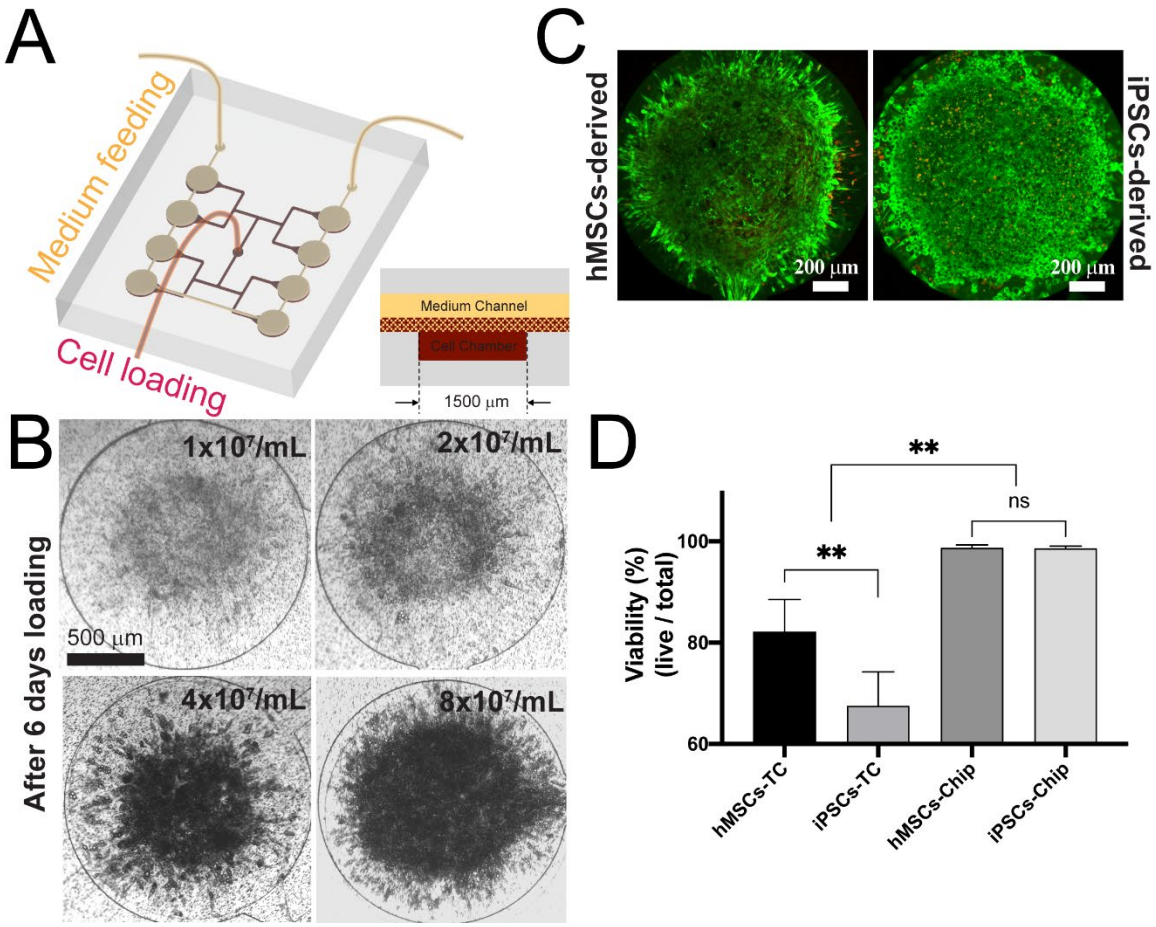

Figure 3-3. Loading density determines survivability of cells in MPS. A) Schematic of the microphysiological device used for modeling. B) Variable cell densities lead to better MPS depot development. C) Live dead assay comparison of hMSCs (left panel) and human iPSC-MSCs (right panel) after 30 days in the MPS. D) Quantification of cells grown in a 24 well plate format vs .in the MPS according to the number of nuclei staining red with ethidium homodimer. Significance denoted with asterisks.

Figure 3-4

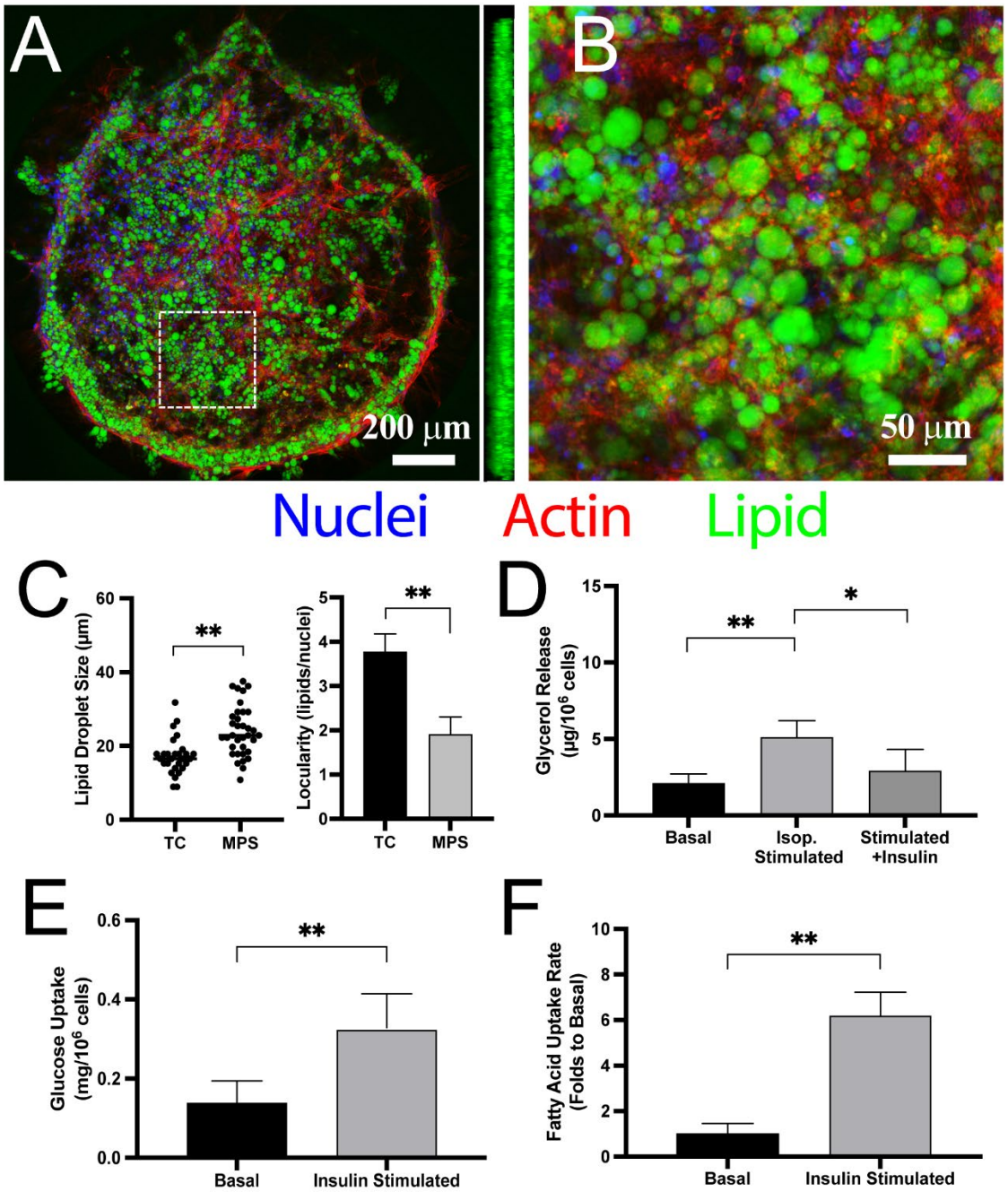

Figure 3-4. Morphological and physiological characteristics of differentiated iPSCs in MPS. A) Maximum intensity projection of a representative well of adipocytes in the MPS after 14 days of differentiation. B) 20x objective of the white box area. C) Lipid droplet size comparison of cells differentiated in a well plate vs. in the MPS. D) Determination of number of lipids per nuclei as a measure of locularity in different formats. E, F) Glucose and Fatty acid uptake of cells in MPS with and without insulin stimulation.

Figure 3-5

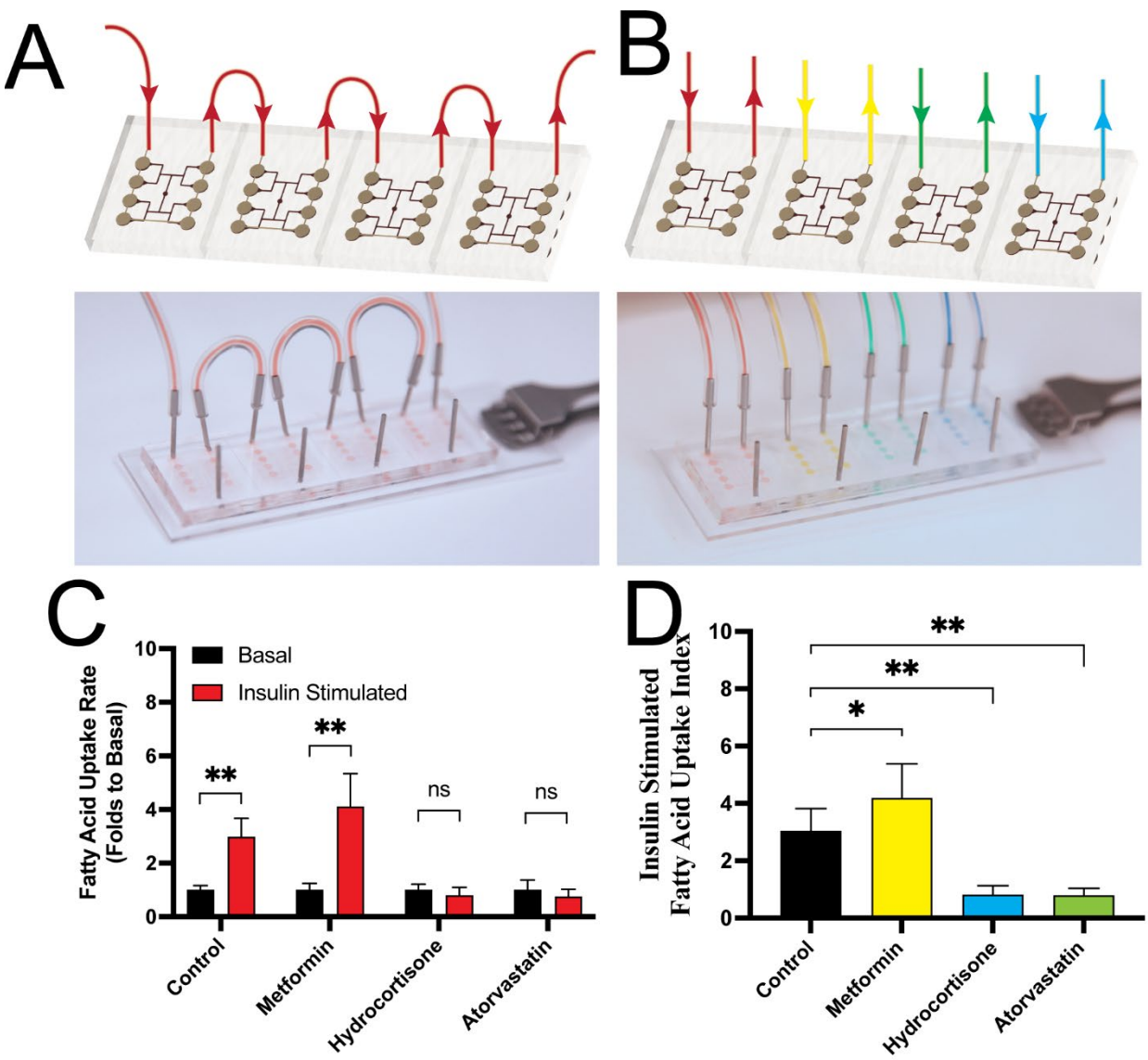

Figure 3-5. Drug screening feasibility in multiunit MPS. A, B) In-series or solo administration of drugs in the designed MPS. C, D) Fatty acid uptake ability of Day 14 differentiated iPSC-MSC in after pretreatment with listed compounds compared to control and basal levels.

Figure 3-6

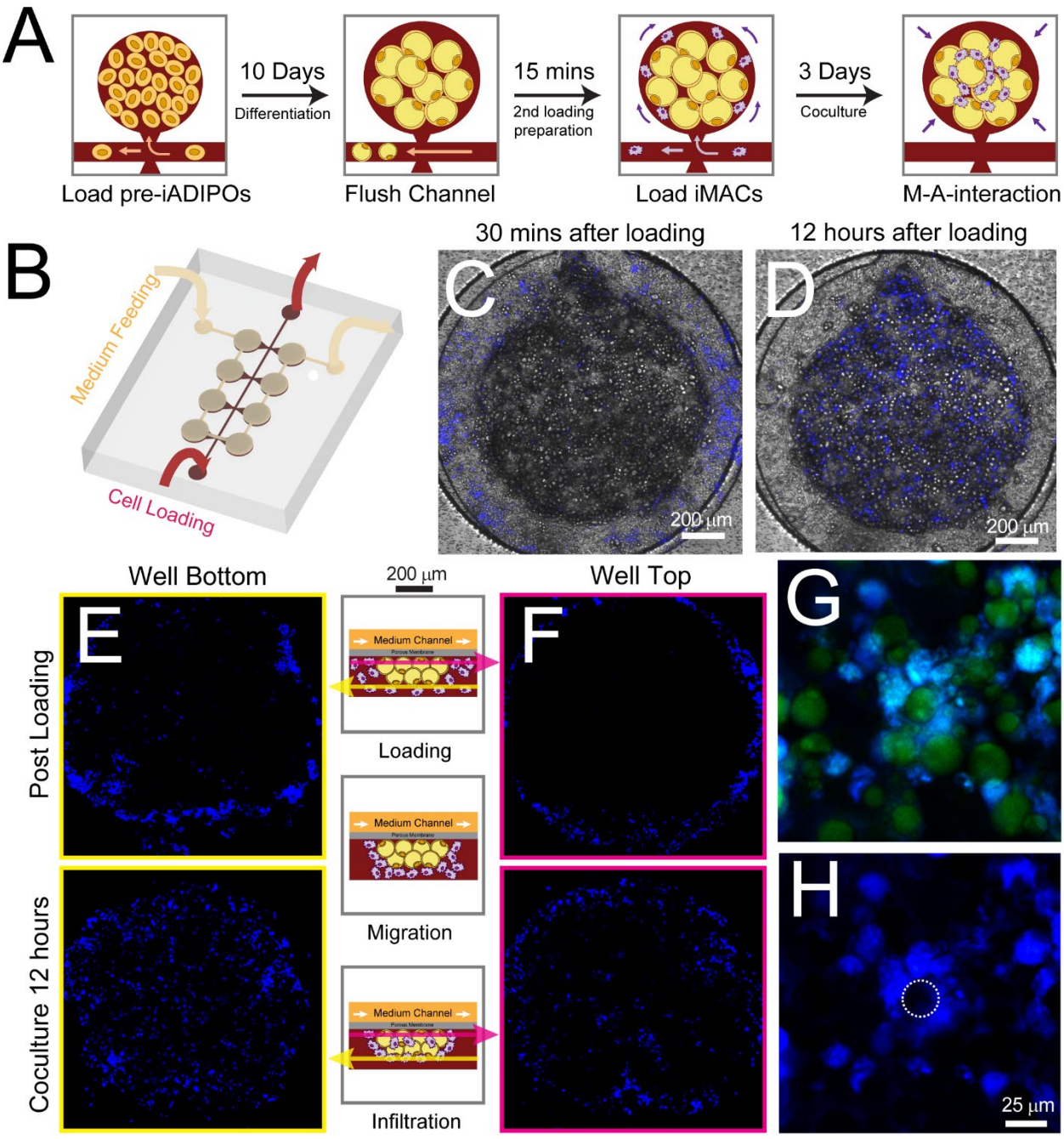

Figure 3-6. IPSC-derived adipocyte and macrophage MPS design. A) Coculture procedure in the MPS. B) Schematic of MPS design. C) iMac location in MPS 30 mins after loading, and D) 12 hours after loading. E, F) similar localization imaging, minus brightfield, of iMAC location relative to the Z axis immediately after loading and 12 hours later. G, H) Pictures showing the development of crown-like structures in the MPS. iMACs were labeled in blue; lipids of iADIPOs were labeled in green.

Figure 3-7

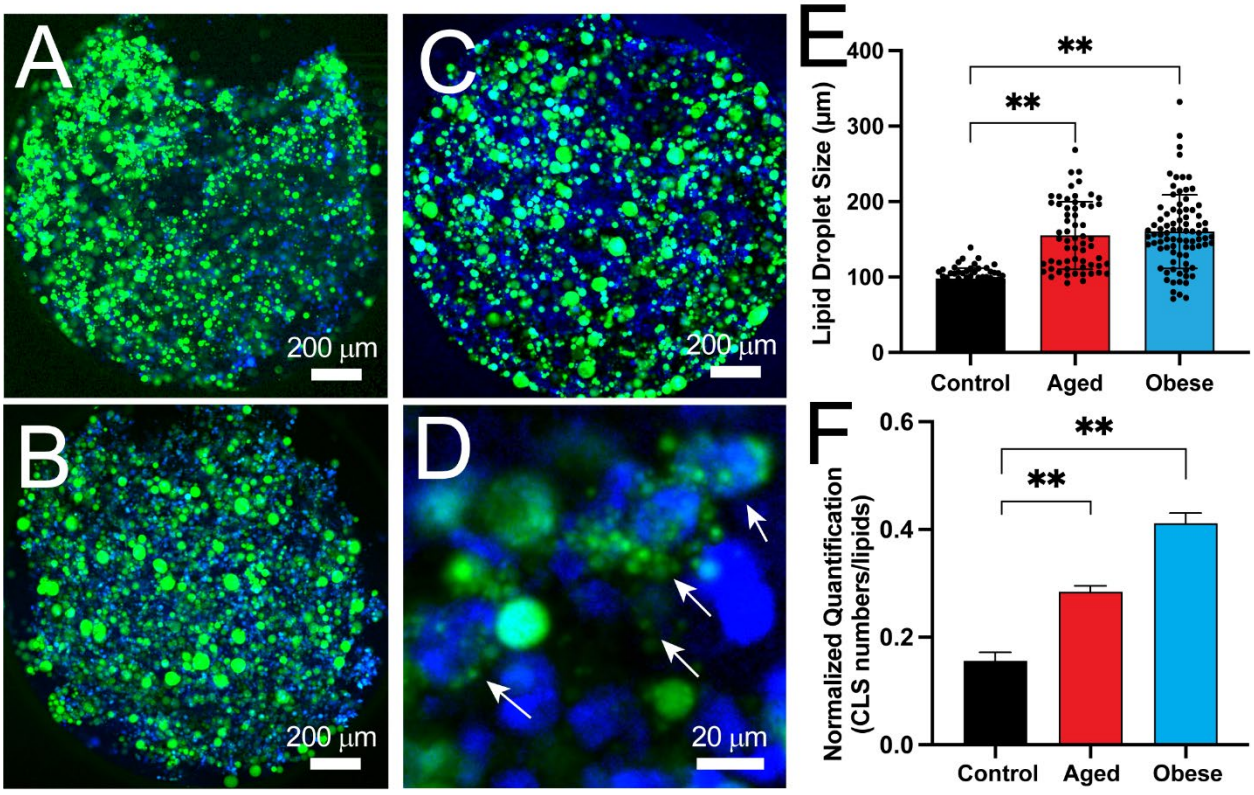

Figure 3-7. Bimodal modeling of unhealthy adipose tissue in MA-MPS. A) Standard day 14 differentiated adipose MPS with the addition of iMACs for 12 hours. B) Aged 74 days adipocytes with iMACs. C) Pamitic-acid loaded cells to simulate obesity. D) Zoom of C. Arrows denote iMACs that exhibit foam cell morphology. E) Lipid droplet size quantitation of iADIPOs in each simulation. F) Quantitation of crownlike structures in each simulation. iMACs were labeled in blue. Lipids of iADIPOs were labeled in green. CLS was quantified based on criterion that >80% of an iADIPO was surrounded or covered by iMACs. N=10 in (e) and N>3 in F).

Figure 3-8

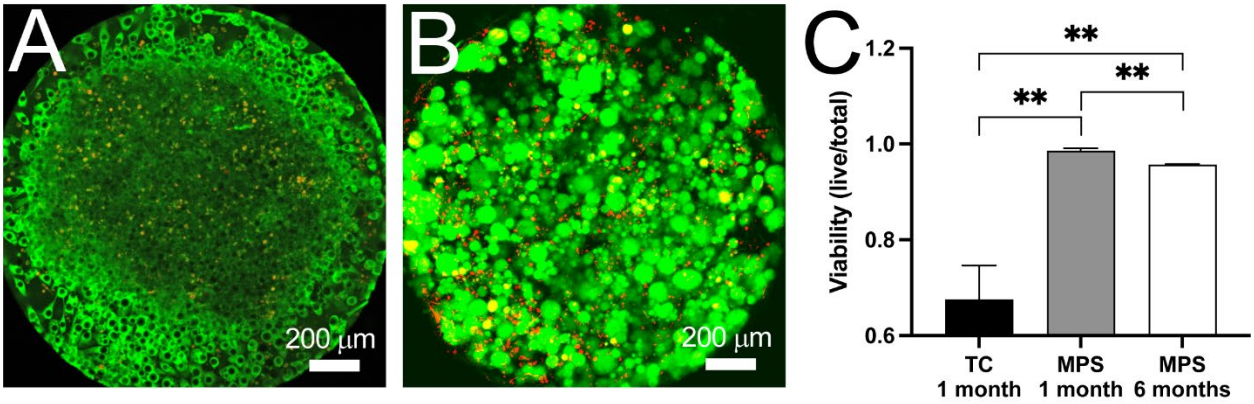

Figure 3-2. Viability of cells after being in device for increasing amounts of time. A) iADIPOs in MPS for 1 month. B) iADIPOs in MPS for 6 months. C) Cell viability quantitation of pictures. n=3 for each condition.

Figure 3-9

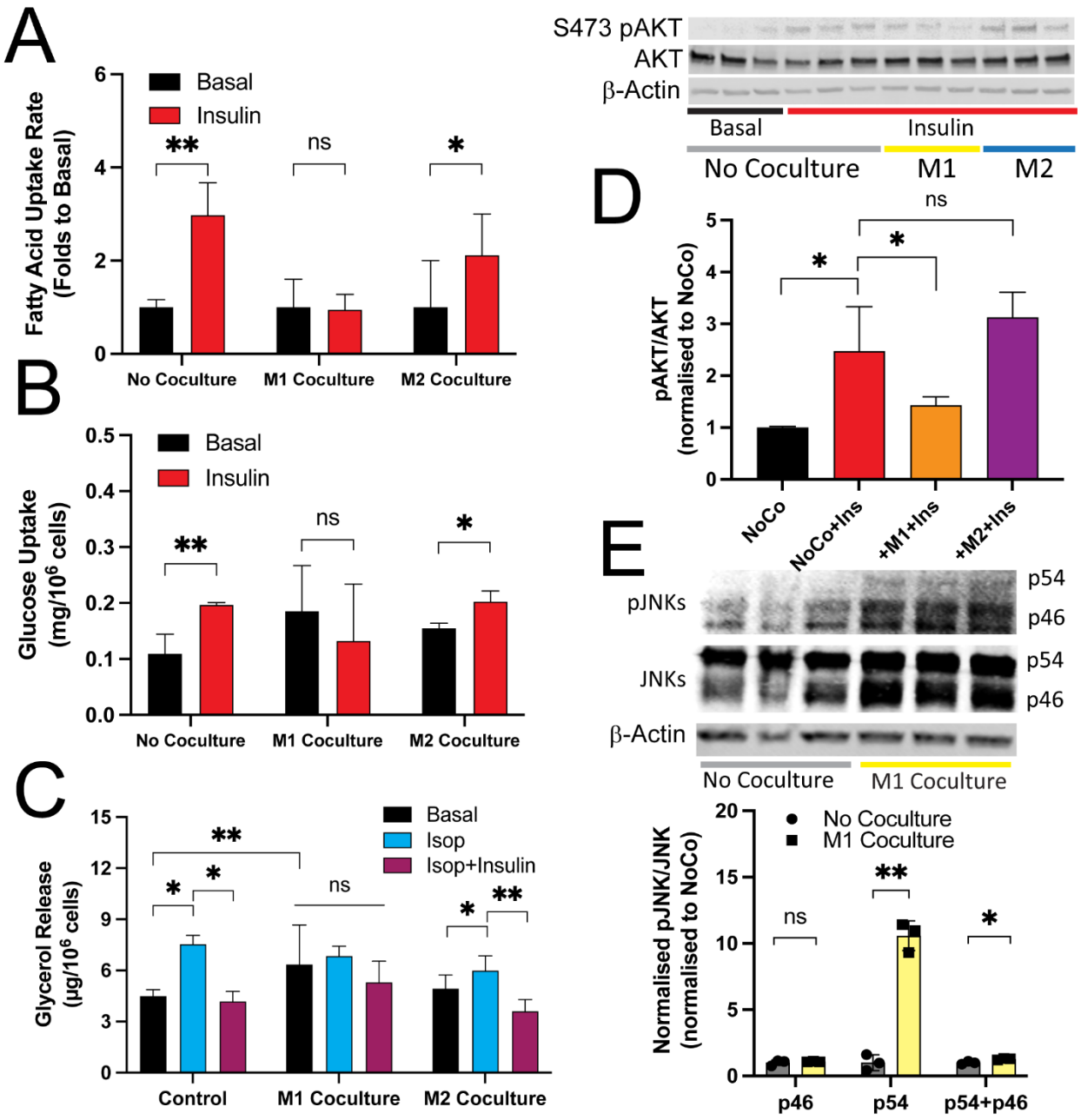

Figure 3-9. Dysregulated metabolic functions in iMAC-iADIPO-MPS depends on Macrophage polarity. A) fatty acid and B) glucose, and also C) dysregulated lipolysis. D) Phosphorylation of Akt (PKB) at ser473 in response to insulin treatment after M1 and M2 coculture. E) Phosphorylation of JNK after M1 coculture. All cocultures lasted for 3 days. n=8 in (a) and n>3 in (b)&(c).

Figure 3-10

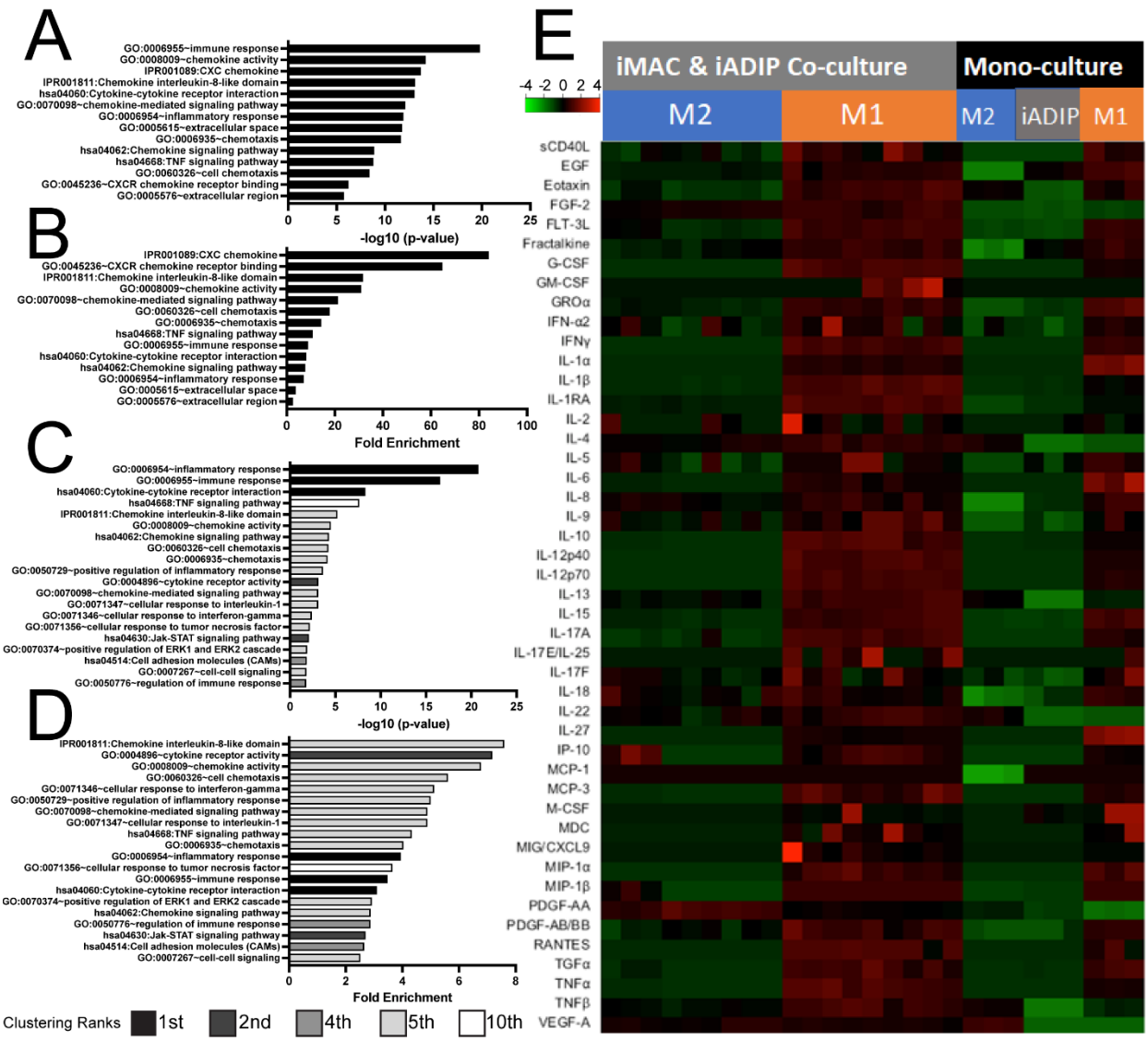

Figure 3-10. RNAseq analysis of iMACs and iADIPOs in pre and post coculture. GO pathway analysis shown in A) -log10 p-value and (b) upregulated fold change. All selected genes were from the group with highest enrichment score in clustering analysis (out of 18). RNA-seq analysis of M1 iMACs after iADIPO coculture vs. monoculture shown in C) -log10 of p-value and D) upregulated folds. Selected genes were from top 1~10 out of 122 groups ranked by enrichment score in clustering analysis. E) Cytokine profiles of culture medium from M1 and M2 coculture with iADIPOs and their respective monocultures. All cocultures were performed in trans-well settings and last for 2 days. n=3 in each group

Figure 3-11

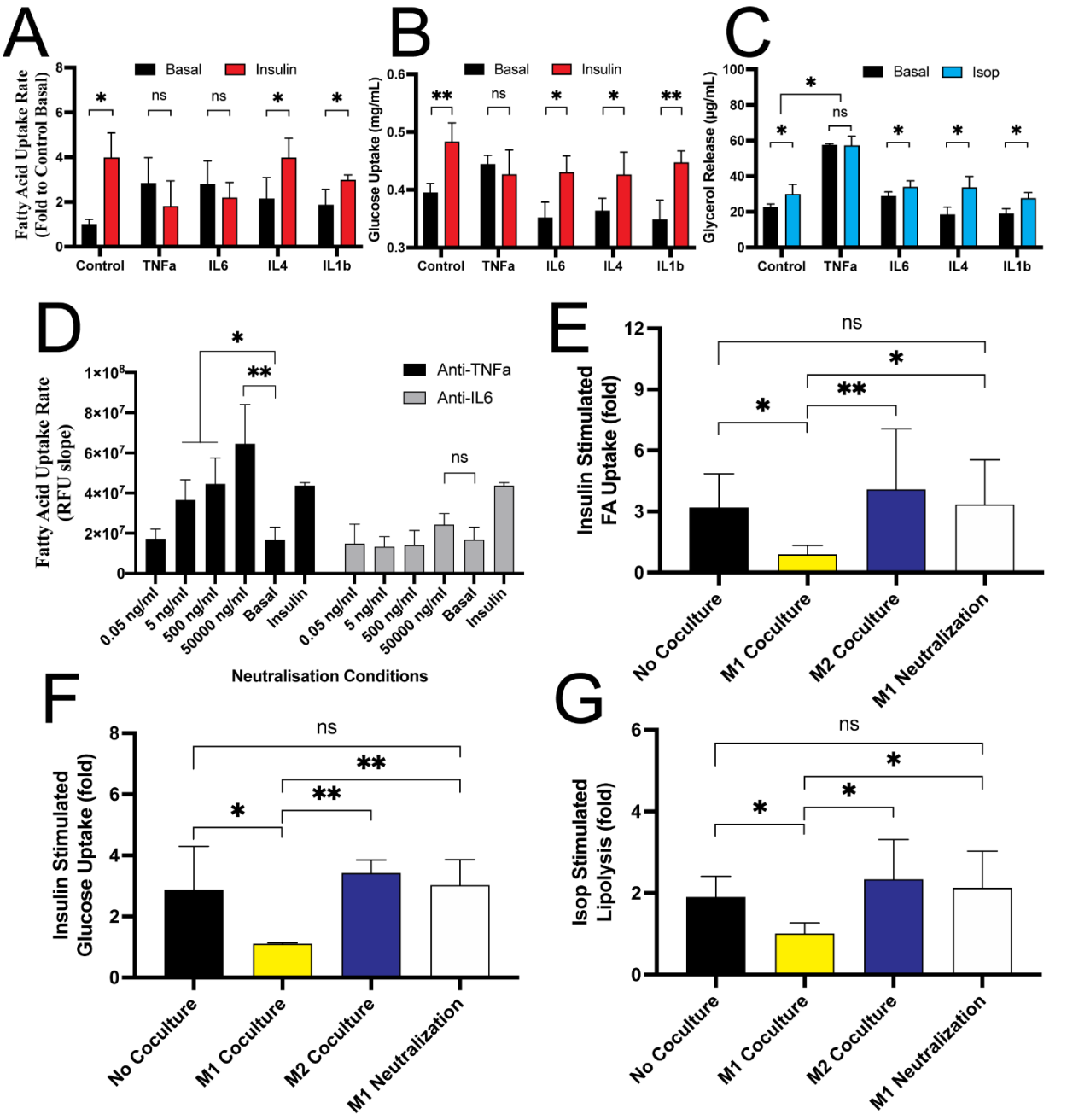

Figure 3-11. Physiological effects of chemokine treatment and coculture. A) Fatty acid uptake, B) glucose uptake and C) lipolysis of iADIPOs after 3-day treatment with selected cytokines at 50 ng/mL. D) Effectiveness of antibodies specific to TNFα and IL6 on insulin sensitivity of iADIPOs after M1 coculture. (e)-(g) Cocktail of anti-TNFα and anti-IL6 cocktail maintained hormonal responsiveness of iADIPOs in measurement of insulin-stimulated (e) fatty acid uptake, (f) glucose uptake and (g) isoproterenol-stimulated lipolysis

Figure 3-12

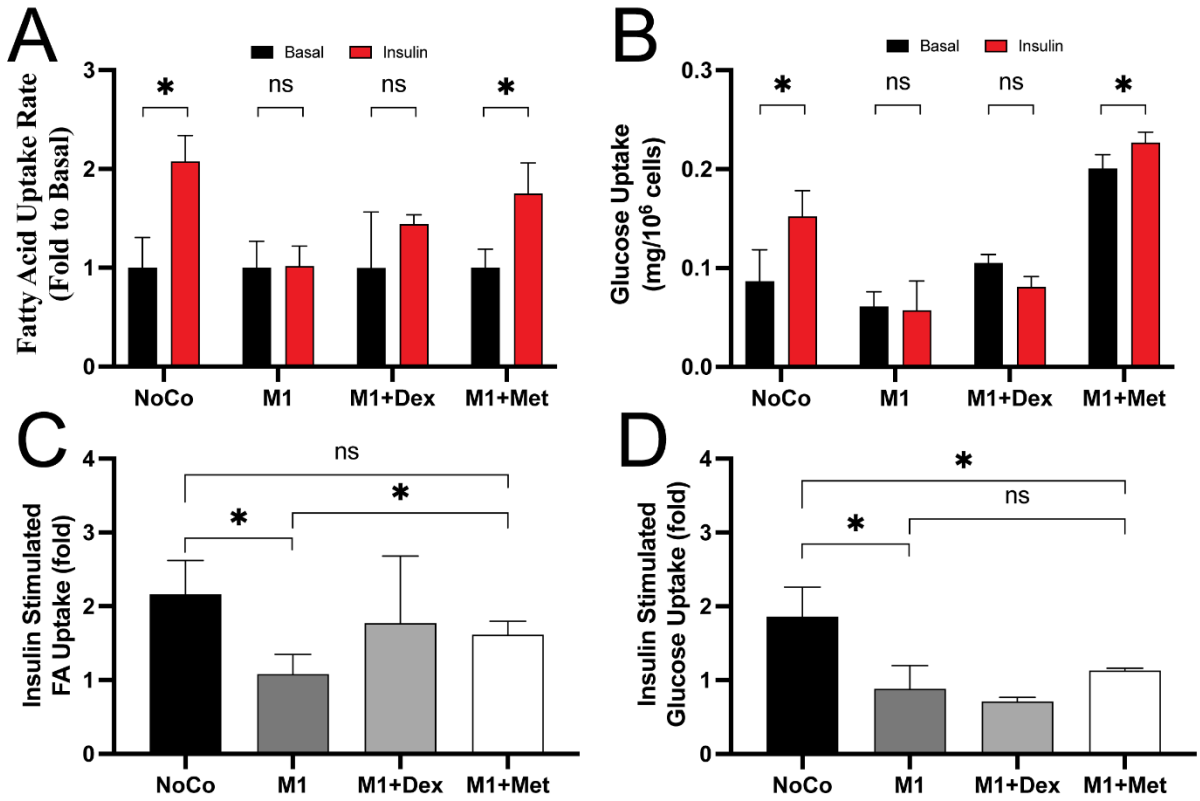

Figure 3-12. Pharmacological intervention of M1-mediated iADIPO dysruption. A, C) Fatty acid uptake rates and total fold change. B, D) Glucose uptake rates and total fold change.

Materials and Methods

Acrylated Hyaluronic Acid (-COOH group)

500kDa and 60kDa sodium hyaluronate were obtained from LifeCore Biomedical and reacted according to the Healy lab published protocols. Briefly, 300mg of 500kDa sodium Hyaluronate (HA) was reconstituted overnight in 100mL of double distilled H_2O at room temperature. 3.9g of adipic acid dihydrazide was then added to the solution and allowed to solubilize for 30 minutes. Next, 575 mg of 1-ethyl-3-[3-(dimethylamino) propyl] carbodiimide (EDC) suspended in 3 mL of 1:1 DMSO:H2O and 507 mg 1-hydroxybenzotriazole (HOBt) suspended in 3 mL DMSO:H2O was added to the stirring solution. pH the solution to 6.8 for at least 6 hours (do not exceed 7.4). pH continues with 1 or 2 Molar NaOH initially then 0.1M NaOH until all the HOBt dissolves. After stirring overnight, transfer the suspension into Spectra/Por 6; 45 mm flat width, 6.4 ml/cm, MWCO:10,000 dialysis membrane and place in 4L of ddH2O with 1.25 g/L NaCl for 12 hours, twice. Next, the HA is dialyzed against 4L of ddH2O for 12 hours, with water changes every 12 hours. Before precipitation we add 5g NaCl/100mL solution. Next, we precipitate the HA with 100% ethanol, filtered with Whatman paper, and resuspended in 100mL of ddH2O. To this, we add 700mg of N-Acryloxysuccinimide and stirred for 24 hours protected from light. This solution was then dialyzed as before. After the three days, we filtered through a Steriflip 50mL (Millipore) spin filter, flash froze in liquid nitrogen, and lyophilized at .024 mBar at -50°C for three days at least. NMR was then performed on the acrylated hyaluronic acid (AcHyA) to determine the percent acrylation, which was usually between 25-35%.

To conjugate the HA with a cysteine terminal peptide, 25mg of AcHyA was dissolved in 10mL ddH2O. At 4°C, 10mg of a peptide (Table 4-1) was added to 1mL of ddH2O with 5.7 mg/mL tris(2-carboxyethyl) phosphine (TCEP) was added to the solution along with 3.0 mg/mL NaOH. This was reacted at room temperature overnight protected from light. The next day, the peptide HA was dialyzed as before and lyophilized again.

Table 4-1. Short adhesion Peptide List and Sequences

Name	Sequence	ECM component	Integrin	Citation
Ag10	CGGNRWHSIYITRFG	Laminin α1		[133]
Ag32	CGGTWYKIAFQRNRK	Laminin γ1	a6b1	[134]
Ag73	CGGRKRLQVQLSIRT	Laminin 2	Syndecan, integrin b1	[135]
bsp_RGD	CGGNGEPRGDTYRAY	Osteopontin	a5b3, a2b1	[136]
C1	CGGGF[HYP]GER	Collagen 1	a1b1, a2b1	[137]
C1(2)	CGGDGEA	Collagen 1	a2b1	[138]
C4	GVKGNPGWPGAP	Collagen 4		[133]
C16	CGGKAFDITYVRLKF	Laminin γ1	a5b1,avb3	[139,140]
Cyc_RGD1	CGGEGYGEGRGDSPG	Fibronectin		[141]
Cyc_RGD1.2	Ac-GCGYGRGDSPG-NH2	Fibronectin		[141]
Fib5	CGGPHSRN	Fibronectin	a5b1, a2bb3	[142]
F9	CGGRYVVLPRPVCFEK	human laminin β1		[143]

Hep1	CGGSPPRRARV	Fibronectin		[144]
P3	CGGVSWFSRHRYSPFAVS	E8 domain of Laminin α	a6b1	[145]
P20	RNAIAEIIKDIGC	CD20		
T1	CGGTTSWSQCSKS	Thrombospondin	a6b1	[146]
Vit1	CGGGKKQRFRHRNRKG	Vitronectin	heparin	[147]
YIGSR	CGGEGYGEGYIGSR	Laminin		[141]
MMP-13	CQPQGLAKC			[148]

Methacrylated Hyaluronic acid (-OH group)

Sodium Hyaluronate of varying molecular weights was obtained from LifeCore Biomedical (Chaska, MN) and stored at -20°C in a food-safe vacuum container until functionalization. To functionalize the HA with an acrylate group for Michael addition-based reactions, we used a method very similar to[149-151], but with some modifications as seen[152] . Briefly, a 1 wt% solution of HA in deionized water was made in a round bottom flask and cooled to 4°C in an ice bath. After reaching 4°C, 8 mL of new methacrylic anhydride (Sigma Millipore, AS: 760-93-0) was added dropwise to the solution per gram of HA. As the pH dropped, NaOH was added slowly to the solution until a pH of 8 was achieved. HA is hydrolyzed at pH above 11, and below four[153], so care was taken to never surpass these levels. Active titration of the pH occurred for at least six hours on the first day of synthesis, which was then placed on a slowly spinning stir plate in a 4°C cold room overnight. The following day, the pH was noted (usually between 4.5 and 5) and increased to 7 using 5N NaOH dropwise. Afterwards, 4 mL of methacrylic anhydride was added to the solution. 1M NaOH was used to pH the solution back up to 8 as needed (roughly every 15 minutes). This occurred for 3 to 4 hours and was then placed back in the cold room until the next day. The resulting solution was then precipitated in ice cold ethanol the following day and portioned out into 50mL conical tubes. The HA/MA mixture was then spun in a tabletop centrifuge at 4347x*g* for 5 mins until the HA precipitate was pelleted. The tubes were decanted into the satellite waste area and inverted onto paper towels to collect any excess ethanol/MA that wasn't removed. Afterward, the pellets were removed to new dry 50mL conicals, portioned out evenly by weight, and then milli-Q water was added to roughly the 40mL mark on the tubes. To drive resolubilization, we placed the Methacrylate HA (MeHA) tubes at 37°C and vortexed them briefly every ten minutes until fully in solution. Tubes were then centrifuged again to remove any precipitated methacrylic anhydride and then placed in a Amicon® Ultra-15 10 kDa filter (EMD Millipore) to further remove any reacted components. Concentrates were then removed using positive displacement pipets (Rainin) and resuspended up to 40mL with milli-Q water for every 250mg of initial HA used. Each conical tube was sterile filtered using a .22µm flip filter (Millipore) and flash frozen in liquid nitrogen. Frozen conical tubes were then capped with a folded double kimwipe and secured with a rubber band before placing on a -50°C lyophilizer depressurized to 0.024 mBar using an amber flask to guard against light damage. Lyophilization was allowed to occur for at least three days or until no ice core was present in the middle of each sample tube. After removal from the lyophilizer, tubes were flushed with Nitrogen gas, parafilmed, and placed at -20°C in a food-safe vacuum container until use.

DBCO Synthesis

DBCO functionalization of sodium hyaluronate for single functionalization, or MeHA for dual functionalization, was performed as previously published[21,154,155]. Briefly, DBCO-Amine (Sigma) was reacted with 60 kDa (average) or 500 kDa HA for 48 hours to before undergoing precipitation and reconstitution in preparation for lyophilization. First, 500 mg HA was dissolved in 30mL MES buffer (50mM, pH 4.0) at room temperature in a stirring round bottom flask until fully dissolved. Next, carboxylic acid groups were activated by an equimolar amount of N-(3-Dimethylaminopropyl)-N'-ethylcarbodiimide (EDC) and N-hydroxysuccinide (NHS) for one hour. 200 mg DBCO-amine was resuspended in 2-4 mL of DMSO and added dropwise to the stirring reaction (0.6 equivalents). Up to 8mL of additional DMSO could be added to the flask if the DMSO DBCO-amine was not remaining in solution. The reaction was protected from light and allowed to proceed at room temperature, stirring, for 48 hours. Precipitation of reacted solution occurred in ice cold acetone if monofunctionalized, or ice-cold ethanol if difunctionalized. The resulting solution was then spun in a tabletop centrifuge at 4347 x *g* for 5 mins until the HA precipitate was pelleted. The tubes were decanted into the satellite waste area and inverted onto paper towels to collect any excess ethanol or acetone that wasn't removed. Afterward, the pellets were removed to new dry 50mL conicals, portioned out evenly by weight, and then milli-Q water was added to roughly the 40mL mark on the tubes. Solutions were concentrated and washed in Amicon® Ultra-15 10 kDa filter columns to remove unreacted reagents, and afterwards were resuspended to 125mg/30mL of ddH_2O. Each conical tube was sterile filtered using a .22µm flip filter (Millipore) and flash frozen in liquid nitrogen. Frozen conical tubes were then capped with a folded double kimwipe and secured with a rubber band before placing on a -50°C lyophilizer depressurized to 0.024 mBar using an amber flask to guard against light damage. Lyophilization was allowed to occur for at least three days or until no ice core was present in the middle of each sample tube. After removal from the lyophilizer, tubes were flushed with Nitrogen gas, parafilmed, and placed at -20°C in a food-safe vacuum container until use.

Rheology

Rheology was carried out on a TA Waters Discovery HR10 parallel plate rheometer using a 20mm sandblasted bottom insert on a temperature controlled peltier plate. One of two top plate inserts was used to perform the measurements, an 8mm sandblasted or a 20mm solvent trap sandblasted. Generally speaking, the 8mm was used for overnight-cured hydrogels where the 20mm was used for kinetic measurements such as gelation timing.

Initial characterization of the hydrogels was performed using a frequency sweep measurement as well as an amplitude sweep in order to determine the optimal testing parameters of these soft gels. For general testing purposes, it was found that a frequency of 0.5 *Hz* and a 5% stress could be used for most measurements, especially pertaining to general hydrogel batch-to-batch quality control experiments.

For general storage and loss modulus data sets, overnight crosslinked hydrogels were removed from their 8mm mold and placed on the preheated bottom plate and the top plate was moved down just touching the hydrogel before trimming off excess material. Then, the top plate was slowly lowered until an axial force of around 0.05 to 0.1 was measured. 20 repeated

measures over a 1-minute period were performed at 0.5 *Hz*, with the direct strain oscillation parameter engaged.

1H NMR Quality Control of HA hydrogels

Nuclear Magnetic Resonance spectroscopy was performed in the College of Chemistry NMR core facility. The primary goal of each experiment was to determine the amount of functionalization of the hydroxyl group, if methacrylate HA was made, or carboxyl group, if DBCO/SPAAC, that occurred during the reaction. 5 mg of HA was dissolved completely in 600 µL of deuterated water (Sigma or Millipore) and loaded into a 5mm NMR tube (Norell) using a positive displacement pipet to minimize the amount of air bubbles being introduced into the solution. Afterwards, the samples were taken to the care facility and placed on their NEO-500 for ^{1}H-NMR. Data of the run was opened and analyzed using MNova (Mestre Labs). Spectra were first processed with an auto phase correction and full auto baseline before selecting the auto peak picking option. For quantitative analysis of the peaks the manual integration tool was used, setting the reference peak at 1.9 ppm for the Methacrylate HA. Next, the peak at 6.1 was selected. That peak area was divided by three (for each of the protons on the added methacrylate group) in order to determine the percentage of methacrylate functionalization of the HA. Alternatively, for a different estimation of percent functionalization, I could instead measure the peak immediately to the right of the reference peak (usually 1.86-1.87) which constitutes the methylene groups within the sample.

For the DBCO modified HA, processing was performed as before, and a reference peak at 1.9 – 2.0 was used to start the manual integration. Next, 4 peaks were identified between 2.5 and 3.0. The proton peak (#4) near the amine group is normalized, and multiplied by the #2 peak, and divide by eight which corresponds to the rate of each hydrogen on the phenyl part of DBCO.

SEM info

Scanning electron microscopy was utilized to visualize the microstructure of the different formulations of MeHA hydrogels. This work was performed in the Electron Microscopy Lab, a core facility at UC Berkeley. Primary visualization was done with a Hitachi TM-4000, a low-vacuum instrument with a thermal electron gun and semiconductor backscattered-electron detector for high resolution, low noise imaging. Hydrogel preparation was performed as suggested in[156,157] due to previous at studying the secondary structure of these gels with SEM yield gray mass alone with no structure[158]. Briefly, ethane was cooled and condensed using the EML Leica EM GP2 Plunge Freezer that was pre-cooled with liquid nitrogen. The resulting liquid ethane was used to plunge freeze 500µL of hydrogel that had been crosslinked the previous evening and allowed to cure overnight at 37°C. It was found that larger volumes of crosslinked hydrogel were required to preserve the structure of the hydrogel during the next step of the process, lyophilization. After freezing in ethane, samples were placed in pierced 50mL conicals and submerged in liquid nitrogen for transport. Liquid nitrogen was removed before placing in an amber flask and attached to a LabConco 2.5L FreeZone -50°C lyophilizer. Lyophilization took place over a 48-hour period at -48°C to -51°C with a median pressure of 0.3mBar. After freeze drying, samples were

carefully cracked and pulled apart to reveal the inner structure of the hydrogels, after which these samples were stub mounted with carbon tape and imaged.

SEM image analysis was performed on three separate areas of the same lyophilized gel at the same magnification. Pore size was quantified according to[159]. 100 pores across the imaged gel were quantified by drawing around their edge. Area data was then exported to excel and organized.

Hydrogel Prep and TC use

MeHA hydrogels were prepared according to previous Kumar lab publications [22,152,158]. Briefly, lyophilized MeHA was weighed out and reconstituted to anywhere between 6-10 weight percent in PBS pH 7.4 (Gibco) depending on the molecular weight of the HA. These hydrogels were reacted overnight at 4°C with short adhesion peptides containing a terminal cysteine that mimic different components of the extracellular matrix. Because cysteines contain a thiol group, they can react with the methacrylate group of the functionalized HA, thus allowing the creation of a cell-tailored niche (Table 4-1). The following morning hydrogels containing the short adhesion peptides were diluted to 3-4wt% total with more PBS and crosslinked with dithiothreitol (Fisher) at a predetermined thiol group to functionalized HA monomer ratio (anywhere from 0.2 to 0.8) depending on the elastic and viscous outcome desired. 10-20µL of DTT-added hydrogel was plated into a 24 well tissue culture plate pre-incubated with Poly-L-Lysine (Sigma) and flattened with a round 12mm type 1 coverslip that had been previously coated in Rain-X to prevent coverslip sticking. The interstitial areas of the plate were then filled with ddH_2O to create a humid environment, and the gels crosslinked overnight. The next morning, coverslips were washed with PBS once and gently removed using curved forceps. Exposed gels were then washed 3x's with DPBS (Gibco) before plating cells.

DBCO gels were also used in similar experiments where 10-20µL of peptide preconjugated HA was plated into a 24 well plate and flattened with a Rain-X coated coverslip. Crosslinking could be achieved as before with thiol/acrylate-based Michael addition, or it could be accomplished with a multi-triazole containing group compound like a bi, quad or octo PEG. 200uM of a 4 arm PEG into a 3 wt% difunctionalized HA was enough to drive crosslinking fast enough to make pipetting into the well difficult.

Additional testing of the hydrogels for their ability to hold on to a triazole modified compound, similar to what we would expect for a conjugated agonist, was conducted using azido-cy5 as a leakable, and traceable, substitute. 2molar excess Az-Cy5 was loaded into each gel and reacted at room temperature overnight protected from light. The next morning the gels were crosslinked using DTT at a 0.6 thiol:monomer ratio in a 12 well tissue culture plate. Gels were crosslinked at 37°C in a CO_2 incubator until the afternoon (6-7 hours). 500uL of PBS was used to wash the hydrogels once before the initial measurement on a fluorescence capable plate reader. Gels were washed once during the morning and once during the afternoon each day for five days, always measuring the fluorescence signal remaining at 12 points in the gel immediately after the afternoon wash. Relative fluorescence units were averaged among the 12 points and used as the daily value for that formulation.

Hydrogel Prep *In vivo* use

In vivo use of the hydrogels was very similar to TC use with special considerations for the ability of the host to remodel the implant. To this end, AG73 and C16 were the primary peptides used in these experiments as they showed reliable ingression of host stem cells over a 10-14 day period. In addition, MMP-degradable crosslinkers were used to further promote the *in-situ* formation of a functional tissue. Experimental setup proceeded as in TC with a 10% hydrogel reconstituting in PBS overnight, or for a few hours at 37°C. Afterwards peptides were added to the mixture according to our previous work listed before and incubated overnight at 4°C. The next day the gels were mixed to their final volumes with additional PBS or non-modified HA, mixed with MMP-13 degradable crosslinker at a 0.6 thiol:HA monomer ratio and loaded into a syringe using a positive displacement pipet. Next, a 20-22 guage needle was attached to the leurlok port, air was ejected, and hydrogel was injected near the inguinal adipose depot of an isoflurane anesthetized animal. Each animal was injected at most twice and were sacrificed using CO_2 and cervical dislocation at 1-, 5- or 10-days post implantation.

Mouse Husbandry and Use

Experiments were performed according to AAALAC guidelines and approved by the University of California, Berkeley Animal Care and Use Committee. 8-week-old male C57BL/6j (Jackson Labs) were group housed for a one-week acclimation period (temperature: 21 ±2°C, humidity: 30--70 %) in Tecniplast cages filled with sani-chip bedding (Harlan) and fed *ad libitum* using LabDiet's 5053 formulation. Breeder colonies of UCP1 promoter-driven Luciferase mice were maintained on the higher fat 5058. Pups were weaned at 21 days of age and placed in sex-specific home cages to prevent unwanted breeding. Males were used for stromovascular fraction isolation.

Tissue Culture

Mouse Preadipocyte cell lines were cultured in DMEM (100mg/L sodium pyruvate, L-Glutamine, 4.5 g/L D-Glucose) plus 10% FBS (EquaFetal, Atlas Biologics) and 1% penicillin streptomycin and were subcultured 10 times during experiments before a new batch was thawed. Much of the work done was performed with two preadipocyte cell lines from Shingo Kajimura that we have previously used [160] for the study of beige and brown adipogenesis. The sWAT cell line is a good model due to their ability to be differentiated into either white or beige adipocytes. sBAT cells are one of the few cells lines that are a decent physiological representation of a brown adipocyte. Both cell lines are easily differentiated toward their experimental end goal using well know protocols for white and brown adipogenesis. For white differentiation, sWAT cells were plated at $1.5x10^5$ cells/mL in a 24 well tissue culture plate where each well received 500µL. The next day, cells should have grown to confluence and differentiation was initiated using 5ug/ml Insulin, 2ug/ml Dexamethasone, 0.5mM IBMX, 0.1uM Rosi. If beige differentiation is desired 1nM T_3 and 0.125mM Indomethacin was also added to the induction media. Induction took place over two days and was followed every two days by maintenance media until ready for an experiment. For maintenance media, only insulin and rosiglitazone were used.

Two human cells were used for some experiments, one MSC from ZenBio (ZBSQ) (lots 60, 61, 65) and another induced pluripotent stem cell line WTC-11. Cells were used for experiments within the first five passages after thawing, roughly equating to total passage eight from receipt of the cells. For experiments, the ZBSQ cells were proliferated in complete medium (DMEM/F12 medium with 10% fetal bovine serum, 1% HEPES, 1% penicillin/streptomycin) with supplements of 0.5 ng/mL human fibroblast growth factor and 0.5 ng/mL human epidermal growth factor plated to almost confluence and allowed to grow for another two. They were then given induction media for three days which consisted of 5ug/ml Insulin, 2ug/ml Dexamethasone, 0.5mM IBMX, and 0.1uM Rosiglitazone. After induction, cells were maintained with Insulin and rosiglitazone alone until at least day 10 of differentiation before experimentation.

For WTC11 cells, prior to adipocyte differentiation, iPSCs were first differentiated into mesenchymal level (iPSC-MSCs) then transfected with exogeneous PPARγ to enhance adipogenesis. After enhancement, cells were grown on culture plates were precoated according to manufacturer's recommendation with ACF protein substrate (Stem Cell Technologies) for at least 2 hours before plating. Cells were lifted with TrypLE (Gibco), spun at 0.2 *rcf* for four minutes. Cells were then plated in ACF media plus ACF supplement, with GlutaMax added. For differentiation, 5uM and SB431542, a TGF-β pathway inhibitor, 1µg/mL doxycycline in DMEM/F12 media was used as the base media along with 5ug/ml Insulin, 2ug/ml Dexamethasone, 0.5mM IBMX, and 0.1uM Rosiglitazone from day 0 of diff to day 3. Days 4 – 9 was a similar media but lacking Dexamethasone and IBMX. Finally, from day 10 to 30 was a half volume media change using the same DM2 media as before.

Mouse MSC populations were also harvested and used for some experiments. Briefly, 3-5 male C57Bl/6j were sacrificed and inguinal or brown adipose tissue was harvested. Similar adipose depots were pooled and minced with scissors until only millimeter chunks remained. Liberase TM (Roche) was added to a pre-warmed serum-free DMEM and minced adipose tissue was added. Dissociation media was then placed on an orbital shaker on an incline rotating at 200rpm for 45 minutes. At 15-minute intervals, the 50mL conicals were taken and briefly vortexed to enhance the tissue breakdown. Dissociated tissue was then placed through a 100µm strainer, centrifuged to pellet, and then a 40µm strainer to obtain single cells. After centrifugation, ACK lysis buffer (Gibco) was used to lyse red blood cells per manufacturers recommendations for the starting tissue volume. ACK lysis buffer was diluted 10-fold in DMEM/F12 + 10% FBS and 1% penn strep with 100µL of Fungizone (Gibco) and 10µL of Geneticin stock (Fisher) for the first three days, replacing the medium every three days. Adhered cells were then allowed to proliferate until 60% confluency and split into three 10cm plates. At 60-80% confluency these cells were then re-plated into their final format and differentiated towards a white or beige fate as previously outlined.

Physiological assays were performed on fully confluent, maturely differentiated, adipocytes. Glucose uptake was performed using the Amplex Red kit from ThermoFisher, measuring the decrease in glucose concentration in the media upon insulin stimulation over a 6–12-hour period. Lipolysis was stimulated with racemic Isoproterenol at 1µM in HBSS + 1% fatty acid-free BSA for 6 hours before measurement with the Free Glycerol Reagent assay from Sigma. Fatty acid uptake was performed as we have previously published[161].

Cytokine analysis

Macrophages and adipocytes were monocultured in 24-well plate or cocultured in trans-well settings with 0.3 mL medium per well. Media were all collected and sent to Eve Technologies (Canada) for analysis with Human Cytokine/Chemokines 65-Plex panel (HD65). Cytokines were plotted in heatmap based on fluorescence intensities.

Gene Expression

RNA was extracted from cells cultured *in vitro* or from adipose tissue taken *in vivo*, using either a trizol (Life)/chloroform (Sigma)-based method or with a New England Biolabs Monarch RNA extraction kit for higher RNA purity. For trizol-based extraction, samples were incubated with up to 1mL for five minutes at room temperature on a rotator. If the sample were tissue, they were broken up with a bead homogenizer using a ball bearing before briefly spinning it down to separate out the lipids. Trizoled samples were incubated with 200µL chloroform for every 1mL of trizol, shaken by hand for 15 seconds, allowed to settle and then centrifuged at 4°C and 12,000x*g* for 15 minutes. The aqueous phase was then removed into a new 1.5mL Eppendorf tube and 0.5mL of isopropanol was added for every 1mL of trizol initially used. Tubes were inverted gently until mixed by placing another tube rack on top and turning upside down repeatedly. Tubes were again centrifuged at 4°C and 12000x*g* for 15 minutes. The supernatant was decanted, gently, and the resulting RNA pellets were washed with 100% ethanol twice, with a brief centrifugation step in-between. Finally, a pipet was used to ensure no ethanol would make it through to the next step, the tube air dried for five minutes, and pellets reconstituted in nuclease-free H_2O. For NEB Monarch kits, the suggested directions were followed exactly, including the option gDNA removal steps.

cDNA synthesis occurred after reconstitution or elution of the RNA and placing on ice to maintain RNA integrity. Samples were then quantified using a Nanodrop One (ThermoFisher). Each sample was loaded according to the least concentration sample which could range to as low as 50ng total depending on the model the RNA was extracted from. This lowest concentration was then loaded into a PCR strip, diluted up to 10uL with water, after which 10uL from the Maxima First Strand synthesis kit (ThermoFisher) was used to create the cDNA used for RT-PCR. A BioRad T100 was used for the thermal reaction which started at 25°C for 10 minutes, followed by a 15-30 minute amplification step at 50°C and ended with a 5 minute incubation at 85°C to inactivate the DNA polymerase. These 20µL samples were then diluted up to 100µL using nuclease-free water and placed at -20°C until qPCR was performed.

qPCR was performed on an ABI Quantstudio 5 in 384w plate using their “standard” cycling parameters for 10uL. This is 50°C for 2 mins, 95°C for 10 mins, then cycled 40x with 95°C for 15 secs, down to 60°C for 1 min with an imaging step at the end. Samples were made up in 10µL volumes, 1µL of which was cDNA. The remainder of the volume was prepared according to the ABI TaqMan Fast Advanced Master Mix, a 2x master mix. TaqMan probes were purchased from IDT and diluted according to their recommendations in nuclease free water before use. For a complete list of all probes used, see Table 4-2.

Table 4-2. qPCR Taqman Probes used

Species	Gene name	Assay ID
Mouse	PPIA	Mm.PT.39a.2.gs
Mouse	TBP	Mm.PT.39a.22214839
Mouse	FABP4	Mm.PT.58.43866459
Mouse	UCP1	Mm.PT.58.7088262
Mouse	PPARγ2	Mm.PT.58.31161924
Mouse	Leptin	Mm.PT.58.13515402
Mouse	Resistin	Mm.PT.58.19073586
Mouse	Col1a1	Mm.PT.58.7562513
Mouse	EBF2	Mm.PT.58.29446261
Mouse	PRDM16	Mm.PT.58.10936929
Mouse	PGC1α	Mm.PT.58.16192665
Mouse	CD36	Mm.PT.58.32162630
Mouse	Myoz3	Mm.PT.58.10845949
Mouse	CTGF	Mm.PT.58.10386125.g
Mouse	Cyr61	Mm.PT.58.10039559.gs
Mouse	Adiponectin	Mm.PT.58.9719546
Mouse	MRTFa/MKL1	Mm.PT.58.31941709
Mouse	CEBPβ	Mm.PT.58.6467976.g
Mouse	CEBPα	Mm.PT.58.30061639.g
Mouse	ZFP423	Mm.PT.58.11752410
Mouse	ZFP516	Mm.PT.58.6635647
Mouse	MRTFb	Mm.PT.58.8277496
Mouse	ADRB1	Mm.PT.58.41132658.g
Mouse	ADRB2	Mm.PT.58.29310038.g
Mouse	ADRB3	Mm.PT.58.31423945
Mouse	CideA	Mm.PT.58.13017856
Mouse	Yap	Mm.PT.58.6477669
Mouse	Taz	Mm.PT.56a.32319022.g
Human	PPIA	Hs.PT.58v.38887593.g
Human	TBP	Hs.PT.58v.39858774
Human	UCP1	Hs.PT.58.39157006
Human	PPARγ	Hs.PT.58.25464465
Human	TBX1	Hs.PT.58.2672803
Human	CITED1	Hs.PT.58.1567731
Human	FABP4	Hs.PT.58.20106818
Human	YAP	Hs.PT.58.14881945
Human	TAZ	Hs.PT.58.40508253
Human	Leptin	Hs.PT.58.38591248.g
Human	Cyr61	Hs.PT.58.27029250.gs
Human	CTGF	Hs.PT.58.14485164.g
Human	TNFα	Hs.PT.58.45380900
Human	TNFαR1	Hs.PT.58.19429998
Human	Adiponectin	Hs.PT.58.26002735

Human	Resistin	Hs.PT.58.20453577.g
Human	Angiotensinogen	Hs.PT.56a.40899792
Human	CXCR1	Hs.PT.58.25079910
Human	CXCR2	Hs.PT.58.41092811
Human	CXCR6	Hs.PT.58.19638752
Human	CD36	Hs.PT.56a.3615957
Human	EBF2	Hs.PT.58.818465
Human	PRDM16	Hs.PT.58.25688289
Human	PGC1α	Hs.PT.58.14965839
Human	ADRB3	Hs.PT.56a.40969747
Human	GRK3	Hs.PT.56a.616076
Human	FATP1	Hs.PT.58.25764893
Human	HSL	Hs.PT.58.40115105
Human	GLUT4	Hs.PT.58.2557238
Human	LPL	Hs.PT.58.20087469

Western Blotting and Protein Expression

Protein extraction was performed according to Abcam's recommendations using a RIPA buffer (Pierce) and a protease/phosphatase inhibitor (Halt 100x, Pierce). If samples came from a tissue, they were bead homogenized using a TissueLyser II from Qiagen. If samples were from tissue culture, they were repeatedly pipetted or scraped and placed in a 1.5mL microcentrifuge tube where they were triterated until cell debris was dispersed. Samples were incubated on ice for 15 mins before centrifuging them at 4°C, 16,000x*g*, for 15 minutes. Afterwards, protein samples were quantified using a BCA assay kit (Pierce), comparing the resulting absorbances to a linear albumin standard. Western samples were made according to their concentrations, loading no more than 50ug of protein per lane. Precast gradient gels were purchased from Bio-Rad in different format to facilitate high numbers or low lysate concentrations. A 6x Laemmli buffer with 10% β-Mercaptoethanol for protein reduction was used to help the samples settle in the gel wells. Gels were then run at 200v for 35-40 minutes, or until the trypan blue dye band was completely off the gel. Transfer was affected using the Bio-Rad Ready-to-Assemble PVDF kit along with the Tranblot Turbo, a semi-dry transfer apparatus that allows for the rapid transfer of protein from the polyacrylamide gel to the PVDF membrane. After transfer, membranes were washed 3x's with Tris buffered Saline plus 1% Tween 20 (TBST). Blocking was performed with 5% milk or BSA in TBST for 20 minutes before replacing with the same blocking buffer with a pre-verified (by manufacturers recommendation) concentration of primary antibody (Table 4-3). After overnight incubation, shaking, at 4°C the blots were washed 3x's with TBST and incubated for 1 hour at room temp with the corresponding secondary antibody(s) that were modified with a fluorescent tag for visualization (Licor). After imaging, bands were quantified using Image Studio Lite, a free western blot analysis package from Licor. Quantitation data was exported to Excel, normalized and averaged, and then graphed with Prism.

Table 4-3. Western Antibodies

Protein	Made in:	Manufacturer	Concentration
AKT	Rabbit	Cell Signaling	1:1k
p-AKT s473	Rabbit	Cell Signaling	1:500
p-AKT t308	Rabbit	Cell Signaling	1:500
HSL	Rabbit	Cell Signaling	1:1k
p-HSL s563	Rabbit	Cell Signaling	1:500
p-HSL s565	Rabbit	Cell Signaling	1:500
p-HSL s633	Rabbit	Cell Signaling	1:500
Glut1	Rabbit	Cell Signaling	1:1k
Glut4	Mouse	Cell Signaling	1:1k
CD36	Mouse	Cell Signaling	1:1k
Leptin	Rabbit	Abcam	1:1k
Adiponectin	Rabbit	Abcam	1:1k
Vinculin	Rabbit	Cell Signaling	1:1k
PAX	Rabbit	Cell Signaling	1:1k
α-Actinin	Rabbit	Cell Signaling	1:1k
Talin1	Rabbit	Cell Signaling	1:1k
β-Actin	Mouse	Cell Signaling	1:2k
β-Tubulin	Mouse	Cell Signaling	1:2k
JNK	Rabbit	Cell Signaling	1:1k
p-JNK t183/tyr185	Rabbit	Cell Signaling	1:1k
UCP1	Rabbit	Cell Signaling	1:500
Tomm20	Mouse	Fisher	1:1k
Anti-Rabbit 800		LiCor	1:10k
Anti-Mouse 680		LiCor	1:10k

Immunofluorescence

Immunofluorescence and fluorescent microscopy were performed in the College of Natural Resources Bioimaging Facility. Two different confocal microscopes were used during the duration of the research. The first, a Zeiss 710, was used to image processed tissue or implant sections. Hydrogel and tissues for cryosectioning were fixed using 4% paraformaldehyde/PBS solution overnight. The next day these samples were placed into a 15% Sucrose in PBS solution. The following day these samples were placed into a 30% sucrose/PBS solution. After another day these fixed samples were placed in OCT compound (TissueTek) and sectioned at 10-15 microns on a Leica CM3050S cryostat. Immunofluorescence was performed on non-serial sections of hydrogel and adipose tissue and was performed according to Abcam's recommendations for paraffin or cryopreserved tissue sections. Briefly, sections on slides were surrounded with a hydrophobic pen to contain the wash and labeling buffers. Sections were gently washed with TBS 2x 5mins and 0.025% Triton X-100 to permeabilize the sections. Sections were then blocked with 10% normal donkey serum and 1% BSA in TBS for 2 hours at room temperature. Afterwards,

primary antibodies were diluted into TBS plus 1% BSA. The next morning, the sections were washed with TBS + 0.025% Triton X-100 2x 5 minutes then incubated in TBS + 1% BSA with the secondary antibody for 1 hour. After incubation, sections were washed 3x in TBS, covered in ProLong Gold antifade mounting solution (Fisher) and covered with a coverslip. The next morning, coverslips were sealed with clear nail polish and taken to the imaging core for visualization on the Zeiss 710.

The second microscope used was an inverted Zeiss 880 that was used to image cells in a dish or multiwell tissue culture plate. For cells in well dishes that were on hydrogel and immunolabeled for protein localization, cells were fixed at room temperature for 10 minutes and washed with PBS 3x for 5 minutes each. Each well was then solubilized with 0.1% Triton X-100 in PBS for 10 minutes before placing in a blocking solution of 1% normal donkey serum, 1% BSA, and 5% FBS for 1 hour. Afterwards, all washes and incubations were performed in this blocking buffer. Antibodies were diluted according to Table 4-4. Final washes before imaging were with PBS alone. Imaging took place within 24 hours due to no antifade being used.

Our migration assay was also carried out on the Zeiss 880 using their Definite Focus 2 package that allowed us to set specific points to image and reimage over a period of hours. Cells were plated sparsely and allowed to adhere for 6 hours before staining with 10nM Hoescht for 1 hours. Labeling media was then gently washed out and the plate was taken to the CNR Bioimaging Facility. Three spots per well/treatment were taken every 15 minutes using Zeiss' GaAsP sensor to limit photobleaching and phototoxicity. Image analysis was performed using IMARIS (Bitplane) spot tracking software package to obtain the track length of each cell within the time course.

For live dyes and cell labeling kits, concentrations were used according to manufacturer's recommendations, and washed in DMEM at least 3x before imaging on the Zeiss 880 inverted scope.

Confocal images were analyzed using ImageJ to obtain localization, area, and mean numbers per cell which were then exported to excel and analyzed there.

Table 4-4. IHC Antibodies and Stains

Protein	Made in:	Manufacturer	Concentration
UCP1	Rabbit	Cell Signaling	1:250
Adiponectin	Mouse	Abcam	1:500
PDGFRa	Rabbit	Cell Signaling	1:500
Endomucin	Mouse	Fisher	1:250
Ly6C	Rabbit	Cell Signaling	1:500
Ly6G	Rabbit	Cell Signaling	1:500
YAP	Rabbit	Cell Signaling	1:300
Tomm20	Mouse	FIsher	1:250
anti-Rab AF488	Donkey	Jackson Immuno	1:1k
anti-Rab AF594	Donkey	Jackson Immuno	1:1k
anti-Rab AF647	Donkey	Jackson Immuno	1:1k
Anti-mouse AF488	Donkey	Jackson Immuno	1:1k
Dapi		Fisher	1µg/mL
Hoechst		Unknown	0.1µg/mL

Cytopainter Green	Abcam	manufacturer
Mitotracker 660	Molecular Probes	manufacturer
Phalloidin 647	Molecular Probes	manufacturer
Calcein AM	Molecular Probes	manufacturer
Ethidium Homodimer	Molecular Probes	manufacturer
BODIPY	Molecular Probes	manufacturer
BODIPY C1C12	Molecular Probes	manufacturer

Statistics

In general, an $n \geq 3$ was used for all major experiments. All results were statistically analyzed by Excel (Microsoft) or Prism (GraphPad). Two-tailed student t-test was used to compare the difference between two groups where appropriate. ANOVA was used for larger grouped analyses. P-value <0.1 as trending significance (†), P-value <0.05 was evaluated as significant (*), <0.01 as highly significant (**), and <0.001 as extremely significant (***). Error bars represent standard error of the mean in each group.

Conclusion

In this dissertation, we have attempted to build novel ways to investigate adipocyte biology as well as modify it in way that would help combat the obesity epidemic. Adipose tissue is a dynamic organ with many different roles and is often maligned due to cultural pressure. We have shown here that with better understanding, adipose tissue can be modified to burn fat instead of storing it. We can use the microphysiological system to test drugs on a patient-by-patient basis to understand how personal genetics could lead to contraindications. In all we have made pointed progress toward the creation of the BAT-MAISI as well as created a human higher throughput isogeneic drug test platform that could help many people in the future.

In Chapter 1 we illustrated the feasibility of an injectable therapeutic that utilized two chemistries, Michael addition and SPAAC, that builds off of previous version that only contained short adhesion peptides and crosslinkers and can now include azide-modified drugs that are bound to the HA and cannot leak out. Here we used Mirabegron, a β_3-Adrenergic receptor agonist but any compound could be used as long as it is modifiable. Further modifications will be necessary in this case in order to get the drug to maintain the ability to induce UCP1 expression and lipolysis, though the hydrogel itself remains viable as a material.

Next, we investigated modifications to our MAT-MACT system in order to determine if it could be made into an injectable that could be used in humans by removing the necessity for cell transplantation creating a BAT-MAISI. By including heparin-bound growth factors we show the ability to increase the gene expression of the cognate receptors in the implant after 10 days. We also investigated two methods that helped make out synthetic tissue more tissue-like, leading to better migration on the new gel surface by preadipocytes.

Finally, we developed a 3D adipose tissue microphysiological device that was supplemented with the hydrogels. This created a niche that allowed for the study of different models of insulin resistance, and even allowed us to add in isogeneically-derived macrophages to perturb the system in physiologically relevant way. These perturbations behaved in ways that pathologists have long reported in obese individuals and reproduced physiological outcomes that mimic patients taking drugs to ameliorate insulin resistance in obesity.

In all we believe compelling progress has been made along these scientific fronts. These data can hopefully be used by others in the future to build off of in order to create functional therapeutic models for the better understanding of human adipose tissue and adipocytes.

References

1 Evan & Bruce. What We Talk About When We Talk About Fat. *Cell* **156**, 20-44, doi:10.1016/j.cell.2013.12.012 (2014).

2 Chouchani, E. T. & Kajimura, S. Metabolic adaptation and maladaptation in adipose tissue. *Nat Metab* **1**, 189-200, doi:10.1038/s42255-018-0021-8 (2019).

3 Cohen, P. & Kajimura, S. The cellular and functional complexity of thermogenic fat. *Nat Rev Mol Cell Biol* **22**, 393-409, doi:10.1038/s41580-021-00350-0 (2021).

4 Sheldon, E. F. The so-called hibernating gland in mammals: A form of adipose tissue. *The Anatomical Record* **28**, 331-347, doi:10.1002/ar.1090280502 (1924).

5 Nnodim, J. O. & Lever, J. D. The pre- and postnatal development and ageing of interscapular brown adipose tissue in the rat. *Anatomy and Embryology* **173**, 215-223, doi:10.1007/bf00316302 (1985).

6 Vitali, A. *et al.* The adipose organ of obesity-prone C57BL/6J mice is composed of mixed white and brown adipocytes. *Journal of Lipid Research* **53**, 619-629, doi:10.1194/jlr.m018846 (2012).

7 Gesta, S., Tseng, Y.-H. & Kahn, C. R. Developmental Origin of Fat: Tracking Obesity to Its Source. *Cell* **131**, 242-256, doi:10.1016/j.cell.2007.10.004 (2007).

8 Cypess, A. M. Reassessing Human Adipose Tissue. *New England Journal of Medicine* **386**, 768-779, doi:10.1056/nejmra2032804 (2022).

9 Himms-Hagen, J. *et al.* Multilocular fat cells in WAT of CL-316243-treated rats derive directly from white adipocytes. *Am J Physiol Cell Physiol* **279**, C670-681, doi:10.1152/ajpcell.2000.279.3.C670 (2000).

10 Wang, Q. A., Tao, C., Gupta, R. K. & Scherer, P. E. Tracking adipogenesis during white adipose tissue development, expansion and regeneration. *Nature Medicine* **19**, 1338-1344, doi:10.1038/nm.3324 (2013).

11 Shao, M. *et al.* Cellular Origins of Beige Fat Cells Revisited. *Diabetes* **68**, 1874-1885, doi:10.2337/db19-0308 (2019).

12 Dewal, R. S. & Stanford, K. I. Effects of exercise on brown and beige adipocytes. *Biochim Biophys Acta Mol Cell Biol Lipids* **1864**, 71-78, doi:10.1016/j.bbalip.2018.04.013 (2019).

13 Lee, Y. H., Petkova, A. P., Mottillo, E. P. & Granneman, J. G. In vivo identification of bipotential adipocyte progenitors recruited by beta3-adrenoceptor activation and high-fat feeding. *Cell Metab* **15**, 480-491, doi:10.1016/j.cmet.2012.03.009 (2012).

14 Oguri, Y. *et al.* CD81 Controls Beige Fat Progenitor Cell Growth and Energy Balance via FAK Signaling. *Cell* **182**, 563-577 e520, doi:10.1016/j.cell.2020.06.021 (2020).

15 O'Mara, A. E. *et al.* Chronic mirabegron treatment increases human brown fat, HDL cholesterol, and insulin sensitivity. *J Clin Invest* **130**, 2209-2219, doi:10.1172/JCI131126 (2020).

16 Cypess, A. M. *et al.* Identification and importance of brown adipose tissue in adult humans. *N Engl J Med* **360**, 1509-1517, doi:10.1056/NEJMoa0810780 (2009).

17 Wolf, K. J. & Kumar, S. Hyaluronic Acid: Incorporating the Bio into the Material. *ACS Biomaterials Science & Engineering* **5**, 3753-3765, doi:10.1021/acsbiomaterials.8b01268 (2019).

18 Saari, H., Konttinen, Y. T., Friman, C. & Sorsa, T. Differential effects of reactive oxygen species on native synovial fluid and purified human umbilical cord hyaluronate. *Inflammation* **17**, 403-415, doi:10.1007/bf00916581 (1993).

19 Kang, L. *et al.* Hyaluronan Accumulates With High-Fat Feeding and Contributes to Insulin Resistance. *Diabetes* **62**, 1888-1896, doi:10.2337/db12-1502 (2013).

20 Ji, E. *et al.* Inhibition of adipogenesis in 3T3-L1 cells and suppression of abdominal fat accumulation in high-fat diet-feeding C57BL/6J mice after downregulation of hyaluronic acid. *International Journal of Obesity* **38**, 1035-1043, doi:10.1038/ijo.2013.202 (2014).

21 Adil, M. M. *et al.* Engineered hydrogels increase the post-transplantation survival of encapsulated hESC-derived midbrain dopaminergic neurons. *Biomaterials* **136**, 1-11, doi:10.1016/j.biomaterials.2017.05.008 (2017).
22 Wolf, K. J. *et al.* A mode of cell adhesion and migration facilitated by CD44-dependent microtentacles. *Proc Natl Acad Sci U S A* **117**, 11432-11443, doi:10.1073/pnas.1914294117 (2020).
23 Chen, K. Y. *et al.* Activating Human Adipose Tissue with the beta3-Adrenergic Agonist Mirabegron. *Methods Mol Biol* **2448**, 83-96, doi:10.1007/978-1-0716-2087-8_5 (2022).
24 Leitner, B. P. *et al.* Kinetics of human brown adipose tissue activation and deactivation. *Int J Obes (Lond)* **43**, 633-637, doi:10.1038/s41366-018-0104-3 (2019).
25 Pozzoli, C., Bertini, S., Poli, E., Placenza, G. & Menozzi, A. Relaxing effects of clenbuterol, ritodrine, salbutamol and fenoterol on the contractions of horse isolated bronchi induced by different stimuli. *Res Vet Sci* **128**, 43-48, doi:10.1016/j.rvsc.2019.10.022 (2020).
26 Colucci, W. S. *et al.* Decreased Lymphocyte Beta-Adrenergic-Receptor Density in Patients with Heart Failure and Tolerance to the Beta-Adrenergic Agonist Pirbuterol. *New England Journal of Medicine* **305**, 185-190, doi:10.1056/nejm198107233050402 (1981).
27 Tharp, K. M. *et al.* Matrix-Assisted Transplantation of Functional Beige Adipose Tissue. *Diabetes* **64**, 3713-3724, doi:10.2337/db15-0728 (2015).
28 Schneider, S., Unger, M., van Griensven, M. & Balmayor, E. R. Adipose-derived mesenchymal stem cells from liposuction and resected fat are feasible sources for regenerative medicine. *Eur J Med Res* **22**, 17, doi:10.1186/s40001-017-0258-9 (2017).
29 Lee, M. J., Wu, Y. & Fried, S. K. Adipose tissue remodeling in pathophysiology of obesity. *Curr Opin Clin Nutr Metab Care* **13**, 371-376, doi:10.1097/MCO.0b013e32833aabef (2010).
30 Peiseler, M. & Kubes, P. More friend than foe: the emerging role of neutrophils in tissue repair. *Journal of Clinical Investigation* **129**, 2629-2639, doi:10.1172/Jci124616 (2019).
31 Schlundt, C. *et al.* Macrophages in bone fracture healing: Their essential role in endochondral ossification. *Bone* **106**, 78-89, doi:10.1016/j.bone.2015.10.019 (2018).
32 Ogle, M. E., Segar, C. E., Sridhar, S. & Botchwey, E. A. Monocytes and macrophages in tissue repair: Implications for immunoregenerative biomaterial design. *Exp Biol Med* **241**, 1084-1097, doi:10.1177/1535370216650293 (2016).
33 Lee, Y. S., Huh, J. Y., Hwang, I., Kim, J. I. & Kim, J. B. Hypoxia-Mediated Chronic Inflammation Is Necessary for Long Term but Not Short Term HFD-Induced Insulin Resistance. *Diabetes* **60**, A436-A436 (2011).
34 Elgazar-Carmon, V., Rudich, A., Hadad, N. & Levy, R. Neutrophils transiently infiltrate intra-abdominal fat early in the course of high-fat feeding. *J Lipid Res* **49**, 1894-1903, doi:10.1194/jlr.M800132-JLR200 (2008).
35 Talukdar, S. *et al.* Neutrophils mediate insulin resistance in mice fed a high-fat diet through secreted elastase. *Nat Med* **18**, 1407-1412, doi:10.1038/nm.2885 (2012).
36 Friedrich, K. *et al.* Perturbation of the Monocyte Compartment in Human Obesity. *Front Immunol* **10**, 1874, doi:10.3389/fimmu.2019.01874 (2019).
37 Hijdra, D., Vorselaars, A. D., Grutters, J. C., Claessen, A. M. & Rijkers, G. T. Phenotypic characterization of human intermediate monocytes. *Front Immunol* **4**, 339, doi:10.3389/fimmu.2013.00339 (2013).
38 Italiani, P. & Boraschi, D. From Monocytes to M1/M2 Macrophages: Phenotypical vs. Functional Differentiation. *Front Immunol* **5**, 514, doi:10.3389/fimmu.2014.00514 (2014).
39 Bergmann, C. E. *et al.* Arteriogenesis depends on circulating monocytes and macrophage accumulation and is severely depressed in op/op mice. *J Leukocyte Biol* **80**, 59-65, doi:10.1189/jlb.0206087 (2006).

40 Arnold, L. *et al.* Inflammatory monocytes recruited after skeletal muscle injury switch into antiinflammatory macrophages to support myogenesis. *J Exp Med* **204**, 1057-1069, doi:10.1084/jem.20070075 (2007).
41 Rosenwald, M., Perdikari, A., Rulicke, T. & Wolfrum, C. Bi-directional interconversion of brite and white adipocytes. *Nat Cell Biol* **15**, 659-667, doi:10.1038/ncb2740 (2013).
42 Guerra, C., Koza, R. A., Yamashita, H., Walsh, K. & Kozak, L. P. Emergence of brown adipocytes in white fat in mice is under genetic control - Effects on body weight and adiposity. *Journal of Clinical Investigation* **102**, 412-420, doi:Doi 10.1172/Jci3155 (1998).
43 Himms-Hagen, J. *et al.* Multilocular fat cells in WAT of CL-316243-treated rats derive directly from white adipocytes. *Am J Physiol-Cell Ph* **279**, C670-C681, doi:DOI 10.1152/ajpcell.2000.279.3.C670 (2000).
44 Seale, P. *et al.* PRDM16 controls a brown fat/skeletal muscle switch. *Nature* **454**, 961-U927, doi:10.1038/nature07182 (2008).
45 Min, S. Y. *et al.* Human 'brite/beige' adipocytes develop from capillary networks, and their implantation improves metabolic homeostasis in mice. *Nature Medicine* **22**, 312-318, doi:10.1038/nm.4031 (2016).
46 Wu, J. *et al.* Beige Adipocytes Are a Distinct Type of Thermogenic Fat Cell in Mouse and Human. *Cell* **150**, 366-376, doi:10.1016/j.cell.2012.05.016 (2012).
47 Shinoda, K. *et al.* Genetic and functional characterization of clonally derived adult human brown adipocytes. *Nature Medicine* **21**, 389-+, doi:10.1038/nm.3819 (2015).
48 Wang, W. S. *et al.* Ebf2 is a selective marker of brown and beige adipogenic precursor cells. *P Natl Acad Sci USA* **111**, 14466-14471, doi:10.1073/pnas.1412685111 (2014).
49 Flynn, L. E., Prestwich, G. D., Semple, J. L. & Woodhouse, K. A. Proliferation and differentiation of adipose-derived stem cells on naturally derived scaffolds. *Biomaterials* **29**, 1862-1871, doi:10.1016/j.biomaterials.2007.12.028 (2008).
50 Hemmrich, K. *et al.* Autologous in vivo adipose tissue engineering in hyaluronan-based gels--a pilot study. *J Surg Res* **144**, 82-88, doi:10.1016/j.jss.2007.03.017 (2008).
51 Burdick, J. A. & Murphy, W. L. Moving from static to dynamic complexity in hydrogel design. *Nat Commun* **3**, 1269, doi:10.1038/ncomms2271 (2012).
52 Engler, A. J., Sen, S., Sweeney, H. L. & Discher, D. E. Matrix elasticity directs stem cell lineage specification. *Cell* **126**, 677-689, doi:10.1016/j.cell.2006.06.044 (2006).
53 Mihai, L. A., Chin, L., Janmey, P. A. & Goriely, A. A comparison of hyperelastic constitutive models applicable to brain and fat tissues. *J R Soc Interface* **12**, 0486, doi:10.1098/rsif.2015.0486 (2015).
54 Cox, T. R. & Erler, J. T. Remodeling and homeostasis of the extracellular matrix: implications for fibrotic diseases and cancer. *Dis Model Mech* **4**, 165-178, doi:10.1242/dmm.004077 (2011).
55 Charrier, E. E., Pogoda, K., Wells, R. G. & Janmey, P. A. Control of cell morphology and differentiation by substrates with independently tunable elasticity and viscous dissipation. *Nat Commun* **9**, 449, doi:10.1038/s41467-018-02906-9 (2018).
56 Cheng, S., Clarke, E. C. & Bilston, L. E. Rheological properties of the tissues of the central nervous system: a review. *Med Eng Phys* **30**, 1318-1337, doi:10.1016/j.medengphy.2008.06.003 (2008).
57 Geerligs, M., Peters, G. W., Ackermans, P. A., Oomens, C. W. & Baaijens, F. P. Linear viscoelastic behavior of subcutaneous adipose tissue. *Biorheology* **45**, 677-688 (2008).
58 Perepelyuk, M. *et al.* Normal and Fibrotic Rat Livers Demonstrate Shear Strain Softening and Compression Stiffening: A Model for Soft Tissue Mechanics. *PLoS One* **11**, e0146588, doi:10.1371/journal.pone.0146588 (2016).
59 Safshekan, F., Tafazzoli-Shadpour, M., Abdouss, M. & Shadmehr, M. B. Viscoelastic Properties of Human Tracheal Tissues. *J Biomech Eng* **139**, doi:10.1115/1.4034651 (2017).

60 Chen, X. *et al.* Quantification of liver viscoelasticity with acoustic radiation force: a study of hepatic fibrosis in a rat model. *Ultrasound Med Biol* **39**, 2091-2102, doi:10.1016/j.ultrasmedbio.2013.05.020 (2013).
61 Levental, I. *et al.* A simple indentation device for measuring micrometer-scale tissue stiffness. *J Phys Condens Matter* **22**, 194120, doi:10.1088/0953-8984/22/19/194120 (2010).
62 Liu, Z. & Bilston, L. On the viscoelastic character of liver tissue: experiments and modelling of the linear behaviour. *Biorheology* **37**, 191-201 (2000).
63 Wu, S. G. & Lee, G. C. On nonlinear viscoelastic properties of arterial tissue. *J Biomech Eng* **106**, 42-47, doi:10.1115/1.3138455 (1984).
64 Chaudhuri, O. *et al.* Substrate stress relaxation regulates cell spreading. *Nat Commun* **6**, 6364, doi:10.1038/ncomms7365 (2015).
65 Tsuji, Y., Li, X. & Shibayama, M. Evaluation of Mesh Size in Model Polymer Networks Consisting of Tetra-Arm and Linear Poly(ethylene glycol)s. *Gels* **4**, doi:10.3390/gels4020050 (2018).
66 Browne, S., Hossainy, S. & Healy, K. Hyaluronic Acid Macromer Molecular Weight Dictates the Biophysical Properties and in Vitro Cellular Response to Semisynthetic Hydrogels. *ACS Biomater Sci Eng* **6**, 1135-1143, doi:10.1021/acsbiomaterials.9b01419 (2020).
67 Fogelstrand, P. & Boren, J. Treatment of hyaluronan accumulation ameliorates high-fat diet-induced insulin resistance in mice. *Diabetes* **62**, 1816-1817, doi:10.2337/db13-0261 (2013).
68 Berry, R. & Rodeheffer, M. S. Characterization of the adipocyte cellular lineage in vivo. *Nat Cell Biol* **15**, 302-308, doi:10.1038/ncb2696 (2013).
69 Kireeva, M. L., Mo, F. E., Yang, G. P. & Lau, L. F. Cyr61, a product of a growth factor-inducible immediate-early gene, promotes cell proliferation, migration, and adhesion. *Mol Cell Biol* **16**, 1326-1334, doi:10.1128/MCB.16.4.1326 (1996).
70 DeBari, M. K. & Abbott, R. D. Adipose Tissue Fibrosis: Mechanisms, Models, and Importance. *Int J Mol Sci* **21**, doi:10.3390/ijms21176030 (2020).
71 Collins, M. N. & Birkinshaw, C. Hyaluronic acid based scaffolds for tissue engineering--a review. *Carbohydr Polym* **92**, 1262-1279, doi:10.1016/j.carbpol.2012.10.028 (2013).
72 Rho, J. G. *et al.* Self-Assembled Hyaluronic Acid Nanoparticles Ameliorate Adipose Tissue Inflammation and Insulin Resistance in Diet-Induced Obese Mice. *Diabetes* **67**, doi:10.2337/db18-2003-P (2018).
73 Wu, J. *et al.* Beige adipocytes are a distinct type of thermogenic fat cell in mouse and human. *Cell* **150**, 366-376, doi:10.1016/j.cell.2012.05.016 (2012).
74 Gong, Z. *et al.* Matching material and cellular timescales maximizes cell spreading on viscoelastic substrates. *Proc Natl Acad Sci U S A* **115**, E2686-E2695, doi:10.1073/pnas.1716620115 (2018).
75 Zhang, C. *et al.* Mechanics-driven nuclear localization of YAP can be reversed by N-cadherin ligation in mesenchymal stem cells. *Nat Commun* **12**, 6229, doi:10.1038/s41467-021-26454-x (2021).
76 Adebowale, K. *et al.* Enhanced substrate stress relaxation promotes filopodia-mediated cell migration. *Nat Mater* **20**, 1290-1299, doi:10.1038/s41563-021-00981-w (2021).
77 Zimmet, P. & Shaw, J. Diabetes: Rising incidence of diabetes mellitus in youth in the USA. *Nat Rev Endocrinol* **13**, 379-380, doi:10.1038/nrendo.2017.59 (2017).
78 Zimmet, P. Z. Diabetes and its drivers: the largest epidemic in human history? *Clin Diabetes Endocrinol* **3**, 1, doi:10.1186/s40842-016-0039-3 (2017).
79 Ortega, F. B., Lavie, C. J. & Blair, S. N. Obesity and Cardiovascular Disease. *Circ Res* **118**, 1752-1770, doi:10.1161/CIRCRESAHA.115.306883 (2016).
80 Polyzos, S. A., Kountouras, J. & Mantzoros, C. S. Obesity and nonalcoholic fatty liver disease: From pathophysiology to therapeutics. *Metabolism* **92**, 82-97, doi:10.1016/j.metabol.2018.11.014 (2019).

81 Lin, J. H. Species similarities and differences in pharmacokinetics. *Drug Metab Dispos* **23**, 1008-1021 (1995).
82 Arabolaza, A. *et al.* Crystal structures and mutational analyses of acyl-CoA carboxylase beta subunit of Streptomyces coelicolor. *Biochemistry* **49**, 7367-7376, doi:10.1021/bi1005305 (2010).
83 Meyer, H., Mueller, J. & Meyer, F. Isolation of an acyl-CoA carboxylase from the tapeworm Spirometra mansonoides. *Biochem Biophys Res Commun* **82**, 834-839, doi:10.1016/0006-291x(78)90858-6 (1978).
84 Song, Z., Xiaoli, A. M. & Yang, F. Regulation and Metabolic Significance of De Novo Lipogenesis in Adipose Tissues. *Nutrients* **10**, doi:10.3390/nu10101383 (2018).
85 Sniderman, A. D., Cianflone, K., Arner, P., Summers, L. K. & Frayn, K. N. The adipocyte, fatty acid trapping, and atherogenesis. *Arterioscler Thromb Vasc Biol* **18**, 147-151, doi:10.1161/01.atv.18.2.147 (1998).
86 Pepino, M. Y., Kuda, O., Samovski, D. & Abumrad, N. A. Structure-function of CD36 and importance of fatty acid signal transduction in fat metabolism. *Annu Rev Nutr* **34**, 281-303, doi:10.1146/annurev-nutr-071812-161220 (2014).
87 Spalding, K. L. *et al.* Dynamics of fat cell turnover in humans. *Nature* **453**, 783-787, doi:10.1038/nature06902 (2008).
88 Jeffery, E., Church, C. D., Holtrup, B., Colman, L. & Rodeheffer, M. S. Rapid depot-specific activation of adipocyte precursor cells at the onset of obesity. *Nat Cell Biol* **17**, 376-385, doi:10.1038/ncb3122 (2015).
89 Wang, Q. A., Tao, C., Gupta, R. K. & Scherer, P. E. Tracking adipogenesis during white adipose tissue development, expansion and regeneration. *Nat Med* **19**, 1338-1344, doi:10.1038/nm.3324 (2013).
90 Vishvanath, L. *et al.* Pdgfrbeta+ Mural Preadipocytes Contribute to Adipocyte Hyperplasia Induced by High-Fat-Diet Feeding and Prolonged Cold Exposure in Adult Mice. *Cell Metab* **23**, 350-359, doi:10.1016/j.cmet.2015.10.018 (2016).
91 Jeffery, E. *et al.* The Adipose Tissue Microenvironment Regulates Depot-Specific Adipogenesis in Obesity. *Cell Metab* **24**, 142-150, doi:10.1016/j.cmet.2016.05.012 (2016).
92 Johannsen, D. L. *et al.* Effect of 8 weeks of overfeeding on ectopic fat deposition and insulin sensitivity: testing the "adipose tissue expandability" hypothesis. *Diabetes Care* **37**, 2789-2797, doi:10.2337/dc14-0761 (2014).
93 Hotamisligil, G. S. & Davis, R. J. Cell Signaling and Stress Responses. *Cold Spring Harb Perspect Biol* **8**, doi:10.1101/cshperspect.a006072 (2016).
94 Rausch, M. E., Weisberg, S., Vardhana, P. & Tortoriello, D. V. Obesity in C57BL/6J mice is characterized by adipose tissue hypoxia and cytotoxic T-cell infiltration. *Int J Obes (Lond)* **32**, 451-463, doi:10.1038/sj.ijo.0803744 (2008).
95 Ye, J., Gao, Z., Yin, J. & He, Q. Hypoxia is a potential risk factor for chronic inflammation and adiponectin reduction in adipose tissue of ob/ob and dietary obese mice. *Am J Physiol Endocrinol Metab* **293**, E1118-1128, doi:10.1152/ajpendo.00435.2007 (2007).
96 Li, C. *et al.* Macrophage polarization and meta-inflammation. *Transl Res* **191**, 29-44, doi:10.1016/j.trsl.2017.10.004 (2018).
97 Divoux, A. *et al.* Fibrosis in human adipose tissue: composition, distribution, and link with lipid metabolism and fat mass loss. *Diabetes* **59**, 2817-2825, doi:10.2337/db10-0585 (2010).
98 Honka, M. J. *et al.* Insulin-stimulated glucose uptake in skeletal muscle, adipose tissue and liver: a positron emission tomography study. *Eur J Endocrinol* **178**, 523-531, doi:10.1530/EJE-17-0882 (2018).

99 O'Doherty, R. M., Halseth, A. E., Granner, D. K., Bracy, D. P. & Wasserman, D. H. Analysis of insulin-stimulated skeletal muscle glucose uptake in conscious rat using isotopic glucose analogs. *Am J Physiol* **274**, E287-296, doi:10.1152/ajpendo.1998.274.2.E287 (1998).
100 Chiasson, J. L., Shikama, H., Chu, D. T. & Exton, J. H. Inhibitory effect of epinephrine on insulin-stimulated glucose uptake by rat skeletal muscle. *J Clin Invest* **68**, 706-713, doi:10.1172/jci110306 (1981).
101 Fisher, R. M. & Gertow, K. Fatty acid transport proteins and insulin resistance. *Curr Opin Lipidol* **16**, 173-178, doi:10.1097/01.mol.0000162322.39548.b1 (2005).
102 Sears, B. & Perry, M. The role of fatty acids in insulin resistance. *Lipids Health Dis* **14**, 121, doi:10.1186/s12944-015-0123-1 (2015).
103 Kahn, S. E., Hull, R. L. & Utzschneider, K. M. Mechanisms linking obesity to insulin resistance and type 2 diabetes. *Nature* **444**, 840-846, doi:10.1038/nature05482 (2006).
104 Ek, I., Arner, P., Bergqvist, A., Carlstrom, K. & Wahrenberg, H. Impaired adipocyte lipolysis in nonobese women with the polycystic ovary syndrome: a possible link to insulin resistance? *J Clin Endocrinol Metab* **82**, 1147-1153, doi:10.1210/jcem.82.4.3899 (1997).
105 Morigny, P., Houssier, M., Mouisel, E. & Langin, D. Adipocyte lipolysis and insulin resistance. *Biochimie* **125**, 259-266, doi:10.1016/j.biochi.2015.10.024 (2016).
106 Raje, V. *et al.* Adipocyte lipolysis drives acute stress-induced insulin resistance. *Sci Rep* **10**, 18166, doi:10.1038/s41598-020-75321-0 (2020).
107 Jiang, J. *et al.* Relationship of obesity to adipose tissue insulin resistance. *BMJ Open Diabetes Res Care* **8**, doi:10.1136/bmjdrc-2019-000741 (2020).
108 Sondergaard, E., De Ycaza, A. E. E., Morgan-Bathke, M. & Jensen, M. D. How to Measure Adipose Tissue Insulin Sensitivity. *J Clin Endocr Metab* **102**, 1193-1199, doi:10.1210/jc.2017-00047 (2017).
109 Ter Horst, K. W. *et al.* Methods for quantifying adipose tissue insulin resistance in overweight/obese humans. *Int J Obes (Lond)* **41**, 1288-1294, doi:10.1038/ijo.2017.110 (2017).
110 Gastaldelli, A., Gaggini, M. & DeFronzo, R. A. Role of Adipose Tissue Insulin Resistance in the Natural History of Type 2 Diabetes: Results From the San Antonio Metabolism Study. *Diabetes* **66**, 815-822, doi:10.2337/db16-1167 (2017).
111 Gastaldelli, A. *et al.* Importance of Changes in Adipose Tissue Insulin Resistance to Histological Response During Thiazolidinedione Treatment of Patients with Nonalcoholic Steatohepatitis. *Hepatology* **50**, 1087-1093, doi:10.1002/hep.23116 (2009).
112 Takahashi, K. & Yamanaka, S. Induction of pluripotent stem cells from mouse embryonic and adult fibroblast cultures by defined factors. *Cell* **126**, 663-676, doi:10.1016/j.cell.2006.07.024 (2006).
113 Shi, Y., Inoue, H., Wu, J. C. & Yamanaka, S. Induced pluripotent stem cell technology: a decade of progress. *Nat Rev Drug Discov* **16**, 115-130, doi:10.1038/nrd.2016.245 (2017).
114 Lau, E., Paik, D. T. & Wu, J. C. Systems-Wide Approaches in Induced Pluripotent Stem Cell Models. *Annu Rev Pathol* **14**, 395-419, doi:10.1146/annurev-pathmechdis-012418-013046 (2019).
115 Mohsen-Kanson, T. *et al.* Differentiation of Human Induced Pluripotent Stem Cells into Brown and White Adipocytes: Role of Pax3. *Stem Cells* **32**, 1459-1467, doi:10.1002/stem.1607 (2014).
116 Warren, C. R. *et al.* Induced Pluripotent Stem Cell Differentiation Enables Functional Validation of GWAS Variants in Metabolic Disease. *Cell Stem Cell* **20**, 547-557 e547, doi:10.1016/j.stem.2017.01.010 (2017).
117 Chal, J. *et al.* Differentiation of pluripotent stem cells to muscle fiber to model Duchenne muscular dystrophy. *Nat Biotechnol* **33**, 962-969, doi:10.1038/nbt.3297 (2015).

118 Matteelli, A. *et al.* Multidrug-resistant and extensively drug-resistant Mycobacterium tuberculosis: epidemiology and control. *Expert Rev Anti Infect Ther* **5**, 857-871, doi:10.1586/14787210.5.5.857 (2007).
119 Kwapiszewska, K., Michalczuk, A., Rybka, M., Kwapiszewski, R. & Brzozka, Z. A microfluidic-based platform for tumour spheroid culture, monitoring and drug screening. *Lab Chip* **14**, 2096-2104, doi:10.1039/c4lc00291a (2014).
120 Sun, J., Warden, A. R. & Ding, X. Recent advances in microfluidics for drug screening. *Biomicrofluidics* **13**, 061503, doi:10.1063/1.5121200 (2019).
121 Louwen, F., Ritter, A., Kreis, N. N. & Yuan, J. Insight into the development of obesity: functional alterations of adipose-derived mesenchymal stem cells. *Obes Rev* **19**, 888-904, doi:10.1111/obr.12679 (2018).
122 Weisberg, S. P. *et al.* Obesity is associated with macrophage accumulation in adipose tissue. *The Journal of clinical investigation* **112**, 1796-1808 (2003).
123 Rosen, E. D. & Spiegelman, B. M. What we talk about when we talk about fat. *Cell* **156**, 20-44 (2014).
124 Matsuo, K. *et al.* ACVR1R206H extends inflammatory responses in human induced pluripotent stem cell-derived macrophages. *Bone* **153**, 116129, doi:10.1016/j.bone.2021.116129 (2021).
125 Zhu, Q., Han, X., Peng, J., Qin, H. & Wang, Y. The role of CXC chemokines and their receptors in the progression and treatment of tumors. *Journal of molecular histology* **43**, 699-713 (2012).
126 Loskill, P. *et al.* WAT-on-a-chip: a physiologically relevant microfluidic system incorporating white adipose tissue. *Lab Chip* **17**, 1645-1654, doi:10.1039/c6lc01590e (2017).
127 Li, X. & Easley, C. J. Microfluidic systems for studying dynamic function of adipocytes and adipose tissue. *Anal Bioanal Chem* **410**, 791-800, doi:10.1007/s00216-017-0741-8 (2018).
128 Rogal, J. *et al.* WAT-on-a-chip integrating human mature white adipocytes for mechanistic research and pharmaceutical applications. *Sci Rep* **10**, 6666, doi:10.1038/s41598-020-63710-4 (2020).
129 Furuhashi, M. *et al.* Adipocyte/macrophage fatty acid-binding proteins contribute to metabolic deterioration through actions in both macrophages and adipocytes in mice. *J Clin Invest* **118**, 2640-2650, doi:10.1172/JCI34750 (2008).
130 Lee, Y. H., Kim, S. N., Kwon, H. J., Maddipati, K. R. & Granneman, J. G. Adipogenic role of alternatively activated macrophages in beta-adrenergic remodeling of white adipose tissue. *Am J Physiol Regul Integr Comp Physiol* **310**, R55-65, doi:10.1152/ajpregu.00355.2015 (2016).
131 Park, S. B. *et al.* Development of in vitro three-dimensional co-culture system for metabolic syndrome therapeutic agents. *Diabetes Obes Metab* **21**, 1146-1157, doi:10.1111/dom.13628 (2019).
132 Liu, Y. *et al.* Adipose-on-a-chip: a dynamic microphysiological in vitro model of the human adipose for immune-metabolic analysis in type II diabetes. *Lab Chip* **19**, 241-253, doi:10.1039/c8lc00481a (2019).
133 Mayo, K. H., Parra-Diaz, D., McCarthy, J. B. & Chelberg, M. Cell adhesion promoting peptide GVKGDKGNPGWPGAP from the collagen type IV triple helix: cis/trans proline-induced multiple proton NMR conformations and evidence for a KG/PG multiple turn repeat motif in the all-trans proline state. *Biochemistry* **30**, 8251-8267, doi:10.1021/bi00247a022 (1991).
134 Meng, Y. *et al.* Characterization of integrin engagement during defined human embryonic stem cell culture. *Faseb J* **24**, 1056-1065, doi:10.1096/fj.08-126821 (2010).
135 Hoffman, M. P. *et al.* Cell type-specific differences in glycosaminoglycans modulate the biological activity of a heparin-binding peptide (RKRLQVQLSIRT) from the G domain of the laminin alpha 1 chain. *J Biol Chem* **276**, 22077-22085, doi:DOI 10.1074/jbc.M100774200 (2001).

136 Harbers, G. M., Gamble, L. J., Irwin, E. F., Castner, D. G. & Healy, K. E. Development and characterization of a high-throughput system for assessing cell-surface receptor-ligand engagement. *Langmuir* **21**, 8374-8384, doi:10.1021/la050396y (2005).
137 Emsley, J., Knight, C. G., Farndale, R. W. & Barnes, M. J. Structure of the integrin alpha2beta1-binding collagen peptide. *J Mol Biol* **335**, 1019-1028, doi:10.1016/j.jmb.2003.11.030 (2004).
138 Marquis, M. E., Lord, E., Bergeron, E., Bourgoin, L. & Faucheux, N. Short-term effects of adhesion peptides on the responses of preosteoblasts to pBMP-9. *Biomaterials* **29**, 1005-1016, doi:10.1016/j.biomaterials.2007.10.047 (2008).
139 Graf, J. *et al.* Identification of an amino acid sequence in laminin mediating cell attachment, chemotaxis, and receptor binding. *Cell* **48**, 989-996, doi:10.1016/0092-8674(87)90707-0 (1987).
140 Nomizu, M. *et al.* Identification of cell binding sequences in mouse laminin gamma1 chain by systematic peptide screening. *J Biol Chem* **272**, 32198-32205, doi:10.1074/jbc.272.51.32198 (1997).
141 Boateng, S. Y. *et al.* RGD and YIGSR synthetic peptides facilitate cellular adhesion identical to that of laminin and fibronectin but alter the physiology of neonatal cardiac myocytes. *Am J Physiol-Cell Ph* **288**, C30-C38, doi:10.1152/ajpcell.00199.2004 (2005).
142 Hozumi, K. *et al.* Mixed Fibronectin-Derived Peptides Conjugated to a Chitosan Matrix Effectively Promotes Biological Activities through Integrins, alpha 4 beta 1, alpha 5 beta 1, alpha v beta 3, and Syndecan. *Bioresearch Open Acc* **5**, 356-366, doi:10.1089/biores.2016.0037 (2016).
143 Wilke, M. S. & Skubitz, A. P. N. Human Keratinocytes Adhere to Multiple Distinct Peptide Sequences of Laminin. *J Invest Dermatol* **97**, 141-146, doi:DOI 10.1111/1523-1747.ep12479311 (1991).
144 Zhu, J. & Marchant, R. E. Design properties of hydrogel tissue-engineering scaffolds. *Expert Rev Med Devices* **8**, 607-626, doi:10.1586/erd.11.27 (2011).
145 Calzada, M. J. *et al.* Recognition of the N-terminal modules of thrombospondin-1 and thrombospondin-2 by alpha(6)beta(1) integrin. *J Biol Chem* **278**, 40679-40687, doi:10.1074/jbc.M302014200 (2003).
146 Lee, S. T. *et al.* Engineering integrin signaling for promoting embryonic stem cell self-renewal in a precisely defined niche. *Biomaterials* **31**, 1219-1226, doi:10.1016/j.biomaterials.2009.10.054 (2010).
147 Klim, J. R., Li, L. Y., Wrighton, P. J., Piekarczyk, M. S. & Kiessling, L. L. A defined glycosaminoglycan-binding substratum for human pluripotent stem cells. *Nat Methods* **7**, 989-U972, doi:10.1038/Nmeth.1532 (2010).
148 Jha, A. K. *et al.* Matrix metalloproteinase-13 mediated degradation of hyaluronic acid-based matrices orchestrates stem cell engraftment through vascular integration. *Biomaterials* **89**, 136-147, doi:10.1016/j.biomaterials.2016.02.023 (2016).
149 Oudshoorn, M. H. M., Rissmann, R., Bouwstra, J. A. & Hennink, W. E. Synthesis of methacrylated hyaluronic acid with tailored degree of substitution. *Polymer* **48**, 1915-1920, doi:10.1016/j.polymer.2007.01.068 (2007).
150 Marklein, R. A. & Burdick, J. A. Spatially controlled hydrogel mechanics to modulate stem cell interactions. *Soft Matter* **6**, 136-143, doi:10.1039/b916933d (2010).
151 Chung, C. *et al.* Effects of auricular chondrocyte expansion on neocartilage formation in photocrosslinked hyaluronic acid networks. *Tissue Eng* **12**, 2665-2673, doi:10.1089/ten.2006.12.2665 (2006).
152 Lei, R. *et al.* Multiwell Combinatorial Hydrogel Array for High-Throughput Analysis of Cell-ECM Interactions. *ACS Biomater Sci Eng* **7**, 2453-2465, doi:10.1021/acsbiomaterials.1c00065 (2021).
153 Tokita, Y. & Okamoto, A. Hydrolytic degradation of hyaluronic acid. *Polymer Degradation and Stability* **48**, 269-273, doi:10.1016/0141-3910(95)00041-j (1995).

154 Deforest, C. A., Polizzotti, B. D. & Anseth, K. S. Sequential click reactions for synthesizing and patterning three-dimensional cell microenvironments. *Nature Materials* **8**, 659-664, doi:10.1038/nmat2473 (2009).
155 Nimmo, C. M., Owen, S. C. & Shoichet, M. S. Diels−Alder Click Cross-Linked Hyaluronic Acid Hydrogels for Tissue Engineering. *Biomacromolecules* **12**, 824-830, doi:10.1021/bm101446k (2011).
156 Gombert, Y., Roncoroni, F., Sánchez-Ferrer, A. & Spencer, N. D. The hierarchical bulk molecular structure of poly(acrylamide) hydrogels: beyond the fishing net. *Soft Matter* **16**, 9789-9798, doi:10.1039/d0sm01536a (2020).
157 Podhorska, B. *et al.* Revealing the True Morphological Structure of Macroporous Soft Hydrogels for Tissue Engineering. *Appl Sci-Basel* **10**, doi:ARTN 6672

10.3390/app10196672 (2020).
158 Ananthanarayanan, B., Kim, Y. & Kumar, S. Elucidating the mechanobiology of malignant brain tumors using a brain matrix-mimetic hyaluronic acid hydrogel platform. *Biomaterials* **32**, 7913-7923, doi:10.1016/j.biomaterials.2011.07.005 (2011).
159 Aston, R., Sewell, K., Klein, T., Lawrie, G. & Grondahl, L. Evaluation of the impact of freezing preparation techniques on the characterisation of alginate hydrogels by cryo-SEM. *Eur Polym J* **82**, 1-15, doi:10.1016/j.eurpolymj.2016.06.025 (2016).
160 Tharp, K. M. *et al.* Actomyosin-Mediated Tension Orchestrates Uncoupled Respiration in Adipose Tissues. *Cell Metab* **27**, 602-615 e604, doi:10.1016/j.cmet.2018.02.005 (2018).
161 Dubikovskaya, E., Chudnovskiy, R., Karateev, G., Park, H. M. & Stahl, A. Measurement of long-chain fatty acid uptake into adipocytes. *Methods Enzymol* **538**, 107-134, doi:10.1016/B978-0-12-800280-3.00007-4 (2014).